University of California

Los Angeles

Computational Quasiconformal Geometry and its Applications on Medical Morphometry and Computer Graphics

A dissertation submitted in partial satisfaction

of the requirements for the degree

Doctor of Philosophy in Mathematics

by

Tsz Wai Wong

2011

© Copyright by
Tsz Wai Wong
2011

The dissertation of Tsz Wai Wong is approved.

Luminita Vese

Paul M. Thompson

Joseph Teran

Tony F. Chan, Committee Chair

University of California, Los Angeles

2011

To my parents . . .

for their love and constant support.

Table of Contents

List of Figures

Acknowledgments

I would like to express my deep gratitude to my advisor, Prof. Tony Chan, who has given me a lot of advice and support in my research during the years of my PhD study. I would also like to thank Prof. Paul Thompson for his support and advice on medical research. I am very thankful to Prof. Shing-Tung Yau for allowing me to visit him at Harvard University and collaborate with him on research. I am thankful to Prof. Lok Ming Lui for his collaboration and contribution to many ideas in this dissertation. I would also like to thank my committee members Prof. Luminita Vese and Prof. Joseph Teran for their suggestions in my oral exams and this dissertation.

Besides, I would like to thank the Department of Mathematics at UCLA for providing me with the opportunity and support to study here, and my friends in the Department of Mathematics who have given me a lot of help and valuable opinions in different ways.

Lastly, I would like to thank my family and friends, especially my parents whose love and encouragement have supported me all of my life.

Vita

1984	Born, Hong Kong, China.
2005	B.S. (Mathematics and Physics), Hong Kong University of Science and Technology, Hong Kong, China.
2005–2006	Teaching Assistant, Department of Mathematics, Hong Kong University of Science and Technology. Taught: Introduction to Lie Groups Linear and Abstract Algebra
2006	M.Phil. (Mathematics), Hong Kong University of Science and Technology.
2008	M.A. (Applied Mathematics), UCLA, Los Angeles, California.
2007–2009	Teaching Assistant, Department of Mathematics, UCLA. Taught: Introduction to Programming Intermediate Programming Advanced Programming Data Structure and Algorithms Probability Theory Probability for Life Science Students Optimization
2009–2011	Research Assistant, Department of Mathematics, UCLA.

Publications

L. M. Lui, T. W. Wong, X. Gu, P. M. Thompson, T. F. Chan, and S. T. Yau, "Compression of surface registrations using Beltrami coefficients", *IEEE Computer Society Conference on Computer Vision and Pattern Recognition (CVPR) 2010*.

L. M. Lui, T. W. Wong, X. Gu, P. M. Thompson, T. F. Chan, and S. T. Yau, "Shape-based diffeomorphic registration on hippocampal surfaces using Beltrami holomorphic flow", *International Conference on Medical Image Computing and Computer Assisted Intervention (MICCAI) 2010*.

L. M. Lui, T. W. Wong, W. Zeng, X. Gu, P. M. Thompson, T. F. Chan, and S. T. Yau, "Detecting shape deformations using Yamabe flow and Beltrami coefficients", *Journal of Inverse Problem and Imaging (IPI): Special Issue in Medical Imaging*, Volume 3, Number 4, December 2009.

L. M. Lui, T. W. Wong, W. Zeng, X. Gu, P. M. Thompson, T. F. Chan, and S. T. Yau, "Representation of surface registrations using Beltrami holomorphic flow", *SIAM Journal on Scientific Computing (SISC), Special Issue on Methods in Medical Imaging*, in press.

Abstract of the Dissertation

Computational Quasiconformal Geometry and its Applications on Medical Morphometry and Computer Graphics

by

Tsz Wai Wong

Doctor of Philosophy in Mathematics

University of California, Los Angeles, 2011

Professor Tony F. Chan, Chair

Conformal geometry has been widely applied in medical imaging and computer graphics, such as in brain registration and texture mapping, where the mappings are constructed to be as conformal as possible to reduce geometric distortions. In reality, most registrations and surface mappings are not conformal and involve non-conformal distortions, which require more general theories to study. A direct generalization of conformal mapping is quasiconformal mapping, where the mapping is allowed to have bounded conformality distortions. In this dissertation, we develop computational algorithms from theories of quasiconformal mappings and quasicoformal geometry and apply them in two directions. First, we propose to study the distortions of surface mappings using the Beltrami coefficient. Second, we propose to represent surface mappings using their Beltrami coefficients for further adjustments. We apply these theories on areas where conformal geometry is used traditionally. These include registration of biological surfaces, shape analysis, medical morphometry, compression and refinement of texture mappings,

and the representation and inpainting of surface diffeomorphisms. Our results demonstrate that quasiconformal geometry is effective in solving shape analysis and surface mapping problems in medical morphometry and computer graphics.

CHAPTER 1

Introduction

Rapid development of computing technology has made possible many computations that were considered complicated or unpractical. This is especially true for the processing of biological surfaces in medical imaging. Surface processing is an important aspect of medical imaging for analyzing thousands of biological shapes for further diagnosis. Several important topics include the detection of abnormality on surfaces, the computation of surface registrations and the representation of surface diffeomorphisms, where many theories have been used to develop new techniques. Besides, surface processing is also important in computer graphics where 3D surfaces are modeled and textured. These areas put classical differential geometry into practical use.

To facilitate these applications, it is necessary to understand the geometry of 3D surfaces. An important tool that can be used is Riemannian geometry, which studies surfaces by considering them as Riemann surfaces admitting a conformal structure. On commonly occurring domains such as a genus zeros surface or a simply connected surface patch, this amounts to parameterize the domain conformally onto the complex plane, the Riemann sphere or the unit disk. In medical imaging, recent development of computational conformal geometry has produced efficient algorithms for parameterizing cortical surfaces conformally onto regular 2D or 3D domains (such as disks or spheres) for further study [AHT99][GWC04][HS09][JSR04][WLG07]. Registration techniques were

also proposed to maximize conformality as much as possible to minimize distortions [LWC07b][LTW08][LTW10][WLC05].

Conformal mappings are well known to preserve angles, and therefore preserve the geometry of surfaces by a scalar factor under the mappings. However, the strong emphasis on preserving local geometry up to a scalar constant places a global limitation of the resulting mappings. Some areas may be enlarged by a large magnification, while some areas are severely shrinked, making it difficult to compare areas which are scaled by different factors. Although conformal registration techniques aim at constructing surface mappings as conformal as possible [LWC07b][LTW08][LTW10][WLC05], the resulting mappings are not conformal most of the time as other constraints are also required to be satisfied, such as the matching of anatomical landmark lines or feature curves. In view of this, this dissertation introduces the use of the more general quasiconformal geometry for medical morphometry and computer graphics.

The organization of this dissertation is as follows. In Chapter 2, we briefly describe the mathematical background related to our work. This includes the definition of conformal and quasiconformal mappings, how to measure the quasiconformality of surface mappings using Beltrami coefficients and how to construct surface mappings with a given Beltrami coefficient.

In Chapter 3, we describe how the Beltrami coefficient can be used to detect abnormalities in biological surfaces. In this application, we register biological surfaces and measure the Beltrami coefficients of the resulting registrations. The abnormalities on the surfaces are modeled as areas with large distortions as given by the Beltrami coefficients. In this way, surface deformities are easily detected.

In Chapter 4, we describe how the Beltrami holomorphic flow (BHF) algorithm can be used to optimize and finely adjust surface registrations. We pro-

pose a framework for representing registrations and surface diffeomorphisms using their Beltrami coefficients. Adjusting the Beltrami coefficient is then equivalent to adjusting the corresponding surface diffeomorphism.

In Chapter 5, we propose to compress surface registrations using Beltrami coefficients. Using the framework in Chapter 4, the compression is performed in the space of Beltrami coefficients by Fourier compression. This greatly lifts the limits imposed by the Jacobian of the diffeomorphisms, requiring it to be positive everywhere.

In Chapter 6, we propose a new registration model by incorporating shape-based features into the minimizer of the L^2-norm of the Beltrami coefficient. By adding geometric features such as the mean and Gaussian curvatures, we propose an algorithm for hippocampal registration by minimizing a new energy function using BHF. Our results show that we can identify areas of statistically significant changes in hippocampi between patients with Alzheimer disease and normal controls.

In Chapter 7, we extend the use of BHF into video processing and computer graphics. With the exact integration of the perturbation given by BHF, we develop an exact algorithm for accurate adjustments of diffeomorphisms on triangular meshes. By working in the space of Beltrami coefficients, our algorithm is further applied on inpainting of missing regions in surface diffeomorphisms and refinement of texture mappings.

CHAPTER 2

Mathematical Background

In this chapter, we briefly describe the mathematical background of our work in this dissertation. First we introduce the basic definitions of Riemann surfaces and Riemannian geometry, which are our main tools to model biological surfaces. Next we introduce the notion of conformality and how Riemann surfaces can be parameterized conformally onto 2D domains. Then we generalize the concept to quasiconformal mappings and define the Beltrami coefficient and the Beltrami equation, which will be the main tool to study mappings between Riemann surfaces. Finally we introduce the Beltrami holomorphic flow method, which we use to reconstruct surface diffeomorphisms satisfying different Beltrami equations. The details of these definitions and theories will be explained in subsequent chapters when they are applied in real applications.

2.1 Riemann Surfaces and Their Conformal Mappings

To study surfaces in medical imaging and computer graphics effectively, one needs a good mathematical model of the surfaces. A well studied class of objects that fits such use are Riemann surfaces, which are surfaces with a conformal structure. Mathematically speaking, a Riemann surface is a real differentiable manifold S of dimension 2 equipped with a smooth varying Riemannian metric g. g can be

represented as a family of inner products $\{g_p\}_{p\in S}$ for every point of S:

$$g_p \colon T_pS \times T_pS \to \mathbb{R}, \quad p \in S. \tag{2.1}$$

The smoothness of the metric means that for all differentiable vector fields X, Y on S, the function $p \mapsto g_p(X(p), Y(p))$ is smooth.

As a differentiable manifold, a Riemann surface S is equipped with an atlas, which is a family of charts $\{U_\alpha, \phi_\alpha\}$, where $\{U_\alpha\}$ forms an open covering of S, and for any two charts (U_α, ϕ_α) and (U_β, ϕ_β) of S where $U_\alpha \cap U_\beta \neq \emptyset$, the atlas transition function $\phi_{\alpha\beta}$ defined as follows is smooth:

$$\phi_{\alpha\beta} = \phi_\beta \circ \phi_\alpha^{-1} \colon \phi_\alpha(U_\alpha \cap U_\beta) \to \phi_\beta(U_\alpha \cap U_\beta). \tag{2.2}$$

The conformal structure condition on S implies that there exists an atlas of S where all atlas transition functions are also conformal. Such atlas is called a conformal atlas. Two conformal atlases are compatible if their union is still a conformal atlas. This relation forms a equivalence relation on the set of conformal atlases on S, and each equivalence class is called a conformal structure.

We can also define conformal mappings between two Riemann surfaces M and N. A mapping $f \colon M \to N$ is conformal if for all $p \in M$, and charts (U_α, ϕ_α) and (U_β, ϕ_β) with $p \in U_\alpha$ and $f(p) \in U_\beta$ respectively, the function $\tilde{f} = \phi_\beta \circ f \circ \phi_\alpha^{-1}$ defined near $\phi_\alpha(p)$ is conformal. In terms of metrics, it means locally, f preserves the surface metrics of M and N up to a multiplicative factor called the conformal factor. This also means that conformal mappings preserve angles.

A fundamental theorem in conformal geometry is the uniformization theorem, which states that any simply connected Riemann surface is conformally equivalent to one of the three domains: the open unit disk, the complex plane, or the Riemann sphere. We will make use of this theorem to study the quasiconformal

geometry of these surfaces, which is a generalization of conformal geometry. In the next section, we illustrate the basic definitions of quasiconformal mappings.

2.2 Quasiconformal Mappings and the Beltrami Coefficient

A generalization of conformal mapping is quasiconformal mapping. Let $f\colon \mathbb{C} \to \mathbb{C}$ be a complex-valued function defined on the complex plane. We define the complex derivatives $\frac{\partial}{\partial z}$ and $\frac{\partial}{\partial \overline{z}}$ as follows:

$$\frac{\partial f}{\partial z} = \frac{1}{2}\Big(\frac{\partial f}{\partial x} - i\frac{\partial f}{\partial y}\Big), \quad \frac{\partial f}{\partial \overline{z}} = \frac{1}{2}\Big(\frac{\partial f}{\partial x} + i\frac{\partial f}{\partial y}\Big). \tag{2.3}$$

We define a quasiconformal mapping as a function $f\colon \mathbb{C} \to \mathbb{C}$ satisfying the Beltrami equation:

$$\frac{\partial f}{\partial \overline{z}} = \mu(z)\frac{\partial f}{\partial z}, \tag{2.4}$$

where $\mu\colon \mathbb{C} \to \mathbb{C}$, called the Beltrami coefficient, is Lebesgue measurable and satisfies $\|\mu\|_\infty < 1$. If f is conformal at $z \in \mathbb{C}$, then the Cauchy-Riemann equations implies that $\frac{\partial f}{\partial \overline{z}} = 0$ at z, and the Beltrami coefficient μ is 0 at z. If f is quasiconformal at $z \in \mathbb{C}$, then the Beltrami coefficient μ measures the local non-conformal distortion at z.

The definition of quasiconformality can be extended to mappings between two Riemann surfaces. Suppose $f\colon M \to N$ is a quasiconformal mapping between two Riemann surfaces. Then the effect of the pullback under f of the usual Euclidean metric ds_N^2 is given by

$$f^*(ds_N^2) = |\frac{\partial f}{\partial z}|^2 |dz + \mu(z)d\overline{z}|^2, \tag{2.5}$$

where the nonconformal distortion is given by the Beltrami coefficient μ.

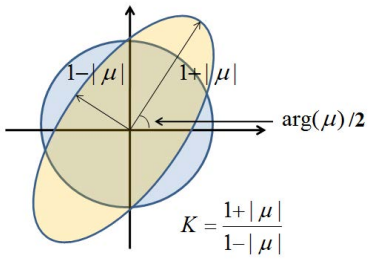

Figure 2.1: Illustration of how Beltrami coefficient μ measures the distortion by a quasi-conformal mapping that maps a small circle to an ellipse with dilation K.

An illustration of how the Beltrami coefficient μ measures non-conformal distortion is shown in Figure 2.1, which shows how a disk is mapped onto an ellipse by the quasiconformal mapping $f\colon \mathbb{C} \to \mathbb{C}$ given by $f(z) = z + \mu\overline{z}$, which has Beltrami coefficient μ. Then the dilation of the ellipse is given by

$$K = \frac{1 + |\mu|}{1 - |\mu|}, \tag{2.6}$$

and the direction of maximal stretching is given by $\arg(\mu)/2$.

In the next section, we consider the theoretical background for us to reconstruct a diffeomorphism from its Beltrami coefficient.

2.3 The Beltrami Holomorphic Flow

To apply tools in quasiconformal geometry on medical morphometry and computer graphics, we need a good theory for quasiconformal mappings on surfaces in 3D. In this dissertation, we are mainly concerned with simply connected 3D surfaces. According to the uniformization theorem, these surfaces are conformally equivalent to either the complex plane $\mathbb{C}$ or the Riemann sphere $\overline{\mathbb{C}}$. Therefore, every diffeomorphism between a pair of simply connected open or closed surfaces can be considered as a diffeomorphism f of $\mathbb{C}$ or $\overline{\mathbb{C}}$. On one hand, we can com-

pute the Beltrami coefficient of f. On the other hand, there are correspondences between the space of diffeomorphisms on $\mathbb{C}$ or $\overline{\mathbb{C}}$, and the space of Beltrami coefficients on $\mathbb{C}$ or $\overline{\mathbb{C}}$. The correspondence for $\overline{\mathbb{C}}$ is given by the following theorem:

Theorem 2.3.1 (Beltrami Holomorphic flow on $\mathbb{S}^2$)**.** *There is a one-to-one correspondence between the set of quasiconformal diffeomorphisms of $\mathbb{S}^2$ that fix the points 0, 1, and ∞ and the set of smooth complex-valued functions μ on $\mathbb{S}^2$ for which $\sup|\mu| = k < 1$. Here, we have identified $\mathbb{S}^2$ with the extended complex plane $\overline{\mathbb{C}}$. Furthermore, the solution f^μ to the Beltrami equation $f_{\overline{z}} = \mu f_z$ depends holomorphically on μ. Let $\{\mu(t)\}$ be a family of Beltrami coefficients depending on a real or complex parameter t. Suppose also that $\mu(t)$ can be written in the form*

$$\mu(t)(z) = \mu(z) + t\nu(z) + t\epsilon(t)(z) \tag{2.7}$$

for $z \in \mathbb{C}$, with suitable μ in the unit ball of $C^\infty(\mathbb{C})$, $\nu, \epsilon(t) \in L^\infty(\mathbb{C})$ such that $\| (\epsilon(t) \|_\infty \to 0$ as $t \to 0$. Then

$$f^{\mu(t)}(w) = f^\mu(w) + t\dot{f}^\mu[\nu](w) + o(|t|) \tag{2.8}$$

locally uniformly on $\mathbb{C}$ as $t \to 0$, for $w \in \mathbb{C}$, and where

$$\dot{f}[\nu](w) = -\frac{f^\mu(w)(f^\mu(w)-1)}{\pi} \int_{\mathbb{C}} \frac{\nu(z)((f^\mu)_z(z))^2}{f^\mu(z)(f^\mu(z)-1)(f^\mu(z)-f^\mu(w))}\, dx\, dy. \tag{2.9}$$

Proof. This theorem is due to Bojarski. For detailed proof, please refer to [2]. □

This theorem provides the theoretical foundation for us to work on the space of Beltrami coefficients for adjustments of diffeomorphisms on simply connected closed surfaces. In fact, Theorem 2.3.1 can be extended to the unit disk $\mathbb{D}$, which allows us to do the same for simply connected open surfaces. The statement of the theorem is as follows:

Theorem 2.3.2 (Beltrami Holomorphic flow on $\mathbb{D}$)**.** *There is a one-to-one correspondence between the set of quasiconformal diffeomorphisms of* $\mathbb{D}$ *that fix the points* 0 *and* 1 *and the set of smooth complex-valued functions* μ *on* $\mathbb{D}$ *for which* $\sup|\mu| = k < 1$*. Furthermore, the solution* f^μ *to the Beltrami equation* $f_{\bar{z}} = \mu f_z$ *depends holomorphically on* μ*. Let* $\{\mu(t)\}$ *be a family of Beltrami coefficients depending on a real or complex parameter* t*. Suppose also* $\mu(t)$ *can be written in the form*

$$\mu(t)(z) = \mu(z) + t\nu(z) + t\epsilon(t)(z) \tag{2.10}$$

for $z \in \mathbb{D}$*, with suitable* μ *in the unit ball of* $C^\infty(\mathbb{D})$*,* $\nu, \epsilon(t) \in L^\infty(\mathbb{D})$ *such that* $\| (\epsilon(t) \|_\infty \to 0$ *as* $t \to 0$*. Then:*

$$f^{\mu(t)}(w) = f^\mu(w) + t\dot{f}^\mu[\nu](w) + o(|t|) \tag{2.11}$$

locally uniformly on $\mathbb{C}$ *as* $t \to 0$*, for* $w \in \mathbb{C}$*, and where*

$$\begin{aligned} \dot{f}[\nu](w) = &-\frac{f^\mu(w)(f^\mu(w)-1)}{\pi} \\ &\Bigg(\int_{\mathbb{D}} \frac{\nu(z)((f^\mu)_z(z))^2}{f^\mu(z)(f^\mu(z)-1)(f^\mu(z)-f^\mu(w))}\, dx\, dy \\ &\quad + \int_{\mathbb{D}} \frac{\overline{\nu(z)}(\overline{(f^\mu)_z(z)})^2}{\overline{f^\mu(z)}(1-\overline{f^\mu(z)})(1-\overline{f^\mu(z)}f^\mu(w))}\, dx\, dy \Bigg). \end{aligned} \tag{2.12}$$

Proof. The proof of this theorem will be presented in details in Chapter 4. □

These two theorems will be used extensively in subsequent chapters to represent and adjust surface diffeomorphisms. A detailed discussion of this framework will be given in Chapter 4. At this point, we have illustrated the main theoretical background of this dissertation, which prepares us to explore the applications of quasiconformal geometry in medical morphometry and computer graphics.

CHAPTER 3

Detection of Shape Deformities Using Yamabe Flow and Beltrami Coefficients

3.1 Introduction

Detecting abnormal changes on surfaces is a central problem in shape analysis, especially in medical research. For example, neuroscientists commonly aim to identify abnormal deformations of cortical and subcortical structures in the brain in order to detect systematic patterns of alterations in brain diseases. In cardiac imaging and oncology, physicians commonly need to track changes or abnormalities in biological organs or tumors, to evaluate the effectiveness of different treatments, or monitor disease progression. Detecting and examining abnormalities with the human eye is inefficient and often inaccurate, especially on complicated surfaces such as the cerebral cortex of the brain. Therefore, it is of great importance to develop automatic methods to detect abnormalities and track abnormal geometric changes over time.

In this chapter, we propose a framework for detecting abnormal changes on elastic surfaces using quasiconformal geometry. Two issues arise in solving this problem. First, we want to find good registrations between surfaces with enforced landmark-correspondences. Second, we want to define a robust measure of deformity, which is invariant under normal (non-rigid) deformations that preserve

local geometry, so that quantitative analysis can be carried out. These goals are related, since good registrations allow accurate detection of abnormalities, while good measures of deformity can be used to set criteria for desirable registrations.

We propose to model deformities between elastic shapes as non-conformal deformations, whereas normal deformations that preserve the local geometry are formulated as conformal deformations. This is a generalization of existing work by Lord et al. and Unal et al. [LHV07b] [US05], which modeled deformities between shapes as non-isometric diffeomorphisms. Using the isometric indicator, the authors proposed to detect abnormalities that are invariant under rigid transformations. Our proposed method is an extension of their approaches, in that we are trying to detect deformities on elastic surfaces that are invariant under non-rigid normal deformations. This is a more general and accurate definition in some situations. For example, we may consider the growth processes of the human body, which is a key area of study in medical imaging and face recognition. As a person grows, different parts of the human body grow locally and the growth rate is somewhat uniform locally [TGW00]. The same organs of two healthy individuals tend to have similar shapes, although they may not be exactly isometric to each other. In other words, local geometry is well preserved under the normal growth process. Conformal maps are well-known to preserve local geometry. Therefore, a good registration between two organs of the same or different individuals should not be far from conformal. This motivates us to define good registrations as conformal registrations, and measure deformities as regions of non-conformality.

The key contribution in this chapter is the use of Beltrami coefficient to detect shape abnormalities. Suppose we are given a registration between a normal and a deformed surface of the same or different subjects. We can compute the Beltrami

coefficient of the registration map, which is a complex-valued function measuring the non-conformal deformation at each point of the map. In our examples, we show that the Beltrami coefficient is an effective measure of shape deformities on elastic surfaces.

To complete our framework for the automatic detection of shape deformities, we propose the following registration algorithm. We first generate a quasiconformal map between the original 3D surface and the surface to be compared with it. The surfaces are first conformally flattened onto 2D rectangles using a novel Yamabe flow method, which computes accurate conformal parameterizations of surfaces. Then, a quasiconformal map is computed to match landmark features between both flattened surfaces. By formulating abnormal changes as non-conformal deformations, we detect abnormalities by computing the Beltrami coefficient, which is uniquely associated with the quasiconformal map. By considering the norm of the Beltrami coefficient, we detect regions with abnormal changes, which are invariant under conformal deformation. Furthermore, by considering the argument of the Beltrami coefficient, we can capture abnormalities induced by local rotational changes. We propose a quantity called the Beltrami index, which allows us to quantitatively describe the degree of abnormality in each region. Experiments applying our algorithm to synthetic surfaces, 3D human face data and real MRI-derived brain surfaces show that our algorithm can effectively detect abnormalities and capture local rotational alterations. The algorithm is also robust under added noise, and it is successful in detecting altered gyrification patterns on cortical surfaces. Quantitative comparisons of the size of abnormality with the Beltrami index show that the detected sizes of abnormalities correspond positively with the sizes of abnormalities. A comparison of the Beltrami coefficient with other commonly used measures like the isometric indicator and gradient show that these measures are not as effective as Beltrami

coefficient and may tend to give misleading results when the compared surfaces undergo normal changes that preserve the local geometry.

This chapter is organized as follows: prior work on related topics is presented in section 2. The basic mathematical theory is discussed in section 3. In Section 4, the details of our proposed model are discussed. In Section 5, our computer algorithm is summarized. Experimental results are discussed in Section 6, and some conclusions and future work are discussed in section 7.

3.2 Previous Work

Many different approaches have been proposed to detect changes in shapes. Most of them take into account properties that depend on the embedding of the shape in space. Tosun et al. [TRL06] proposed the use of three different shape measures – the shape index, curvedness, and L2 norm of mean curvature – to quantify cortical gyrification and complexity. While the curvature measure is an important geometric measure of surface properties, it is also affected by healthy changes like normal growth, which increases surface size and decreases curvature. Moreover, since the curvature is a second order geometric measure, it is more sensitive to noise in data, especially in triangular meshes. Extra preprocessing is required to guarantee the robustness of the measure. In contrast, the Beltrami coefficient we use is a first order geometric measure. This leads to less perturbation due to noise. By computing surface Jacobian and applying statistical inference via random field theory on cortical surfaces processed by diffusion smoothing, Chung et al. [CWR03] studied changes in cortical surface area, thickness, and curvature, as well as the change of the total gray matter volume over time. While surface Jacobian can detect area changes caused by abnormalities, it can also be affected by healthy deformations like normal growth, which also causes area changes of

surface registrations. By looking at the Beltrami coefficients, we are able to minimize the effects caused by such changes. We are also able to detect rotational distortions caused by abnormalities. Shi et al. [SRL07] suggested the use of Hamilton-Jacobi skeletons on cortical surfaces to study gyrification patterns in Williams syndrome. In this approach, the degree of gyrification is measured by the number of branches in the Hamilton-Jacobi skeleton. While this method is easily computable and gives a fast measure of complexity of the cortical surface, subtle changes could occur within a branch of the cortical surface, which require a finer measure to detect. To overcome this problem, our approach provides an local and intrinsic measure of surface distortion to detect such changes.

Registration is broadly used in medical imaging and face recognition. It aims to produce a desirable registration for obtaining good correspondences or performing further analysis. Grenander et al. [GM98] surveyed existing methods of computational anatomy and proposed a framework to compute deformation maps and empirical probability laws for disease testing. Early work such as Gaser et al. [GVK99] compute an initial correspondence field between surfaces to ease the detection of abnormalities. Such applications often involve models of the human face or organs of the human body. Some existing methods model deformities between shapes in terms of nonrigid or non-isometric diffeomorphisms [LHV07b] [US05]. This may make their algorithms classify normal growth in living organisms as abnormal. This motivates us to model abnormalities as non-conformal diffeomorphisms, and good registrations as ones that are as conformal as possible. We support our view with the following points. First, normal changes such as growth in humans tend to preserve local geometry well, and hence are conformal. Second, by modeling good registrations as those that are conformal, we are still able to get a correct registration when the proper registration is indeed isometric.

In most methods for detecting shape changes, an accurate registration between two shapes has to be computed. The area has been extensively studied. Unal et al. [US05] proposed the use of coupled PDEs for joint segmentation and registration. However, technique does not support the matching of user-defined landmarks. Pohl et al. [PFG06] proposed an expectation maximization-based method to solve the problem, which takes into account of image artifacts, anatomical labelmaps, and a structure-dependent hierarchical mapping from the atlas to the image space. This allows some controls over the matched areas, but user-defined landmark constraints may not be matched. Lord et al. [LHV07b] [LHV07a] proposed to match hippocampal surfaces by finding maps minimizing the deviation from isometry under the constraints of piecewise deformation homogeneity, with local asymmetry quantified. The authors defined asymmetries between paired shapes as non-rigid diffeomorphisms between shapes. However, under normal conditions, like growth, non-rigid shape changes naturally occur. In one of our examples, it is shown that the maps of a correctly matched pair of surfaces can be non-isometric in normal as well as abnormal regions. Such occasions call for a more flexible definition of shape abnormality.

It has become increasingly popular to study shape changes by computing diffeomorphisms with desired properties, as they give one-to-one correspondences of shapes for local comparisons. Using control theory and large-deformation continuum mechanics, variational metrics have been developed on the space of diffeomorphisms [GM98] [VMY04]. In computing diffeomorphisms, one of the goals is to preserve local geometry as far as possible while consistently aligning important anatomical features lying within a surface. Gu et al. [GWC04] proposed to find an optimal Möbius transformation between two surfaces to minimize a landmark mismatch error. Wang et al. [WLC05][LWC07b] defined a new energy functional based on harmonic energy to optimize the conformal parameterization of cortical

surfaces, while fixing landmark correspondences. The harmonic energy method was applied by Shi et al. [STD07] to match implicitly-defined surfaces by solving PDEs on them using level set methods. Using integral flows of smooth vector fields, Lui et al. [LTW08] further proposed to compute a landmark-matching diffeomorphism with shape-based correspondences between landmark curves.

Recently, conformal geometry has been used for 3D non-rigid surface matching and registration. Harmonic maps have been used to track non-rigid motions of 3D surfaces, which requires tracking of boundary correspondences. This challenge was addressed in [ZZW08][WLG07], where different conformal mappings induced by different holomorphic differentials were combined to achieve accurate and robust matching results. Even so, holomorphic differentials cannot handle surfaces with complicated topology; the Ricci flow method is much more flexible and general. The surface-based Ricci flow was introduced in [Ham88]. The theory of discrete surface Ricci flow was introduced in [CL03]. Euclidean Ricci flow has been applied to 3D shape analysis in [ZSG10], where all the Gaussian curvatures of the surface are concentrated on several singularities. To remove these singularities, the discrete hyperbolic Ricci flow was introduced in [ZYZ08], which improves the accuracy and robustness of the matching and registration. In practice, the Ricci flow method imposes constraints on the triangulation of the discrete surface, whereas the discrete Yamabe flow can handle much more general triangulations. Furthermore, the Yamabe flow can achieve a higher level of conformality than the Ricci flow. The theory of discrete Yamabe flow is established in [Luo04], where the existence, uniqueness and stability of the solution is rigorously proven.

3.3 Theoretical Background

In this section, we describe some basic mathematical concepts relevant to describing our algorithm.

A surface S with a conformal structure is called a *Riemann surface*. Given two Riemann surfaces M and N, a map $f : M \to N$ is *conformal* if it preserves the surface metric, up to a multiplicative factor called the *c*onformal factor. An immediate consequence is that every conformal map preserves angles. With the angle-preserving property, a conformal map effectively preserves the local geometry of the surface structure.

A generalization of conformal map is called the *quasiconformal* map which is an orientation-preserving homeomorphism between Riemann surfaces with bounded conformality distortion, in the sense that the first order approximation of the quasiconformal homeomorphism takes small circles to small ellipses of bounded eccentricity. Thus, a conformal homeomorphism that maps a small circle to a small circle can also be regarded as quasiconformal. Mathematically, f is quasiconformal provided that it satisfies the Beltrami's equation:

$$\frac{\partial f}{\partial \overline{z}} = \mu(z)\frac{\partial f}{\partial z} \tag{3.1}$$

for some complex-valued Lebesgue-measurable μ satisfying $|\mu|_\infty < 1$. In terms of the metric tensor, consider the effect of the pullback under f of the usual Euclidean metric ds_E^2; the resulting metric is given by:

$$f^*(ds_E^2) = |\frac{\partial f}{\partial z}|^2 |dz + \mu(z)d\overline{z})|^2 \tag{3.2}$$

which, relative to the background Euclidean metric dz and $d\overline{z}$, has eigenvalues $(1+|\mu|)^2\frac{\partial f}{\partial z}$ and $(1-|\mu|)^2\frac{\partial f}{\partial z}$. μ is called the *Beltrami coefficient*, which is a measure of conformality. In particular, the map f is conformal around a small neighborhood

of p when $\mu(p) = 0$. Also, the gradient and the Beltrami coefficient of the map are closely related. Suppose $f = (f_1, f_2)$ under the conformal parameter domains. The Jacobian matrix J of f can be written as $(\nabla f_1, \nabla f_2)$ which is a 2×2 matrix. The Jacobian is closely related to $|\mu_f|$. Mathematically,

$$\det(J) = (1 - |\mu_f|^2)(|\nabla f_1|^2 + |\nabla f_2|^2 + \det(J))/4$$

While $|\det(J)|$ gives us information about the area distortion under the map f, $|\mu_f|$ gives us information about the conformality distortion. In other words, $|\mu_f|$ measures the regions of deformations that do not preserve local geometry.

Infinitesimally, around a point p, f may be expressed with respect to its local parameter as follows:

$$\begin{aligned} f(z) &= f(p) + f_z(p)z + f_{\overline{z}}(p)\overline{z} \\ &= f(p) + f_z(p)(z + \mu(p)\overline{z}) \end{aligned} \tag{3.3}$$

Obviously, f is not conformal if and only if $\mu(p) \neq 0$. Inside the local parameter domain, f may be considered as a map composed of a translation of $f(p)$ together with a stretch map $S(z) = z + \mu(p)\overline{z}$, which is postcomposed by a multiplication of $f_z(p)$ which is conformal. All the conformal distortion of $S(z)$ is caused by $\mu(p)$. $S(z)$ is the map that causes f to map a small circle to a small ellipse. From $\mu(p)$, we can determine the angles of the directions of maximal magnification as well as the amount of maximal magnification and maximal shrinking. Specifically, the angle of maximal magnification is $arg\mu(p)/2$ with magnifying factor $1 + |\mu(p)|$; the angle of maximal shrinking is the orthogonal angle $(arg\mu(p) - \pi)/2$ with shrinking factor $1 - |\mu(p)|$. The distortion or dilation is given by:

$$K = \frac{1 + |\mu(p)|}{1 - |\mu(p)|} \tag{3.4}$$

Thus, the Beltrami coefficient μ gives us all the information about the conformaity of the map (See Figure 5.1). This motivates its use as a measure of ab-

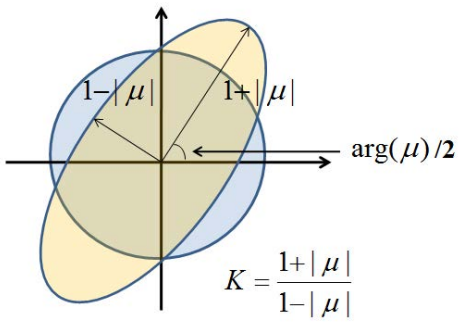

Figure 3.1: Illustration of how Beltrami coefficient μ measures the distortion by a quasiconformal mapping that maps a small circle to an ellipse with dilation K.

normal deformation, as abnormalities tend to cause significant distortions in the conformality of the deformation map.

It is often convenient to conformally map 3D surfaces to planar domains, to simplify subsequent computations. Yamabe flow offers a rigorous and efficient way to do this. Suppose S is a surface embedded in the 3D Euclidean space $\mathbb{R}^3$, then it has the induced Euclidean metric denoted by $\mathbf{g} = (g_{ij})$. Let $u : S \to \mathbb{R}$ be a function on S, then $\bar{\mathbf{g}} = e^{2u}\mathbf{g}$ is another Riemannian metric of S, which is conformal to $\mathbf{g}$. If the Gaussian curvatures induced by $\mathbf{g}$ and $\bar{\mathbf{g}}$ are K and $\bar{K}$, then they are related by the following *Yamabe equation*

$$\bar{K} = e^{2u}(-\Delta_{\mathbf{g}} u + K), \tag{3.5}$$

where $\Delta_{\mathbf{g}}$ is the Laplace-Beltrami operator under the original metric $\mathbf{g}$.

It is fundamentally important to design a Riemannian metric $\bar{\mathbf{g}}$ with a prescribed curvature $\bar{K}$, which is equivalent to solving the Yamabe equation. The surface Yamabe flow (or equivalently the Ricci flow) is a powerful tool for solving it. Intuitively, the surface Yamabe flow deforms the metric in proportion to the Gaussian curvature, such that the Gaussian curvature evolves according to a heat

diffusion process.

$$\frac{dg_{ij}}{dt} = (\bar{K} - K)g_{ij}. \tag{3.6}$$

It has been proven [Luo04] that if $\bar{K} \equiv 0$ everywhere and the total area is preserved during the flow, the Yamabe flow converges and leads to a metric with constant Gaussian curvature. Note that, for higher-dimensional Riemannian manifolds, the Ricci flow and Yamabe flow are different. On discrete surfaces, the discrete Yamabe flow produces better conformality than the discrete Ricci flow.

3.4 Our Proposed Model

In our method, we propose to use the Beltrami coefficient to detect abnormalities on surfaces. This is done by formulating abnormal changes as non-conformal deformations. Conversely, a conformal deformation is considered as normal. This definition is based on the fact that the local geometries of shape are well-preserved under normal changes, such as biological shape deformations. Conformal maps are well known to preserve local geometry and thus it is plausible to use them to characterize normal deformation. When shapes undergo abnormal changes, significant local distortions in conformality are often observed. This motivates us to consider the Beltrami coefficient, which measures the degree of conformality distortion, for abnormality detection. Our proposed algorithm has three main steps. First, the original 3D surface and the deformed surface are conformally parameterized onto 2D rectangles using the Yamabe flow method. This simplifies the problem by transforming the 3D surface problem into a 2D problem. Second, a quasiconformal map is obtained between the two surfaces by computing a harmonic map between their conformal parameter domains, which also accommodates constraints to match internal landmarks based on their shapes. This gives

a one-to-one correspondence (registration) between the two surfaces. Finally, the Beltrami coefficient associated with the quasiconformal map is computed as an index of abnormal changes. We describe each step in detail next.

3.4.1 Conformal Parameterization Using the Yamabe Flow

To detect regions with abnormalities, the first step is to find a one-to-one correspondence (registration) between the original and deformed surfaces. With this registration, we can detect the distortion in conformality of the deformation at each point by computing the associated Beltrami coefficient. Computing the surface registration directly on surfaces is difficult, especially on complicated surfaces such as the cortical surface of the brain. Therefore, it is advantageous for us to first parameterize the surfaces conformally onto the 2D parameter domain. This simplifies the process by transforming the surface problem into a 2D problem. Under the conformal parameterizations, determining conformality distortion between surfaces is equivalent to determining it between their conformal parameter domains. Of course, the computation of conformal parameterizations has to be accurate in order to effectively detect changes in conformality. The Yamabe flow (3.6) provides us with an efficient and accurate way to compute these conformal maps.

In practice, all surfaces are approximated by piecewise linear triangular meshes $M(V, E, F)$, where V, E and F represent the vertex, edge and face set of the mesh. We use v_i to denote the i-th vertex, $[v_i, v_j]$ the edge connecting v_i and v_j, $[v_i, v_j, v_k]$ the face connecting v_i, v_j, v_k. The *discrete metric* is the edge length function $\ell : E \to \mathbb{R}^+$ satisfying triangle inequality. The *vertex discrete curvature*

is defined as angle deficiency,

$$K_i = \begin{cases} 2\pi - \sum_{[v_i,v_j,v_k]\in F} \theta_i^{jk} & v_i \notin \partial M \\ \pi - \sum_{[v_i,v_j,v_k]\in F} \theta_i^{jk} & v_i \in \partial M \end{cases}$$

where θ_i^{jk} is the corner angle at v_i in the face $[v_i, v_j, v_k]$, ∂M is the boundary of M. Let $\mathbf{u} : V \to \mathbb{R}$ be the discrete conformal factor. The edge length of $[v_i, v_j]$ is defined as

$$\ell_{ij} := \exp(u_i)\exp(u_j)\ell_{ij}^0,$$

where ℓ_{ij}^0 is the original edge length in $\mathbb{R}^3$. The discrete Yamabe flow is defined as

$$\frac{du_i}{dt} = \bar{K}_i - K_i,$$

with the constraint $\sum_i u_i = 0$. The discrete Yamabe flow converges, and the final discrete metric induces the prescribed curvature; a detailed proof can be found in [Luo04]. The discrete Yamabe flow is the negative gradient flow of the following *Yamabe energy*,

$$E(\mathbf{u}) = \int_{\mathbf{u}_0}^{\mathbf{u}} \sum_i (\bar{K}_i - K_i) du_i,$$

where $\mathbf{u}_0 = (0, 0, \cdots, 0)$. This energy is convex and has a unique global minimum, which corresponds to the desired metric. Using Newton's method, the Yamabe energy can be optimized very efficiently. The Hessian matrix $H = (h_{ij})$ of the Yamabe energy has an explicit form. If $[v_i, v_j]$ is an edge on the mesh, $[v_i, v_j, v_k]$ and $[v_j, v_i, v_l]$ are the two faces adjacent to $[v_i, v_j]$, then $h_{ij} = \cot\theta_k^{ij} + \cot\theta_l^{ij}$, θ_k^{ij} is the corner angle at v_k in the face $[v_i, v_j, v_k]$. The diagonal element h_{ii} equals to $\sum_{j\neq i} h_{ij}$.

To compute a conformal mapping of a simply connected surface S, we set the target curvature to be zeros for all interior vertices, and the total curvature of boundary vertices to be 2π. For example, in order to map a human face surface

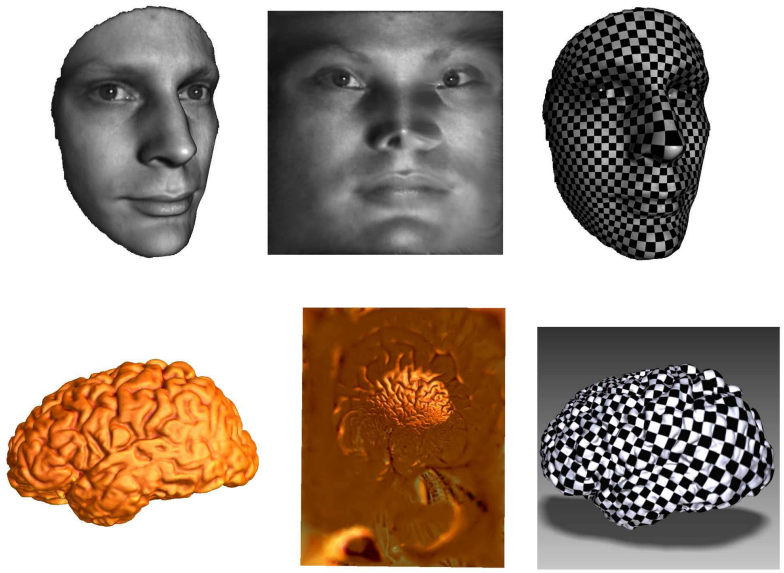

Figure 3.2: Conformal mappings of a real human face and a real brain cortical surface, using Yamabe flow method. Four corners are picked, whose target curvatures are set to be $\frac{\pi}{2}$, and the target curvatures are set to be zeros everywhere.

to a rectangle, we select four corner vertices, and set their target curvatures to be $\frac{\pi}{2}$. The target curvatures for all other vertices are zeros. Using the Yamabe flow, we can obtain the desired metric. Then we flatten the mesh isometrically face by face using the resulting metric. Figure 3.2 shows two examples of conformal surface mappings using Yamabe flow method. The conformality is demonstrated using checkerboard texture mapping.

3.4.2 Quasiconformal Map between Surfaces

After parameterizing the surfaces conformally, the next step is to determine a quasiconformal registration between the conformal parameter domains. There may be important curves on the surfaces representing landmark features[LWC07a], so we look for the optimized harmonic diffeomorphism that exactly matches landmark features via a variational approach. However, minimizing the energy func-

tional over the search space of landmark-matching surface diffeomorphisms is difficult. Following [LTW08], we formulate our problem as a variational energy defined on a search space of smooth vector fields $\overrightarrow{V}$. The diffeomorphism may then be generated through the integral flow of $\overrightarrow{V}$. $\overrightarrow{V}$ are restricted only to those that do not flow across the landmark curves (to enforce exact landmark correspondence). Our energy has 2 terms: (1) a harmonic energy term to optimize the harmonicity of the parametrization maps; (2) a smoothness energy term to ensure the smoothness of the vector field.

Denote the conformal parameter domains of S_1 and S_2 by D_1 and D_2 respectively. We look for harmonic diffeomorphisms $\tilde{f}_1 : D_1 \to \Omega$ and $\tilde{f}_2 : D_2 \to \Omega$ that match landmark curves to a consistent location C. The composition map $\tilde{f}_2^{-1} \circ \tilde{f}_1$ is a landmark-matching harmonic diffeomorphism from D_1 to D_2. To start with, we compute any arbitrary maps $f_{01} : D_1 \to \Omega$ and $f_{02} : D_2 \to \Omega$. We then iteratively look for the smooth vector field $\vec{X}_i$ on Ω such that the composition map $\tilde{f}_i = \Phi^{\vec{X}_i} \circ f_{0i} : D_i \to \Omega$ is the landmark matching harmonic diffeomorphism ($i = 1, 2$). Here, $\Phi^{\vec{X}_i} : \Omega \to \Omega$ is the time-1 integral flow of the vector field $\vec{Y}_i = P_C \vec{X}_i$ satisfying the integral flow equation:

$$\frac{\partial \Phi^{\vec{X}_i}}{\partial t}(\mathbf{x}, t) = \vec{X}_i(\Phi^{\vec{X}_i}(\mathbf{x}, t)),$$
$$\Phi^{\vec{X}_i}(\mathbf{x}, 0) = \mathbf{x}.$$

$\vec{Y}$ is the projection of the vector field $\vec{X}_i$ such that it is tangential to C. This ensures the exact landmark matching property of $\tilde{f}_i$.

The vector fields $\vec{X}_i = a_i \frac{\partial}{\partial x} + b_i \frac{\partial}{\partial y}$ minimizes the following energy functional:

$$J[a_i, b_i] = \int_\Omega |\nabla \tilde{f}_1|^2 \ + |\nabla \tilde{f}_2|^2 \, dx + \lambda \int_C \left(\kappa_1(\tilde{f}_1) - \kappa_2(\tilde{f}_2)\right)^2 \, ds_D \qquad (3.7)$$
$$+\beta \int_\Omega |\nabla \vec{X}_1|^2 + |\nabla \vec{X}_2|^2 \, dx$$

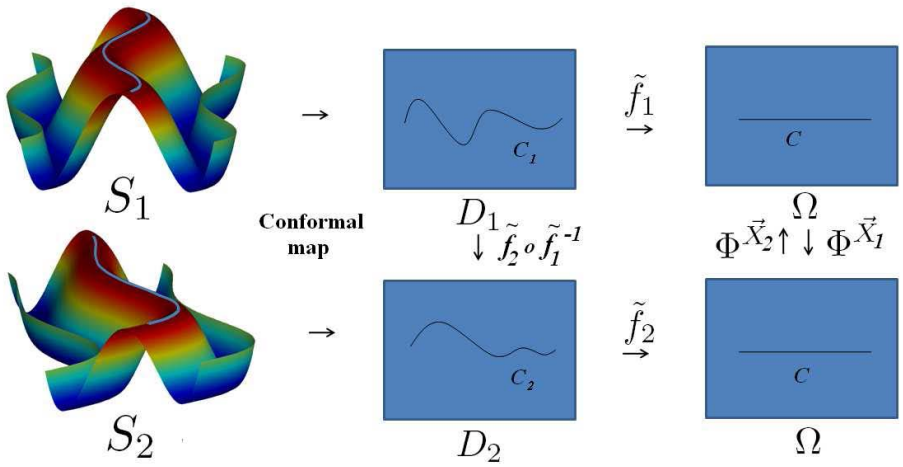

Figure 3.3: How quasiconformal registration is constructed between two surfaces.

The variational problem is then formulated to be defined over the space of C^1 smooth vector fields on Ω. The last integral in the energy is the smoothness term for the vector fields $\vec{X}_i$. The first two integrals are the harmonic terms, which aim to preserve the harmonicity of the parameterization as much as possible. The second term is a *symmetric* shape term defined as an arc length integral, where the shape measure is defined according to the curvature. The proposed energy functional can be minimized by modifying the vector field iteratively according to the following Euler-Lagrange equation:

$$\frac{da_i}{dt} = \int_0^1 B_i(\phi_s^{\vec{Y}_i})\ \Psi_i(\phi_s^{\vec{Y}_i}, 1)\ \Psi_i^{-1}(\phi_s^{\vec{Y}_i}, s)\ P_C\vec{e}_1\ \ |D\phi_s^{\vec{Y}_i}|\ ds - \beta\Delta a_i \tag{3.8}$$

$$\frac{db_i}{dt} = \int_0^1 B_i(\phi_s^{\vec{Y}_i})\ \Psi_i(\phi_s^{\vec{Y}_i}, 1)\ \Psi_i^{-1}(\phi_s^{\vec{Y}_i}, s)\ P_C\vec{e}_2\ \ |D\phi_s^{\vec{Y}_i}|\ ds - \beta\Delta b_i, \tag{3.9}$$

where:

$B_i := -\Delta\tilde{f}_i\ Df_{0,i}\ +\ \lambda\chi_A\ \big((-1)^{i-1}\big(\kappa_1(\tilde{f}_1) - \kappa_2(\tilde{f}_2)\big)\nabla\kappa_i - \nabla\cdot C_i\big)\ Df_{0,i}\ |\nabla H(\phi)|$;
Ψ_i is the orthogonal fundamental matrix for the homogeneous system of

$$\frac{\partial}{\partial t}P_i(x,t) = \eta P_C\vec{e}_1\ (\Phi^{\vec{Y}_i}(x,t)) + D\vec{Y}_i(\Phi^{\vec{Y}_i}(x,t))\ P_i(x,t),$$
$$P_i(x,0) = \mathbf{0}.$$

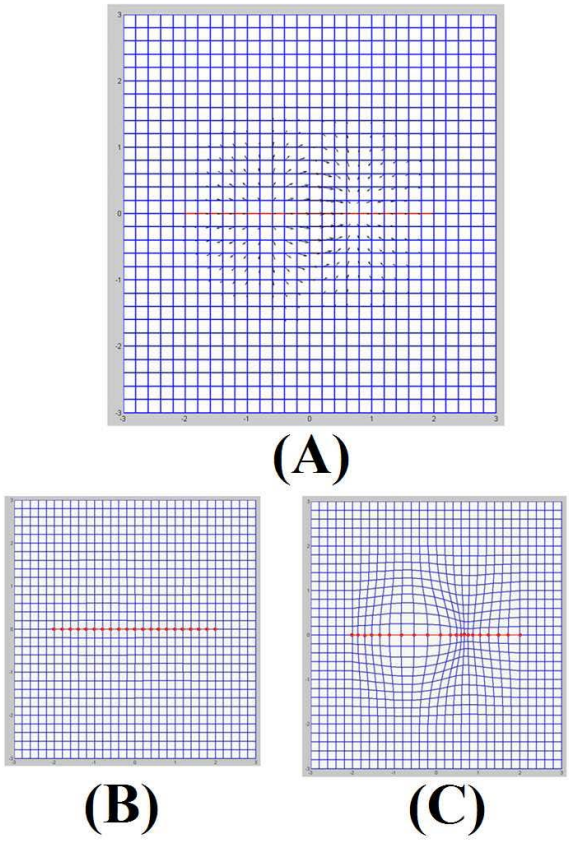

Figure 3.4: (A) shows the vector field defined on the domain. The vector field on the landmark is tangential to the curve. (B) shows the grid lines on the domain. Several points are labeled on the landmark to visualize its displacement under the integral flow. (C) shows the result of the integral flow of the vector field. A diffeomorphism with exact landmark matching is obtained. Note that points slide along the landmark curve, instead of flowing across the curve.

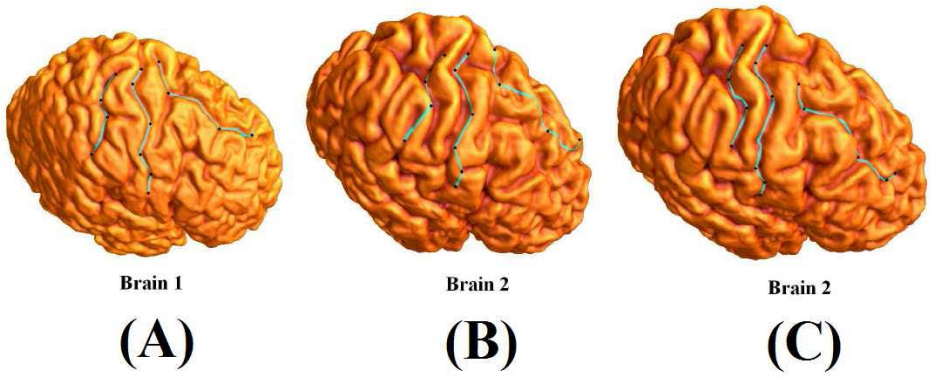

Figure 3.5: Illustration of the result of matching the cortical surfaces with several sulcal landmarks. (A) shows brain surface 1. It is mapped to brain surface 2 under the conformal parameterization as shown in (B). (C) shows the result of matching under our proposed parameterization.

Figure 3.3 shows a schematic diagram of our quasiconformal map construction. Figure 3.4 shows how the constraint vector field can be used to obtain the desired registration with exact landmark matching based on the shape information. Figure Figure 3.5 illustrates the matching results for cortical surfaces with several sulcal landmarks labeled. Figure 3.5(A) shows brain surface 1 with several landmarks labeled. It is mapped to brain surface 2 under the conformal parameterization as shown in Figure 3.5(B). The sulcal landmarks on Brain 1 are only mapped approximately to the sulcal regions on Brain 2. Figure 3.5(C) shows the matching result under the parameterization we proposed. The corresponding landmarks are mapped exactly. Also, the correspondence between the landmark curves follows the shape information (corners to corners; see the black dot).

Using harmonic maps for registration is beneficial as they tend to preserve conformality as much as possible. They effectively capture the region of conformal deformation and help to identify regions of non-conformal deformation. By computing the Beltrami coefficient μ of the registration, we can detect abnormalities. In cases where the deformed surface does not undergo any abnormal

(non-conformal) deformations, the harmonic map obtained will be close to conformal and μ will approximately be zero.

3.4.3 Computing the Beltrami Coefficient

Given the conformal parameterizations together with the registration between the conformal parameter domains, we can detect the abnormal region by computing the Beltrami coefficient. The Beltrami coefficient measures the change in conformality. Suppose the conformal parameterizations of S_o and S_d are $\phi_o : S_o \to D_1$, $\phi_d : S_d \to D_2$ respectively. Denote the registration between the parameter domains by $F : D_1 \to D_2$. The composition map $\tilde{F} = \phi_d^{-1} \circ F \circ \phi_o : S_o \to S_d$ will give a landmark matching harmonic registration between the original and deformed surface. By computing the Beltrami coefficient $\mu_{\tilde{F}}$ of $\tilde{F}$, we can detect which point on the surface undergoes abnormal (non-conformal) deformation. The Beltrami coefficient is invariant under conformal maps. In other words, $|\mu_{f\circ g}| = |\mu_g|$ and $|\mu_{g\circ f}| = |\mu_f|$ if g is conformal. Since ϕ_o and ϕ_d are both conformal diffeomorphisms, we have:

$$|\mu_{\tilde{F}}| = |\mu_{\phi_d^{-1}\circ F\circ\phi_o}| = |\mu_F| \tag{3.10}$$

Thus, to compute $\mu_{\tilde{F}}$, it suffices to compute μ_F. Since F is a map defined on the 2D complex plane, we can compute its Beltrami coefficient easily by:

$$\mu_F = \frac{F_{\overline{z}}}{F_z} = \frac{\frac{\partial F}{\partial x} + i\frac{\partial F}{\partial y}}{\frac{\partial F}{\partial x} - i\frac{\partial F}{\partial y}} \tag{3.11}$$

The Beltrami coefficient is a complex-valued function. When the deformation near a point p is conformal, then $\mu_{\tilde{F}}(p) = 0$. At the point where abnormal deformation happens around its immediate neighborhood, $\mu_{\tilde{F}}$ will be non-zero. We can easily detect regions of abnormality by computing the norm of the Beltrami coefficient $|\mu_{\tilde{F}}|$.

To measure the degree of abnormality quantitatively, we introduce a measure called Beltrami Index (BI) which measures the average of the Beltrami coefficient over a certain region. Mathematically, it is defined as:

$$BI(D) = \int_D |\mu(z)|dz / \int_D |dz| \tag{3.12}$$

The Beltrami Index can effectively measure the degree of abnormalities in different regions on the surface (see Figure 3.17).

Also, as described in section 3, the argument of $\mu_{\tilde{F}}$ measures the angle of complex dilation. This can be used to describe any local rotational change of the abnormal shape. By representing $\mu_{\tilde{F}}$ as a vector field $\vec{V} = (\mathbf{Re}(\mu_{\tilde{F}}), \mathbf{Im}(\mu_{\tilde{F}}))$ on the parameter domain, we can easily visualize the rotational change of the abnormal shape (see Figure 3.9).

3.5 Computer Algorithm

The computer algorithm can be summarized as follows:

1 Compute the conformal parameterizations of the original surface S_o and deformed surface S_d: $\phi_o : S_o \to D_1$ and $\phi_d : S_d \to D_2$;

2 Compute the landmark-matching harmonic registration between the conformal domains: $\tilde{F} : D_1 \to D_2$;

3 Compute the Beltrami coefficient $\mu_{\tilde{F}}$ of $\tilde{F}$. Compute $|\mu_{\tilde{F}}|$ to detect regions of abnormality. The rotational change of the abnormal shape can be visualized by the vector field $\vec{V} = (\mathbf{Re}(\mu_{\tilde{F}}), \mathbf{Im}(\mu_{\tilde{F}}))$ on the parameter domain.

3.6 Experimental Results

We tested our proposed algorithm on synthetic surfaces, 3D human face data and MRI-derived models of human brain cortical surfaces, to detect abnormalities.

In Figure 3.6, we tested our proposed algorithm using synthetic data. Figure 3.6(A) shows the original surface. Figure 3.6(B) shows the deformed surface with both conformal and non-conformal deformations. Figure 3.6(C) shows the plot of $|\mu|$. It effectively detect the deformity on the surface. Figure 3.6(D) shows the plot of the isometric indicator $|f^*(ds_E^2) - \mathbf{Identity}|$. It is equal to 0 if f is isometric. Figure 3.6(E) shows the gradient norm of the deformation field. Note that both the isometric indicator and the gradient of the deformation field are not good measures for detecting deformities. Figure 3.7 shows another example on synthetic surfaces. Figure 3.7(A) shows the original surface. Figure 3.7(B) shows the deformed surface with both conformal and non-conformal deformations. Figure 3.7(C) shows the plot of $|\mu|$. Figure 3.7(D) shows the distribution of μ as a complex number. It represents a vector field on the conformal parameter domain- this can be used to visualize the rotational change of the abnormal shape. Again, it is observed that μ can be used effectively as an indicator to segment the abnormal regions on the surface (see the shaped segmented region on the surface in Figure 3.7(B)).

In Figure 3.8, we illustrate our idea on a human face. Figure 3.8(A) shows the original human face without abnormality. Figure 3.8(B) shows the deformed human face with abnormal swollen area. Figure 3.8(C) shows the the plot of $|\mu|$ versus the conformal parameter domain. Figure 3.8(D) shows the distribution of $|\mu|$ by color. Observe that μ can effectively reflect the swollen area on the human face.

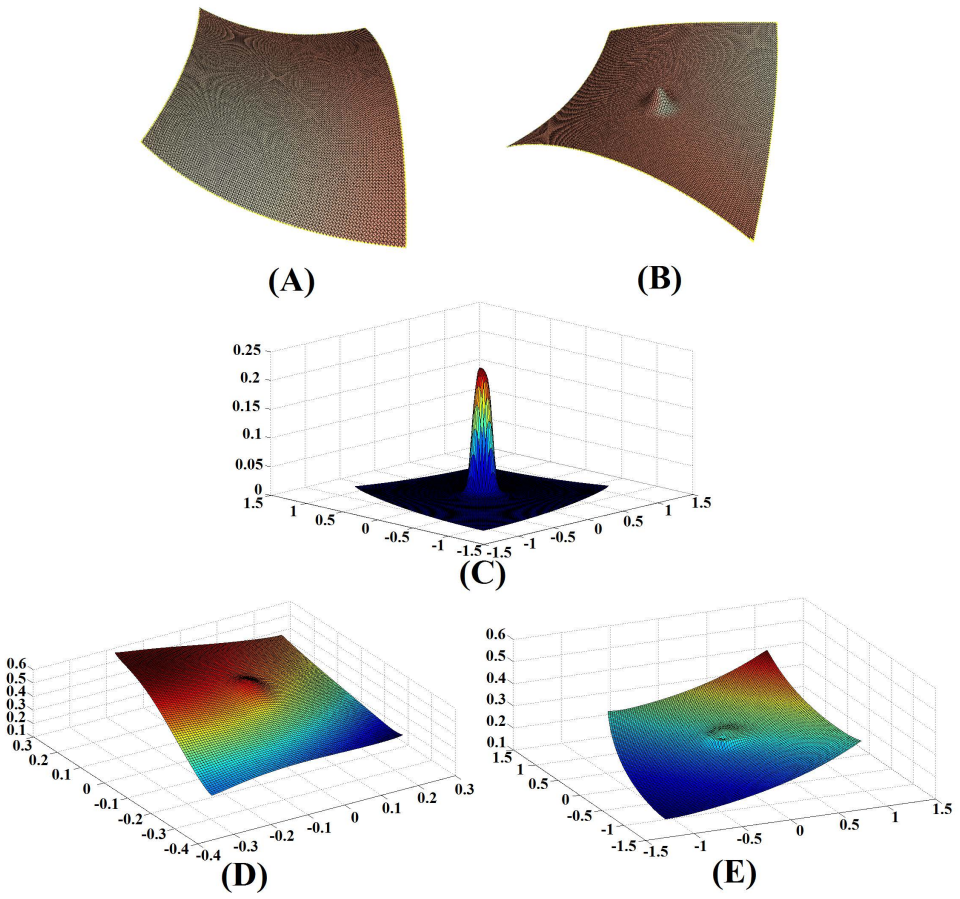

Figure 3.6: (A) shows the original surface. (B) shows the deformed surface with both conformal and non-conformal deformations. (C) shows the plot of $|\mu|$. (D) shows the plot of the isometric indicator $|f^*(ds_E^2) - \mathbf{Identity}|$. It is equal to 0 if f is isometric. (E) shows the gradient norm of the deformation field. Note that both the isometric indicator and the gradient of the deformation field are not good measures for detecting deformities.

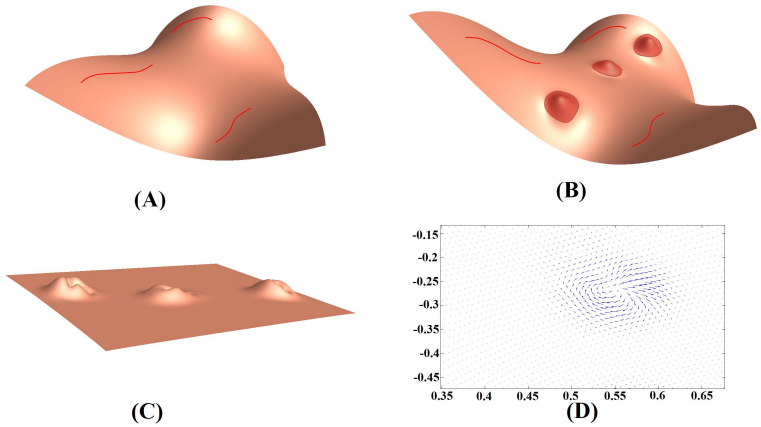

Figure 3.7: (A) shows the original surface. (B) shows the deformed surface with both conformal and non-conformal deformations. (C) shows the plot of $|\mu|$. (D) shows the distribution of μ as a complex number. It represents a vector field on the conformal parameter domain. Observe that μ can be used effectively as an indicator to segment the abnormal regions on the surface.

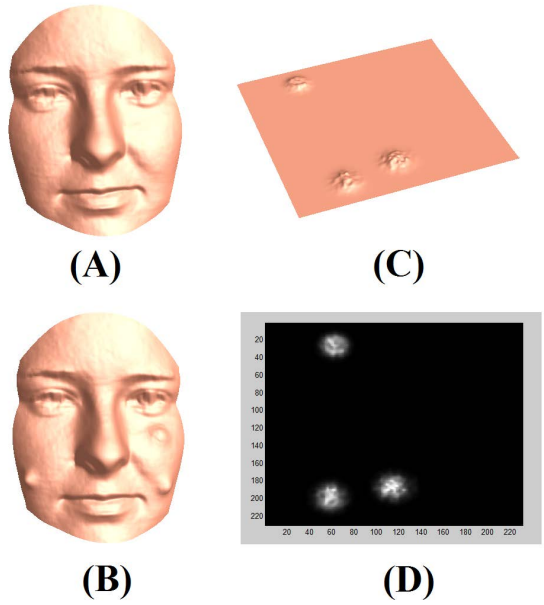

Figure 3.8: (A) shows the original human face and (B) shows a deformed version of the human face with an abnormally swollen area. (C) shows the plot of $|\mu|$ versus the parameter domain. (D) shows the distribution of $|\mu|$ by color.

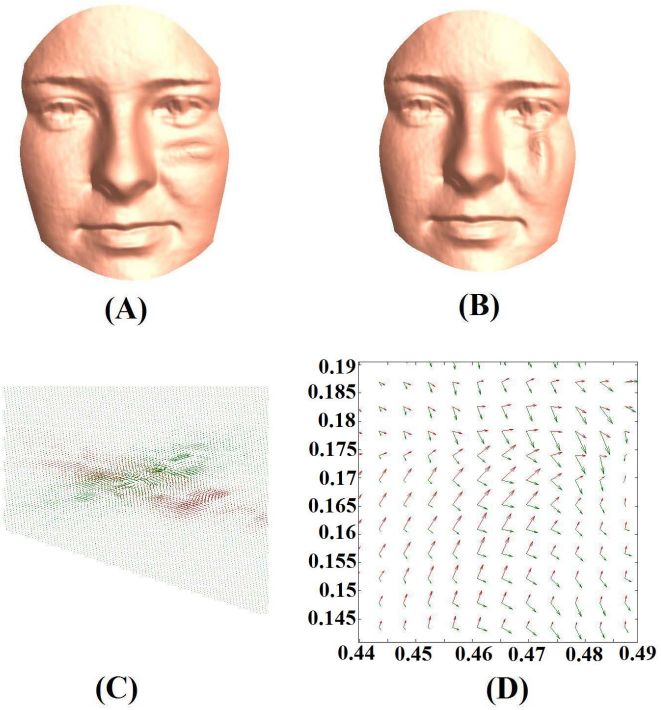

Figure 3.9: (A) shows a human face with an abnormal swollen area. In (B), the swollen area is rotated. (C) plots the Beltrami coefficients μ on the parameter domain. (D) shows a zoomed-in region. The green and red colors represent the Beltrami coefficients for (A) and (B) respectively. Observe that the Beltrami coefficients effectively reflects the rotational change of the swollen area.

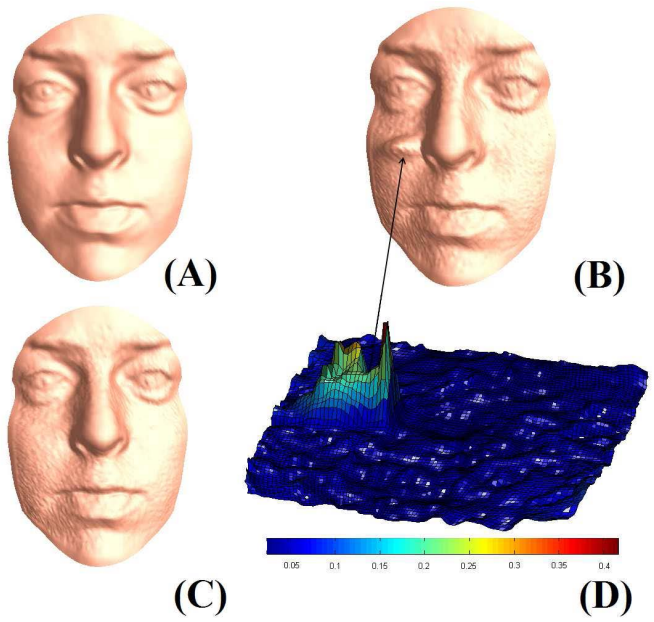

Figure 3.10: (A) shows the original clean human face. (B) shows the deformed human face with noise. (C) shows the original human face with noise. (D) shows the plot of μ computed under noise.

Figure 3.9 shows how the complex-valued Beltrami coefficient μ can be used to detect rotational change of abnormal shape. It is done by visualizing μ as a vector field $\vec{V} = (\mathbf{Re}(\mu_{\tilde{F}}), \mathbf{Im}(\mu_{\tilde{F}}))$ on the parameter domain. Figure 3.9(A) shows a human face with an abnormally swollen area. In Figure 3.9(B), the swollen area is rotated. Figure 3.9(C) plots the complex-valued Beltrami coefficients μ on the parameter domain. Figure 3.9(D) shows the same area zoomed in. The green and red colors represent the Beltrami coefficients for (A) and (B), respectively. Observe that the Beltrami coefficients effectively reflect the rotational change of the swollen area. The abnormal shape is generally rotated by 90 degrees.

In Figure 3.10, we test our proposed algorithm on noisy data. Figure 3.10(A) shows the original clean human face. Figure 3.10(B) shows the deformed human face with noise. Figure 3.10(C) shows the original human face with noise. (D) shows the plot of μ computed under noise. Note that our method is stable under

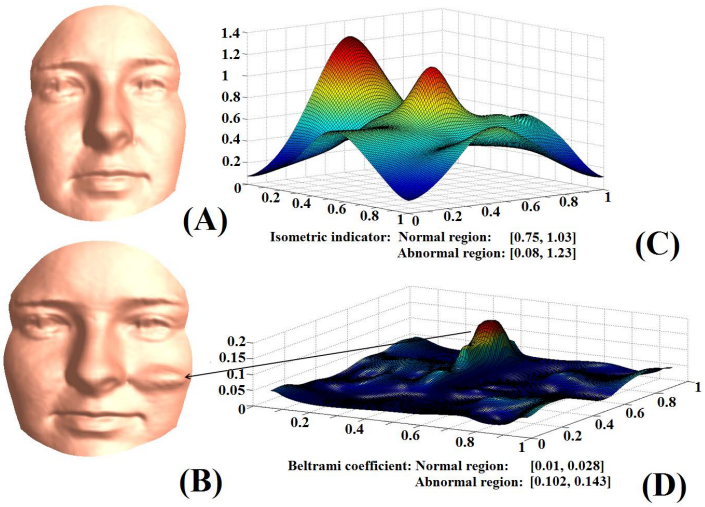

Figure 3.11: (A) shows the original human face. (B) shows the deformed human face. The deformed face is fatter and abnormality is observed. The local geometry is well preserved (except for the abnormal region), although the face has become fatter. (C) shows the plot of the isometric indicator. (D) shows the plot of $|\mu|$.

noise and can effectively detect deformities on noisy surface data.

In Figure 3.11, 3.13 and 3.14, we illustrate our proposed algorithm on a human brain cortical surface. Figure 3.11 shows the original brain surface (Brain 1) and the deformed brain surface (Brain 2) with abnormal gyral thickening. The gyral thickening can be observed inside the circled region. Figure 3.13 shows a zoom-in of the abnormal region. Gyral thickening is clearly observed. Figure 3.13(A) shows the plot of $|\mu|$ versus the parameter domain. Figure 3.13(B) shows the distribution of $|\mu|$ in color. Again, the Beltrami coefficient μ can effectively detect the gyral thickening region.

Figure 3.15 shows another example of detecting abnormalities on brain surfaces. Figure 3.15(A) shows the original brain surface. Figure 3.15(B) shows the deformed brain surface with gyral thickening in the circled regions. Figure 3.15(C) shows the distribution of $|\mu|$. The Beltrami coefficient μ again clearly reflects the region of abnormal changes on the human brain cortical surface.

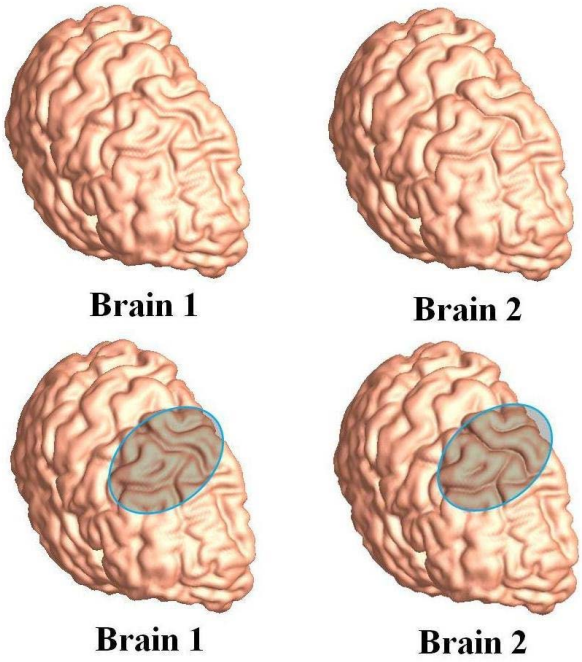

Figure 3.12: The figure shows the original brain surface (Brain 1) and the deformed brain surface (Brain 2) with an abnormal thickening of the gyri, which can be observed inside the circled region.

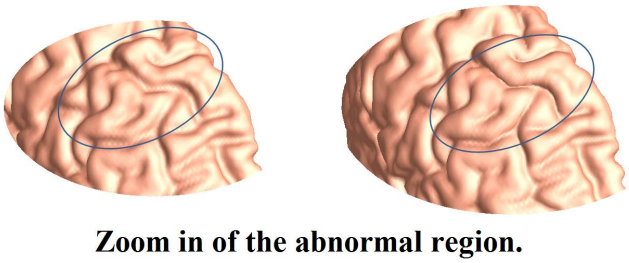

Figure 3.13: The figure shows a zoomed-in version of the abnormal region. Gyral thickening can be clearly observed.

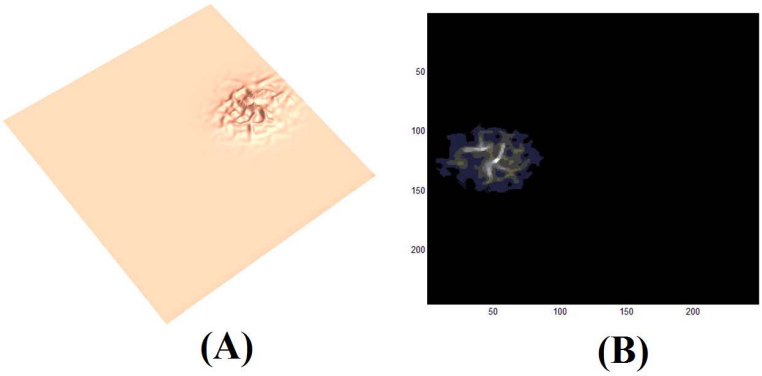

Figure 3.14: (A) shows the plot of $|\mu|$ versus the parameter domain of the brain surfaces. (B) shows the distribution of $|\mu|$ by color.

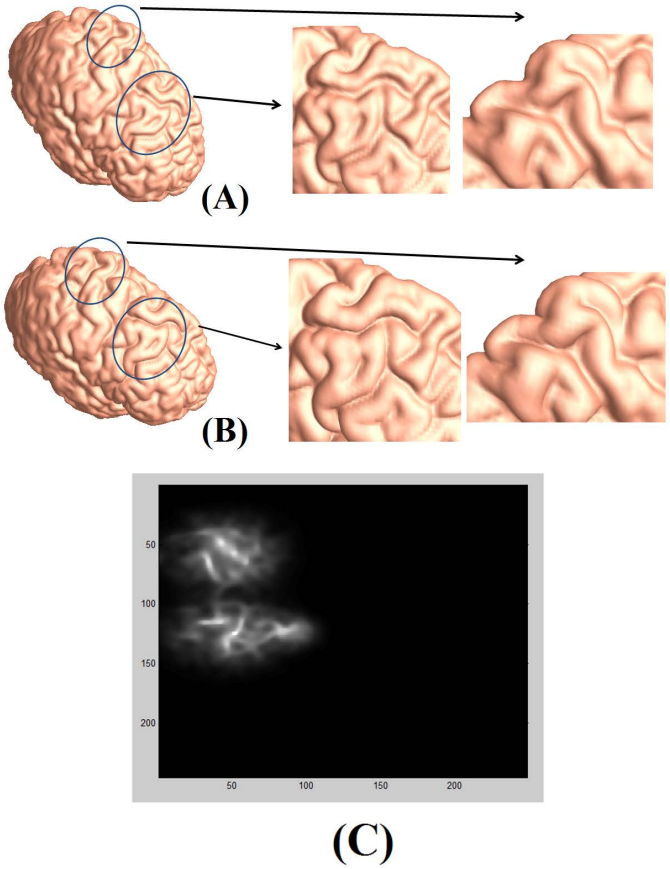

Figure 3.15: The figure shows another example of detecting abnormalities on brain surfaces. (A) shows the original brain surface. (B) shows the deformed brain surface with gyral thickening inside the circled regions. (C) shows the distribution of $|\mu|$.

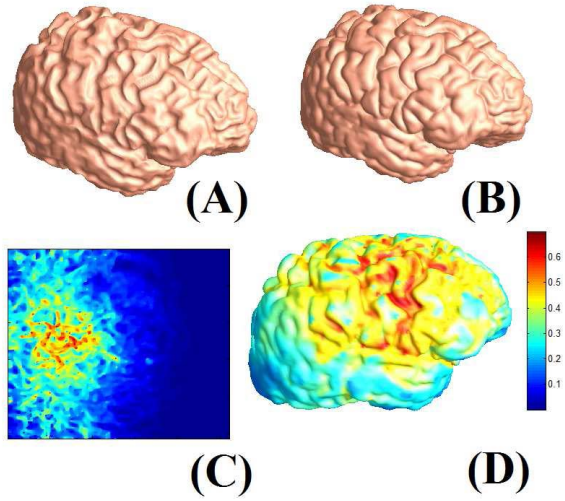

Figure 3.16: (A) shows a real human brain cortical surface. (B) shows the deformed cortical surface. The brain has undergone different degrees of gyrification in different regions. (C) shows the colormap of the brain determined by the Beltrami coefficient. Red color indicates a high value of the Beltrami coefficient, whereas blue colors mean low values of Beltrami coefficient. (D) shows the colormap on the conformal parameter domain.

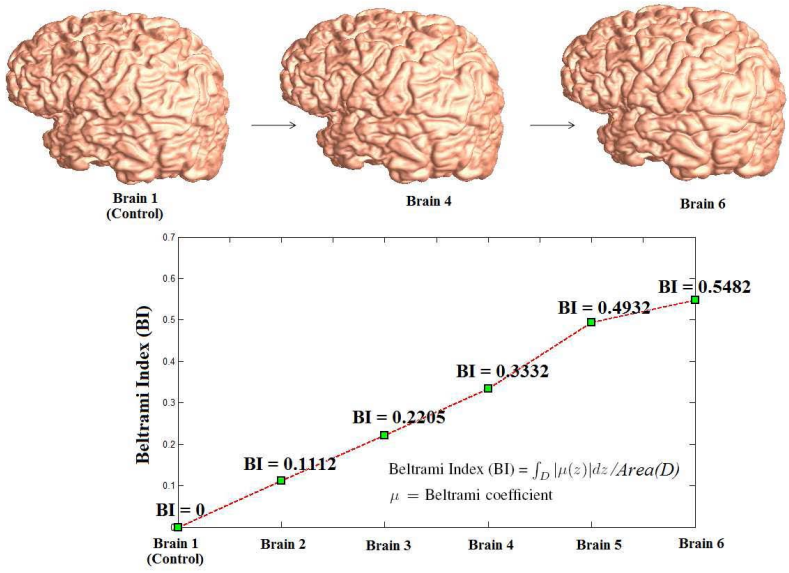

Figure 3.17: The top shows a series of brain surfaces undergoing more and more gyri thickening. The bottom shows how the Beltrami Index (BI) can effectively measure the gyrification.

Figure 3.16 illustrates how we can use Beltrami coefficient to capture the gyrification pattern on the human brain surface. Figure 3.16(A) shows a real human brain cortical surface. Figure 3.16(B) shows the deformed cortical surface. The brain has undergone different degrees of gyrification at different regions. Figure 3.16(C) shows the colormap of the brain determined by the Beltrami coefficient. Red color means high value of Beltrami coefficient whereas blue color means low value of Beltrami coefficient. Figure 3.16(C) shows the colormap on the conformal parameter domain. Observe that the colormap of the Beltrami coefficient effectively captures the gyrification pattern on the brain surface.

Figure 3.17 shows how we can qualitatively measure the degree of abnormalities using the Beltrami Index (BI). The top shows a series of brain surfaces which are undergoing more and more gyral thickening. The bottom shows the plot of the Beltrami Index (BI) of each deformed brain surfaces. Observe that the value of the Beltrami Index becomes bigger as the gyral thickening becomes more severe. It shows that the Beltrami Index (BI) can effectively measure the degree of the abnormal changes.

3.7 Conclusion

In conclusion, we developed an effective algorithm to detect abnormalities on surfaces using quasiconformal geometry. To do this, we computed a landmark-matching harmonic registration between the original and deformed 3D surfaces, together with its associated Beltrami coefficient, μ. Experimental results show that the Beltrami coefficient can effectively detect regions with abnormalities, which are invariant under normal (conformal) deformation. By visualizing μ as a vector field defined on the parameter domain, we can capture the rotational change of the abnormal shape. In future, we will apply our algorithm to study

human brain diseases such as Williams syndrome, which results from genetically-mediated developmental abnormalities in cortical folding. We will also develop more efficient numerical schemes to speed up the computation.

3.8 Appendix

Numerical Implementation of the Quasiconformal Registration Algorithm

We describe how the quasiconformal registration algorithm can be implemented. In practice, all surfaces are represented by meshes which consists of vertices, edges and triangular faces. The functions and their partial derivatives in the iterative scheme are defined on each vertex and linearly interpolated to define the value on each triangular face. They can be computed as follows:

- Laplacian of a function F can be computed as: $\Delta F = \sum_{[u,v]\in N_v} k_{uv}(F(v) - F(u))$, where: N_v is a set of triangles around v that forms a neighborhood of v; $k_{uv} = (\cot\alpha + \cot\beta)/2$, where α and β are the opposite angles of the edge $[u, v]$. For detail, please see [PP93].

- Gradient $\nabla\kappa_i$ can be computed as: $\nabla\kappa_i = \sum_{[u,v,w]\in N_v} \frac{\nabla_{[u,v,w]}\kappa_i}{n}$, where $\nabla_{[u,v,w]}\kappa_i$ is the gradient of κ_i on the triangle $[u, v, w]$. The value of κ_i on $[u, v, w]$ is linearly interpolated. n is the number of faces in N_v.

- $Df_{0,i}$ is defined as $Df_{0,i} = (\nabla f^1_{0,i}, \nabla f^2_{0,i})$ which is a 2×2 matrix, where $f_{0,i} = (f^1_{0,i}, f^2_{0,i})$. Similarly, $DY_i := (\nabla\vec{Y}^1_i, \nabla\vec{Y}^2_i)$, where $\vec{Y}_i = (Y^1_i, Y^2_i)$

- The orthogonal fundamental matrix $\Psi_i(\vec{x}, s)$ is defined as:

  $\Psi_i(\vec{x}, s) := exp(\int_0^s D\vec{Y}_i(\Phi^{\vec{Y}_i}(\vec{x}, t))dt)$. Suppose the interval $[0, 1]$ is discretized as: $s_0 = 0 < s_1 < ... < s_n = 1$. $\Psi_i(\vec{x}, s)$ can be computed as:

$\Psi_i(\vec{x}, s_k) := exp(\sum_{j=1}^{k} D\vec{Y}_i(\Phi^{\vec{Y}_i}(\vec{x}, s_j))(s_j - s_{j-1}))$.

- The function δ_ϵ is defined to be a positive function that is compactly supported in $(-\epsilon, \epsilon)$ and can be computed mathematically as:

  $\delta_\epsilon(x) = \frac{1}{a(\epsilon)\sqrt{\pi}} exp(-\frac{x^2}{a(\epsilon)^2})$

- η_{ep} is a smooth function on Ω such that $\eta_{ep} = 0$ at the endpoints of the open curves $\Gamma_k \subset C$, $k = 1, 2, ..N$. It can be computed mathematically as: $\eta_{ep} = 1 - \sum_{i=1}^{2N} \delta_\epsilon^i(x)$, where $\delta_\epsilon^i(x) = exp(-(x - a_i)/\epsilon^2)$ and $a_1, a_2, ..., a_{2N}$ are the set of end points of the landmark curves.

- The initial map f_{0i} maps the landmark curves C_i to the common curve $C_{standard,i}$. It can be computed as follows: Given a set of landmark curves $C_i(t)$ on the parameter domain and a set of corresponding common curves $C_{standard,i}(t)$. Starting from the initial map $f_0 = \mathbf{Id}$, we can iteratively flow the map to get a diffeomorphism which matches $C_i(t)$ to $C_{standard,i}(t)$ as follow. We can define a vector fields on $f^n(C_i(t))$ as $\vec{V}^n(t) = C_{standard,i}(t) - f^n(C_i(t))$ and smoothly extend to the parameter domain by Gaussian convolution $G * \vec{V}^n(t)$. The iterative scheme can then be written as: $f^{n+1} = f^n + dt\vec{V}_n(f^n)$.

CHAPTER 4

Optimization of Surface Registrations Using Beltrami Holomorphic Flow

4.1 Introduction

Surface registration is a process of finding an optimal 1-1 correspondence between surfaces. It is of great importance in different research areas, such as computer graphics and medical imaging. For example, in medical imaging, surface registration is always needed for statistical shape analysis, morphometry and processing of signals on brain surfaces (e.g., denoising or filtering). In many such applications, a surface must be non-rigidly aligned with another surface, while matching various features that lie within the two surfaces. Finding an optimal surface registration that best matches the required constraints is difficult, especially on complicated surfaces such as human brains. It is therefore necessary to develop an effective algorithm to compute the best surface registration.

In order to obtain the best 1-1 correspondence between two surfaces, an optimization of surface registrations is often required. *Optimization of surface registrations* refers to a process of selecting an optimal surface diffeomorphism within a large class of admissible smooth mappings, that best satisfies certain properties. Mathematically, it can usually be formulated as a variational problem:

$$\min_{f \in \mathbb{F}_{Diff}} E_0(f) \tag{4.1}$$

where $\mathbb{F}_{Diff} = \{f : S_1 \to S_2 : f \text{ is a diffeomorphism}\}$ is the space of all surface diffeomorphisms from S_1 to S_2.

Solving this type of variational problem is generally difficult, since the space of all surface diffeomorphisms $\mathbb{F}_{Diff}$ is a complicated functional space. For example, $\mathbb{F}_{Diff}$ is inherently infinite dimensional and has no natural linear structure. Constructing an efficient optimization scheme that guarantees to obtain a minimizer in the search space of diffeomorphisms becomes a big challenge. For example, a loss of bijectivity of the surface map (overlapping) is often observed during the optimization process. To solve this problem, it is necessary to develop a simple representation of surface diffeomorphisms, which helps to simplify the optimization procedure.

In this chapter, we propose a simple representation of surface diffeomorphisms using Beltrami coefficients (BCs). The BCs are any complex-valued functions defined on the surface with L^∞-norm strictly less than 1. Fixing any 3 points on a pair of surfaces, there is a one-to-one correspondence between the set of surface diffeomorphisms and the set of BCs. Hence, every bijective surface map can be represented by a unique BC. Conversely, given a BC, we can reconstruct the unique surface map associated to it, using the Beltrami Holomorphic flow (BHF) method introduced in this chapter. The BHF formulates the variation of the associated map under the variation of BC. Hence, the variational problem over the space of surface diffeomorphisms can be easily reformulated into a variational problem over the space of BCs:

$$\min_{\mu \in \mathbb{F}_{BC}} E(\mu) \tag{4.2}$$

where $\mathbb{F}_{BC} = \{\mu : S_1 \to \mathbb{D} : |\mu|_\infty < 1\}$ is the set of BCs.

The space of BCs is a much simpler functional space, which captures many essential features of a surface map. There are no restrictions on the BC that it has

to be 1-1, surjective or satisfy some constraints on the Jacobian. By adjusting BCs, we can adjust the surface registration accordingly to obtain the desired properties of the map. This makes the minimization procedure much easier. More importantly, a bijective surface map is guaranteed to be obtained during the optimization process. We applied our proposed algorithm on synthetic examples and real medical applications for surface registration, which demonstrate the effectiveness of our proposed method.

In summary, our work contributes to the following three aspects:

- We propose a simple representation of surface diffeomorphisms, which facilities the optimization of surface registrations;
- We develop a reconstruction algorithm of the surface diffeomorphism from a given BC, using the Beltrami holomorphic flow method. This completes the representation scheme and allows us to move back and forth between BCs and surface diffeomorphisms.
- We formulate the variation of the associated surface map under the variation of BC. It allows us to reformulate the variational problem over the space of surface diffeomorphisms into a variational problem over the space of BCs. It greatly simplifies the optimization procedure.

A flow chart summarizing the framework proposed in this chapter is shown in Figure 4.1

4.2 Previous Work

Surface registration has been studied extensively by different research groups. Most methods compute the optimal surface registration by minimizing certain

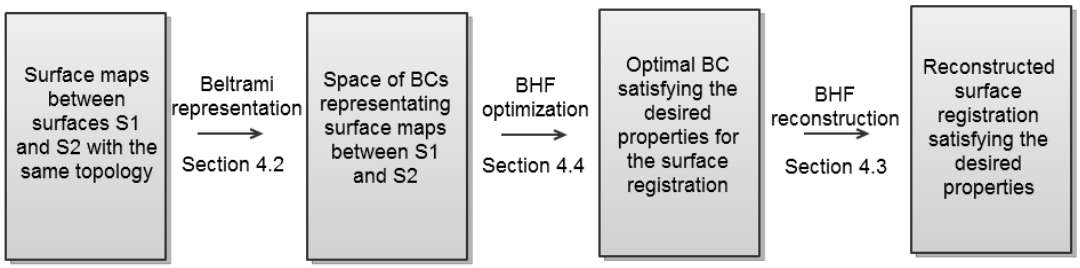

Figure 4.1: A flow chart summarizing the framework proposed in this chapter.

kinds of energy functionals. We will briefly describe some related methods that are commonly used.

Conformal surface registration has been widely studied to obtain a smooth 1-1 correspondence between surfaces, that minimizes the angular distortion [AHT99] [GWC04][HS09][JSR04][LPR02][WLG07]. Conformal maps are usually computed variationally by optimizing some energy functionals, such as the harmonic energy [GWC04] or the least square energy based on the Cauchy-Riemann equation [LPR02]. A 1-1 correspondence between surfaces can be obtained at the optimal state. However, the above registration is not guaranteed to map anatomical features, such as sulcal landmarks, consistently from subject to subject.

To obtain a surface registration that matches important landmark features, landmark-based diffeomorphisms are often used. Optimization of surface diffeomorphisms by landmark matching has been extensively studied. Gu et al. [GWC04] improves the conformal parameterization by composing an optimal Möbius transformation so that it minimizes a landmark mismatch energy. The resulting parameterization remains conformal, although features cannot be perfectly matched. Wang et al. [WLC05][LWC07b] proposed a variational framework to compute an optimized conformal registration which aligns landmarks as good

as possible. Landmarks are not matched exactly and diffeomorphisms cannot be guaranteed when there is a a large amount of landmark features. Glaunès et. al [GVM04] proposed to generate large deformation diffeomorphisms of the sphere onto itself, given the displacements of a finite set of template landmarks. The diffeomorphism obtained can better match landmark features. Lui et al. [LTW10] proposed to compute the shape-based landmark matching registration between brain surfaces, using the integral flow method. The one parameter subgroup within the set of all diffeomorphisms are considered and represented by smooth vector fields. Landmarks can be perfectly matched and the correspondence between landmark curves are based on the shape information. Leow et al. [LYL05] proposed a level set-based approach for matching different types of features, including points and 2D or 3D curves represented as implicit functions. These matching fields in the parameter domain were then pulled back onto the surfaces to compute a correspondence field. Later, Shi et al. [STD07] computed a direct harmonic mapping between two surfaces by embedding both surfaces as the level set of an implicit function, and representing the mapping energy as a Dirichlet functional in the 3D volume domains. Although such an approach can incorporate landmark constraints, it is not proven to yield diffeomorphic mappings.

In case there is no well-defined landmarks on surfaces, some authors have proposed driving features into correspondence based on shape information. Lyttelton et al. [LBR07] computed surface parameterizations that match surface curvature. Fischl et al. [FST99] improved the alignment of cortical folding patterns by minimizing the mean squared difference between the average convexity across a set of subjects and that of the individual. Wang et al. [WCT05] computed surface registrations that maximize the mutual information between mean curvature and conformal factor maps across subjects. Lord et al. [LHV07b]

matched surfaces by minimizing the deviation from isometry. In most situations, extra attention has to be paid to ensure the optimal map computed is diffeomorphic. Hence, developing an effective optimization algorithm that guarantees to give a diffeomorphic surface registration is necessary. This motivates us to look for a simple representation of surface diffeomorphisms which helps to simplify the optimization procedure.

4.3 Theoretical Background

In this section, we describe some basic mathematical concepts related to our algorithms. For details, we refer readers to [GL00] and [SY94].

A surface S with a conformal structure is called a *Riemann surface*. Given two Riemann surfaces M and N, a map $f : M \to N$ is *conformal* if it preserves the surface metric up to a multiplicative factor called the *conformal factor*. An immediate consequence is that every conformal map preserves angles. With the angle-preserving property, a conformal map effectively preserves the local geometry of the surface structure. A generalization of conformal maps is the *quasi-conformal* maps, which are orientation-preserving diffeomorphisms between Riemann surfaces with bounded conformality distortion, in the sense that their first order approximations takes small circles to small ellipses of bounded eccentricity [GL00]. Thus, a conformal homeomorphism that maps a small circle to a small circle can also be regarded as quasi-conformal. Figure 4.2 illustrates the idea of conformal and quasiconformal maps.

Mathematically, $f\colon \mathbb{C} \to \mathbb{C}$ is quasi-conformal provided that it satisfies the Beltrami equation:

$$\frac{\partial f}{\partial \overline{z}} = \mu(z)\frac{\partial f}{\partial z}. \tag{4.3}$$

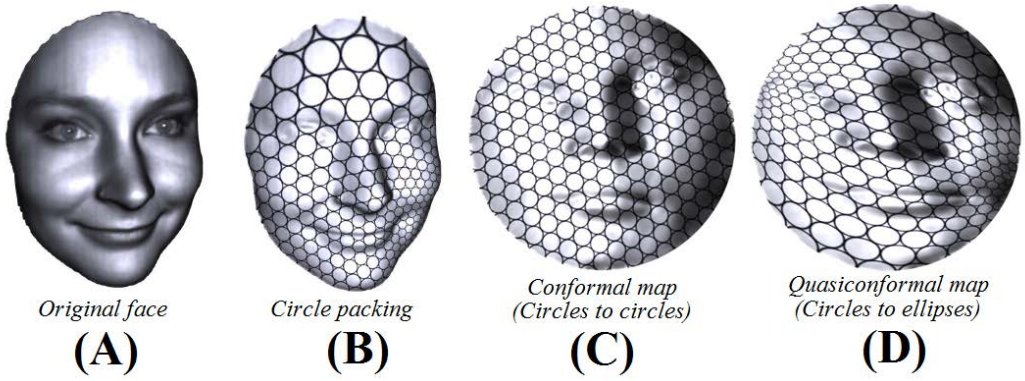

Figure 4.2: Illustration of conformal map and quasiconformal map. (A) shows a human face. A circle packing pattern is plotted in (B). (C) shows the conformal parameterization, which maps circles to circles. (D) shows the quasiconformal parameterization, which maps circles to ellipses.

for some complex valued Lebesgue measurable μ satisfying $||\mu||_\infty < 1$. In terms of the metric tensor, consider the effect of the pullback under f of the usual Euclidean metric ds_E^2; the resulting metric is given by:

$$f^*(ds_E^2) = |\frac{\partial f}{\partial z}|^2 |dz + \mu(z)d\overline{z}|^2. \tag{4.4}$$

which, relative to the background Euclidean metric dz and $d\overline{z}$, has eigenvalues $(1 + |\mu|)^2 \frac{\partial f}{\partial z}$ and $(1 - |\mu|)^2 \frac{\partial f}{\partial z}$. μ is called the *Beltrami coefficient*, which is a measure of non-conformality. In particular, the map f is conformal around a small neighborhood of p when $\mu(p) = 0$. Infinitesimally, around a point p, f may be expressed with respect to its local parameter as follows:

$$\begin{aligned} f(z) &= f(p) + f_z(p)z + f_{\overline{z}}(p)\overline{z} \\ &= f(p) + f_z(p)(z + \mu(p)\overline{z}). \end{aligned} \tag{4.5}$$

Obviously, f is not conformal if and only if $\mu(p) \neq 0$. Inside the local parameter domain, f may be considered as a map composed of a translation to $f(p)$ together with a stretch map $S(z) = z + \mu(p)\overline{z}$, which is postcomposed by a multiplication of $f_z(p)$, which is conformal. All the conformal distortion of $S(z)$ is caused by

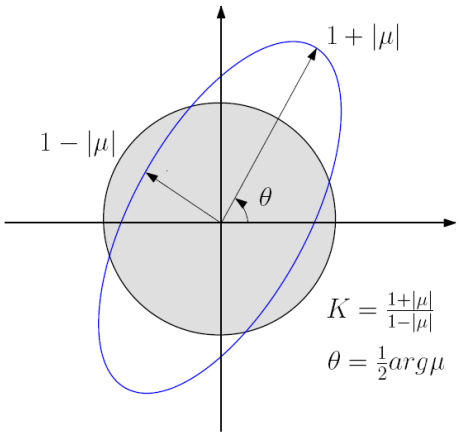

Figure 4.3: Illustration of how the Beltrami coefficient μ measures the distortion of a quasi-conformal mapping that maps a small circle to an ellipse with dilation K.

$\mu(p)$. $S(z)$ is the map that causes f to map a small circle to a small ellipse. From $\mu(p)$, we can determine the angles of the directions of maximal magnification and shrinking and the amount of them as well. Specifically, the angle of maximal magnification is $\arg(\mu(p))/2$ with magnifying factor $1+|\mu(p)|$; The angle of maximal shrinking is the orthogonal angle $(\arg(\mu(p)) - \pi)/2$ with shrinking factor $1-|\mu(p)|$. The distortion or dilation is given by:

$$K = (1+|\mu(p)|)/(1-|\mu(p)|). \tag{4.6}$$

Thus, the Beltrami coefficient μ gives us important information about the properties of the map (See Figure 4.3).

Now, suppose μ and σ are the Beltrami coefficients of the quasiconformal maps f^μ and f^σ respectively. Then the Beltrami coefficient τ of the composition map $f^\tau = f^\sigma \circ (f^\mu)^{-1}$ can be computed as:

$$\tau = \left(\frac{\sigma-\mu}{1-\overline{\mu}\sigma}\frac{1}{\theta}\right) \circ (f^\mu)^{-1}, \tag{4.7}$$

where $\theta = \frac{\overline{p}}{p}$ and $p = \frac{\partial}{\partial z} f^\mu(z)$. In particular, if f^σ is the identity, that is, if $\sigma = 0$,

then

$$\tau = -(\mu\frac{p}{\overline{p}}) \circ (f^{\mu})^{-1}. \tag{4.8}$$

4.4 Main Algorithms

In this section, we discuss in detail the main algorithms in this chapter. Our goal is to look for a simple representation scheme for the space of surface diffeomorphisms, with least constraint as possible, to simplify the optimization process.

4.4.1 Beltrami Holomorphic Flow

In this subsection, we describe two theorems about the Beltrami Holomorphic Flow on the sphere $\mathbb{S}^2$ and the unit disk $\mathbb{D}$. All the algorithms developed in this chapter are based solely on these two theorems.

Theorem 4.4.1 (Beltrami Holomorphic flow on $\mathbb{S}^2$)**.** *There is a one-to-one correspondence between the set of quasiconformal diffeomorphisms of $\mathbb{S}^2$ that fix the points 0, 1, and ∞ and the set of smooth complex-valued functions μ on $\mathbb{S}^2$ for which $\sup|\mu| = k < 1$. Here, we have identified $\mathbb{S}^2$ with the extended complex plane $\overline{\mathbb{C}}$. Furthermore, the solution f^{μ} to the Beltrami equation depends holomorphically on μ. Let $\{\mu(t)\}$ be a family of Beltrami coefficients depending on a real or complex parameter t. Suppose also that $\mu(t)$ can be written in the form*

$$\mu(t)(z) = \mu(z) + t\nu(z) + t\epsilon(t)(z) \tag{4.9}$$

for $z \in \mathbb{C}$, with suitable μ in the unit ball of $C^{\infty}(\mathbb{C})$, $\nu, \epsilon(t) \in L^{\infty}(\mathbb{C})$ such that $\| (\epsilon(t) \|_{\infty} \to 0$ as $t \to 0$. Then

$$f^{\mu(t)}(w) = f^{\mu}(w) + t\dot{f}^{\mu}[\nu](w) + o(|t|) \tag{4.10}$$

locally uniformly on $\mathbb{C}$ *as* $t \to 0$*, for* $w \in \mathbb{C}$*, and where*

$$\dot{f}[\nu](w) = -\frac{f^\mu(w)(f^\mu(w)-1)}{\pi} \int_{\mathbb{C}} \frac{\nu(z)((f^\mu)_z(z))^2}{f^\mu(z)(f^\mu(z)-1)(f^\mu(z)-f^\mu(w))}\, dx\, dy. \tag{4.11}$$

Proof. This theorem is due to Bojarski. For detailed proof, please refer to [2]. □

Theorem 4.4.1 simply states that any diffeomorphism of $\mathbb{S}^2$ that fixes $0, 1$ and ∞ can be represented uniquely by a Beltrami coefficient. In fact, the 3-point correspondence can be arbitrary, instead of fixing $0, 1$ and ∞ only. This can be done easily by composing Mobius transformations to the diffeomorphism. Let $f : \mathbb{S}^2 \to \mathbb{S}^2$ be any diffeomorphism of $\mathbb{S}^2$ and given any 3-point coresspondence $\{a, b, c \in \mathbb{S}^2\} \leftrightarrow \{f(a), f(b), f(c) \in \mathbb{S}^2\}$. We can look for Mobius transformations ϕ_1 and ϕ_2 that map $\{a, b, c\}$ and $\{f(a), f(b), f(c)\}$ to $0, 1, \infty$ respectively. ϕ_1 and ϕ_2 are uniquely determined. The composition map $\widetilde{f} := \phi_2 \circ f \circ \phi_1^{-1}$ is a diffeomorphism of $\mathbb{S}^2$ that fixes $0, 1$ and ∞ and can be represented by a unique Beltrami coefficient. In other word, given a diffeomorphism f of $\mathbb{S}^2$ and any 3-point correspondence, we can represent f uniquely by a Beltrami coefficient.

The theorem also gives the variation of the diffeomorphism under the variation of the Beltrami coefficient. In order to adjust the diffeomorphism, we can simply adjust the Beltrami coefficient by using the variational formula.

Theorem 4.4.1 can be further extended to diffeomorphisms of the unit disk $\mathbb{D}$.

Theorem 4.4.2 (Beltrami Holomorphic flow on $\mathbb{D}$)**.** *There is a one-to-one correspondence between the set of quasiconformal diffeomorphisms of* $\mathbb{D}$ *that fix the points* 0 *and* 1 *and the set of smooth complex-valued functions* μ *on* $\mathbb{D}$ *for which* $\sup|\mu| = k < 1$*. Furthermore, the solution* f^μ *depends holomorphically on* μ*. Let* $\{\mu(t)\}$ *be a family of Beltrami coefficients depending on a real or complex*

parameter t. Suppose also $\mu(t)$ can be written in the form

$$\mu(t)(z) = \mu(z) + t\nu(z) + t\epsilon(t)(z) \tag{4.12}$$

for $z \in \mathbb{D}$, with suitable μ in the unit ball of $C^\infty(\mathbb{D})$, $\nu, \epsilon(t) \in L^\infty(\mathbb{D})$ such that $\| (\epsilon(t) \|_\infty \to 0$ as $t \to 0$. Then:

$$f^{\mu(t)}(w) = f^\mu(w) + t\dot{f}^\mu[\nu](w) + o(|t|) \tag{4.13}$$

locally uniformly on $\mathbb{C}$ as $t \to 0$, for $w \in \mathbb{C}$, and where

$$\begin{aligned} \dot{f}[\nu](w) = &-\frac{f^\mu(w)(f^\mu(w)-1)}{\pi} \\ &\Bigg(\int_{\mathbb{D}} \frac{\nu(z)((f^\mu)_z(z))^2}{f^\mu(z)(f^\mu(z)-1)(f^\mu(z)-f^\mu(w))}\, dx\, dy \\ &\quad + \int_{\mathbb{D}} \frac{\overline{\nu(z)}(\overline{(f^\mu)_z(z)})^2}{\overline{f^\mu(z)}(1-\overline{f^\mu(z)})(1-\overline{f^\mu(z)}f^\mu(w))}\, dx\, dy \Bigg). \end{aligned} \tag{4.14}$$

Proof. The proof of this theorem can be found in the Appendix. □

Theorem 4.4.2 states that any diffeomorphism of $\mathbb{D}$ that fixes 2 points (i.e. 0 and 1) can be represented uniquely by a Beltrami coefficient. Again, the 2-point correspondence can be arbitrary. Let $g : \mathbb{D} \to \mathbb{D}$ be a diffeomorphism of $\mathbb{D}$ and given any 2-point correspondence $\{a, b \in \mathbb{D}\} \leftrightarrow \{g(a), g(b) \in \mathbb{D}\}$. We can find two unique Mobius tranformations of $\mathbb{D}$, ϕ_1 and ϕ_2, that map $\{a, b\}$ and $\{g(a), g(b)\}$ to $\{0, 1\}$ respectively. The composition map $\widetilde{g} := \phi_2 \circ g \circ \phi_1^{-1}$ is a diffeomorphism of $\mathbb{D}$ that fixes 0 and 1 and can be represented by a unique Beltrami coefficient. Theorem 4.4.2 also gives the variation of the diffeomorphism of $\mathbb{D}$ under the variation of the Beltrami coefficient. Therefore, we can again adjust the diffeomorphism of $\mathbb{D}$ by adjusting the Beltrami coefficient, which is a much simpler functional space.

Theorem 4.4.1 and Theorem 4.4.2 can be extended to genus 0 closed surfaces and open surfaces with disk topology. Therefore, they can be applied to

representing general surface diffeomorphisms, which will be discussed in Section 4.4.2.

4.4.2 Representation of Surface Homeomorphisms Using BCs

As mentioned earlier, it is crucial to look for a simple representation for the space of all surface diffeomorphisms so that the optimization procedure can be simplified. Surface registration is commonly represented by 3D coordinate functions in $\mathbb{R}^3$. This representation requires lots of storage space and is difficult to manipulate. For example, the 3D coordinate functions have to a satisfy certain constraint on the Jacobian J (namely, $J > 0$) in order to preserve the 1-1 correspondence of the surface maps. Enforcing this constraint adds extra difficulty in manipulating and adjusting surface maps. It is therefore important to have a simpler representation with as few constraints as possible.

Theorem 4.4.1 and 4.4.2 allow us to represent surface diffeomorphisms of $\mathbb{S}^2$ and $\mathbb{D}$ by Beltrami coefficients. The theorems can be further extended to genus 0 closed surfaces and open surfaces with disk topology.

Let S_1 and S_2 be two genus 0 closed surfaces, and given 3 points correspondence between them: $\{p_1, p_2, p_3 \in S_1\} \leftrightarrow \{q_1, q_2, q_3 \in S_2\}$. By Riemann mapping theorem, S_1 and S_2 can both be uniquely parameterized by conformal maps $\phi_1 : S_1 \to \mathbb{S}^2$ and $\phi_2 : S_2 \to \mathbb{S}^2$ respectively, such that $\phi_1(p_1) = 0, \phi_1(p_2) = 1, \phi_1(p_3) = \infty$ and $\phi_2(q_1) = 0, \phi_2(q_2) = 1, \phi_2(q_3) = \infty$. Given any surface diffeomorphism $f : S_1 \to S_2$. The composition map $\widetilde{f} := \phi_2 \circ f \circ \phi_1^{-1} : \mathbb{S}^2 \to \mathbb{S}^2$ is a diffeomorphism from $\mathbb{S}^2$ to itself fixing $0, 1$ and ∞. By Theorem 4.4.1, $\widetilde{f}$ can be uniquely represented by a Beltrami coefficient $\widetilde{\mu}$ defined on $\mathbb{S}^2$. Hence, f can be uniquely represented by a Beltrami coefficient $\mu := \widetilde{\mu} \circ \phi_1^{-1}$ defined on S_1. In other words, we have proven the following Corollary:

Corollary 4.4.3. *Let S_1 and S_2 be two genus 0 closed surfaces. Suppose $f : S_1 \to S_2$ is a surface diffeomorphism from S_1 and S_2 . Given 3 points correspondence $\{p_1, p_2, p_3 \in S_1\} \leftrightarrow \{f_(p_1), f_(p_2), f_(p_3) \in S_2\}$. f can be represented by a unique Beltrami coefficient $\mu : S_1 \to \mathbb{C}$.*

Similarly, theorem 4.4.2 can be extended to open surfaces with disk topology. Let M_1 and M_2 be two genus 0 open surfaces. Given two points correspondence between them: $\{p_1, p_2 \in M_1\} \leftrightarrow \{q_1, q_2 \in M_2\}$. We can again uniquely parameterize M_1 and M_2 conformally that map the corresponding points to 0 and 1. Denote them by $\phi_1 : M_1 \to \mathbb{D}$ and $\phi_2 : M_2 \to \mathbb{D}$. The composition map $\widetilde{f} := \phi_2 \circ f \circ \phi_1^{-1} : \mathbb{D} \to \mathbb{D}$ is a diffeomorphism of $\mathbb{D}$ fixing 0 and 1. Again, $\widetilde{f}$ can be uniquely represented by a Beltrami coefficient $\widetilde{\mu}$ defined on $\mathbb{S}^2$. Hence, f can be uniquely represented by a Beltrami coefficient $\mu := \widetilde{\mu} \circ \phi_1^{-1}$ defined on M_1. So, we have the following Corollary.

Corollary 4.4.4. *Let M_1 and M_2 be two genus 0 open surfaces with disk topology. Suppose $f : M_1 \to M_2$ is a surface diffeomorphism from M_1 and M_2 . Given 2 points correspondence $\{p_1, p_2 \in M_1\} \leftrightarrow \{f_(p_1), f_(p_2) \in M_2\}$. f can be represented by a unique Beltrami coefficient $\mu : M_1 \to \mathbb{C}$.*

Corollary 4.4.3 and 4.4.4 allows us to represent diffeomorphisms of genus 0 closed surfaces or open surfaces with disk topology by Beltrami coefficients. Thus, we can use the Beltrami coefficient μ_f associated uniquely to f to represent f. We first compute the Beltrami coefficient $\widetilde{\mu}_{\widetilde{f}}$ of the composition map $\widetilde{f} = \phi_2 \circ f \circ \phi_1^{-1} : D \to D$. Mathematically, $\widetilde{\mu}_{\widetilde{f}}$ is given by the following formula:

$$\widetilde{\mu}_{\widetilde{f}} = \frac{\partial \widetilde{f}}{\partial \overline{z}} / \frac{\partial \widetilde{f}}{\partial z} = \frac{1}{2}(\frac{\partial \widetilde{f}}{\partial x} + \sqrt{-1}\frac{\partial \widetilde{f}}{\partial y}) / \frac{1}{2}(\frac{\partial \widetilde{f}}{\partial x} - \sqrt{-1}\frac{\partial \widetilde{f}}{\partial y}). \tag{4.15}$$

The Beltrami coefficient μ_f can then be computed by $\mu_f := \widetilde{\mu}_{\widetilde{f}} \circ \phi_1^{-1} : S_1 \to \mathbb{C}$. μ_f is a complex-valued functions defined on S_1 with $\sup |\mu_f| < 1$. There are no

restrictions on μ_f that it has to be 1-1, surjective or satisfy some constraints on the Jacobian. With this representation, we can easily manipulate and adjust surface maps.

In practice, surfaces are commonly approximated by discrete meshes comprising of triangular or rectangular faces. The parameterizations map the surface meshes onto the mesh D in $\mathbb{C}$. The partial derivatives (or gradient) can be discretely approximated on each face of D. By taking average, the partial derivatives and hence the Beltrami coefficient can be computed on each vertex. The detailed numerical implementation can be found in the Appendix.

The Beltrami coefficient consists of two real functions only, namely the real and imaginary parts. Compared to the representation using 3D coordinate functions, this representation reduces 1/3 of the original storage space.

The computational algorithm can be summarized as follow:

Algorithm 4.1. *Beltrami Representation of Surface Diffeomorphisms*
Input: Surface diffeomorphism $f : S_1 \to S_2$*; points correspondence* $\{p_i\} \leftrightarrow \{q_i = f(p_i)\}$.
Output: Beltrami representation $\mu_f : S_1 \to \mathbb{C}$ *of* $f : S_1 \to S_2$.

1. *Compute the conformal parameterizations of* S_1 *and* S_2 *that map* $\{p_i\}$ *and* $\{q_i\}$ *to consistent locations on the parameter domain* D*. Denote them by* $\phi_1 : S_1 \to D$ *and* $\phi_2 : S_2 \to D$

2. *Set* $\widetilde{f} = \phi_2 \circ f \circ \phi_1^{-1} : D \to D$ *and compute the Beltrami coefficient* $\widetilde{\mu}_{\widetilde{f}}$ *by Equation 4.15.*

3. *Compute the Beltrami coefficient* $\mu_f : S_1 \to \mathbb{C}$ *by* $\mu_f := \widetilde{\mu}_{\widetilde{f}} \circ \phi_1^{-1}$.

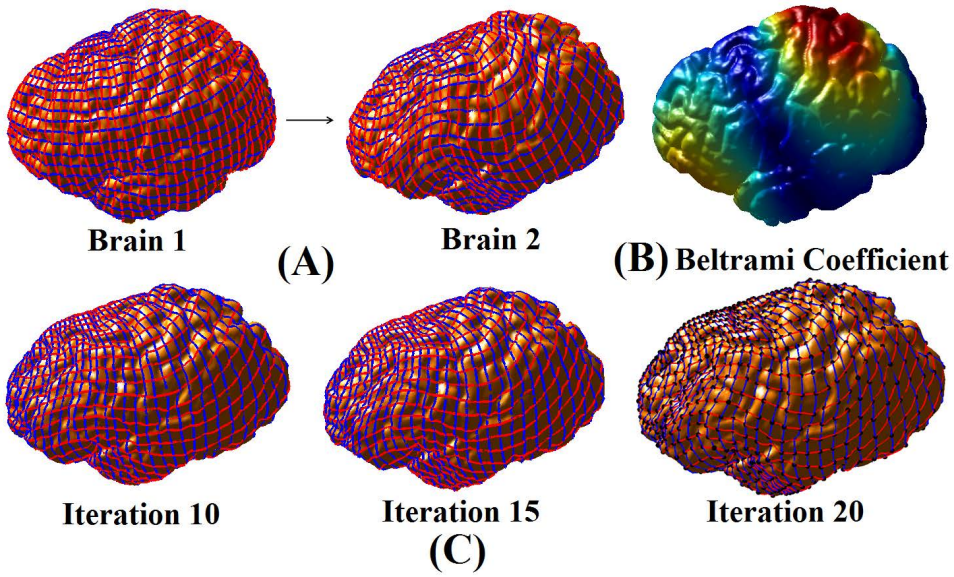

Figure 4.4: Beltrami representation and reconstruction of a surface diffeomorphism f on the brain surface. The top left shows a surface diffeomorphism between two different brain surfaces. The top right shows the Beltrami representation μ of f. The colormap of $|\mu|$ is shown. The bottom row shows the reconstructed map at different iterations N during the BHF reconstruction. When $N = 20$, the map closely resembles to the original map (the black dots shows the exact positions under the original map)

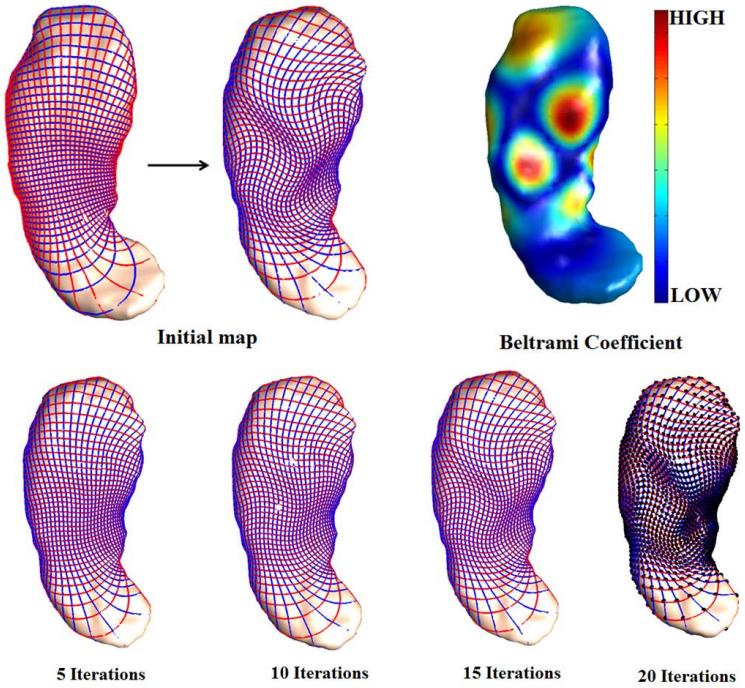

Figure 4.5: Beltrami representation and reconstruction of a surface diffeomorphism f on the hippocampal surface. The top left shows a surface diffeomorphism between two different hippocampal surfaces. The top right shows the Beltrami representation μ of f. The colormap of $|\mu|$ is shown. The bottom row shows the reconstructed map at different iterations N during the BHF reconstruction. When $N = 20$, the map closely resembles to the original map (the black dots shows the exact positions under the original map)

4.4.3 Reconstruction of Surface Diffeomorphisms from BCs

Given the Beltrami coefficient μ defined on S_1. It is important to have a reconstruction scheme to compute the associated quasi-conformal diffeomorphism f^μ. This allows us to move back and forth between BCs and surface diffeomorphisms. We propose the *Beltrami Holomorphic flow* (BHF) method to reconstruct the surface diffeomorphism $f^\mu \colon S_1 \to S_2$ associated with μ. The BHF iteratively flows the identity map to f^μ. In this subsection, we describe the BHF method in detail.

The variation of f^μ under the variation of μ can be expressed explicitly. Sup-

pose $\widetilde{\mu}(z) = \mu(z) + t\nu(z) + \mathcal{O}(t^2)$ $(z = x + iy)$. Then, $f^{\widetilde{\mu}(z)}(w) = f^{\mu}(w) + tV(f^{\mu}, \nu)(w) + \mathcal{O}(t^2)$, where

$$V(f^{\mu}, \nu)(w) = \int_D K(z, w) dxdy. \tag{4.16}$$

where:

$$K(z,w) = \begin{cases} -\frac{f^{\mu}(w)(f^{\mu}(w)-1)}{\pi}\left(\frac{\nu(z)((f^{\mu})_z(z))^2}{f^{\mu}(z)(f^{\mu}(z)-1)(f^{\mu}(z)-f^{\mu}(w))}\right) & \text{if } D = \mathbb{S}^2; \\ -\frac{f^{\mu}(w)(f^{\mu}(w)-1)}{\pi}\left(\frac{\nu(z)((f^{\mu})_z(z))^2}{f^{\mu}(z)(f^{\mu}(z)-1)(f^{\mu}(z)-f^{\mu}(w))}\right. & \\ \qquad\left. + \frac{\overline{\nu(z)}(\overline{(f^{\mu})_z(z)})^2}{\overline{f^{\mu}(z)}(1-\overline{f^{\mu}(z)})(1-\overline{f^{\mu}(z)}f^{\mu}(w))}\right) & \text{if } D = \mathbb{D}. \end{cases} \tag{4.17}$$

We can also write $V(f^{\mu}, \nu)(w)$ as:

$$V(f^{\mu}, \nu)(w) = \int_D \begin{pmatrix} G_1\nu_1 + G_2\nu_2 \\ G_3\nu_1 + G_4\nu_2 \end{pmatrix} dxdy. \tag{4.18}$$

where $\nu = \nu_1 + i\nu_2$ and G_1, G_2, G_3, G_4 are real-valued functions defined on D.

Using this fact, we propose the BHF method to iteratively flow the identity map to f^{μ}. Given the parameterizations $\phi_1 \colon S_1 \to D$ and $\phi_2 \colon S_2 \to D$, we look for the map $\widetilde{f}^{\mu} = \phi_2 \circ f^{\mu} \circ \phi_1^{-1} \colon D \to D$ associated uniquely with $\widetilde{\mu} = \mu \circ \phi_1^{-1} \colon D \to \mathbb{C}$. f^{μ} can then be obtained by $f^{\mu} = \phi_2^{-1} \circ \widetilde{f}^{\mu} \circ \phi_1$.

We start with the identity map **Id** of which the Beltrami coefficient is equal to 0. Let N be the number of iterations. Define $\widetilde{\mu}_k = k\widetilde{\mu}/N$, $k = \{0, 1, 2, ..., N\}$. Let $\widetilde{f}^{\widetilde{\mu}_k}$ be the map associated with $\widetilde{\mu}_k$. Note that $\widetilde{f}^{\widetilde{\mu}_0} = \mathbf{Id}$ and $\widetilde{f}^{\widetilde{\mu}_N} = \widetilde{f}^{\mu}$. Equation 5.5 allows us to iteratively compute $\widetilde{f}^{\widetilde{\mu}_k}$ and thus obtain a sequence of maps flowing from **Id** to $\widetilde{f}^{\mu}$. Mathematically, the iterative scheme is given by:

$$\widetilde{f}^{\widetilde{\mu}_{k+1}} = \widetilde{f}^{\widetilde{\mu}_k} + V(\widetilde{f}^{\widetilde{\mu}_k}, \frac{\widetilde{\mu}}{N}); \quad \widetilde{f}^{\widetilde{\mu}_0} = \mathbf{Id} \tag{4.19}$$

The computational algorithm of the reconstruction scheme can be summarized in Algorithm 4.2. The detailed numerical implementation can be found in Appendix.

Algorithm 4.2. *Reconstruction of surface diffeomorphisms from BCs*

Input: BC μ on S_1; Conformal parameterizations of S_1 and S_2: ϕ_1 and ϕ_2; Iterations N

Output: Surface diffeomorphism $f^\mu : S_1 \to S_2$ associated to μ

1. *Set $k = 0$; $\widetilde{f}^{\widetilde{\mu}_0} = \mathbf{Id}$*
2. *Set $\widetilde{\mu}_k := k\widetilde{\mu}/N$; Compute $\widetilde{f}^{\widetilde{\mu}_{k+1}} = \widetilde{f}^{\widetilde{\mu}_k} + V(\widetilde{f}^{\widetilde{\mu}_k}, \frac{\widetilde{\mu}}{N})$; $k = k + 1$*
3. *Repeat Step 2 until $k = N$; Set $f^\mu := \phi_2^{-1} \circ \widetilde{f}^\mu \circ \phi_1 : S_1 \to S_2$.*

Figure 4.4 and 4.5 illustrate the idea of reconstructing surface diffeomorphisms from BCs on human brain surfaces and hippocampal surfaces respectively. BHF computes a sequence of surface maps $\{\widetilde{f}^{\widetilde{\mu}_k}\}$ converging to $\widetilde{f}^\mu$. The approximation of $\widetilde{f}^{\widetilde{\mu}_k}$ is more accurate with a smaller time step or equivalently a larger number of iterations N. Figure 4.6 shows the error the the reconstructed map f^{Re} versus different number of iterations N used in the BHF process. The error is defined as $Error = \sup ||f^{Re} - f||$, where f is the original map. As expected, the error decreases as N increases. In practice, the approximations are very accurate when $N \geq 15$. In our experiments, we set $N = 20$.

4.4.4 BHF Optimization of Surface Registrations

We have described a simple representation scheme for surface diffeomorphisms using BCs. The space of BCs is a simple functional space with least amount of constraints. The commonly used representation using coordinate functions requires the enforcement of the Jacobian constraints to ensure the bijectivity of the surface maps. The Jacobian constraint is a complicated partial differential inequality, which adds extra difficulty for the optimization problem. In contrary, there are no restrictions on the BC that it has to be 1-1, surjective or satisfy

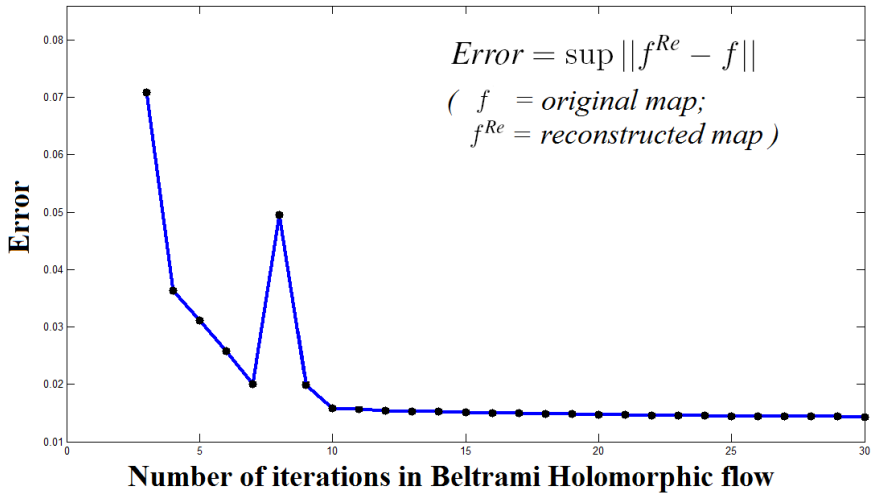

Figure 4.6: The error of the reconstructed map f^{Re} versus the number of iterations used in the BHF process.

some constraints on the Jacobian. With BCs, we can easily manipulate and adjust surface maps.

Theorem 4.4.1 and 4.4.2 give us the variation of the surface map under the variation of its BC (Equation 5.5 and 4.17). This allows us to perform the optimization on the space of BCs, instead of working directly on the space of surface diffeomorphisms.

Given an energy functional E defined on the space of surface diffeomorphisms, we can easily reformulate E to be defined on the space of BCs. With the BHF variation, we can derive the Euler-Lagrange equation to optimize BCs iteratively. To demonstrate the idea, we consider a simple example to optimize surface maps between two human brain surfaces.

Example 4.1 Consider two different human brain surfaces S_1 and S_2 as shown in Figure 4.7. Denote the conformal parameterizations of them by $\phi_1 : S_1 \to D$ and $\phi_2 : S_2 \to D$. In surface registration, it is often important to find an optimal

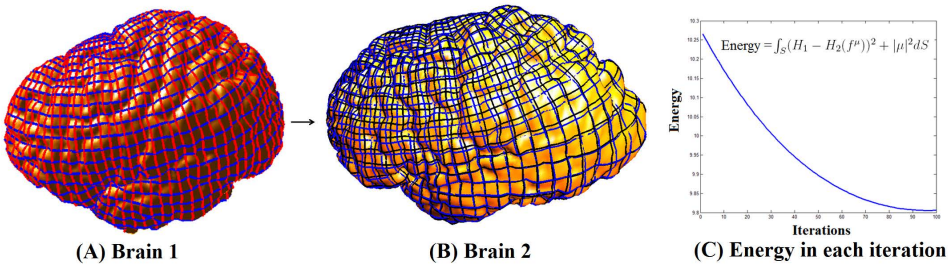

(A) Brain 1 (B) Brain 2 (C) Energy in each iteration

Figure 4.7: Illustration of BHF optimization scheme on brain surfaces. This example shows the optimization result matching functions F_1 and F_2 defined on the two brain surfaces. The blue grid represents the initial map. The black grid represents the optimized map.

1-1 correspondence that matches the intensities defined on each surfaces. Let $F_1 : S_1 \to \mathbb{R}$ and $F_2 : S_2 \to \mathbb{R}$ be two intensities (functions) defined on S_1 and S_2 respectively. Here, we define F_1 and F_2 as $F_1 := \phi_1^{-1}(5.2x^2 + 3.3y^2)$; $F_2 := \phi_2^{-1}(6.8x^2 + 2.8y)$. We propose to find $f : S_1 \to S_2$ minimizing $E(f) = \int_{S_1}(F_1(w) - F_2(f(w)))^2 dw$. We can formulate the energy functional to be defined on the space of BCs over the conformal parameter domain D. That is,

$$E(\mu) = \int_D (F_1(w) - F_2(f^\mu))^2 dw \tag{4.20}$$

The Euler-Lagrange equation can be derived as follow:

$$\begin{aligned}
\frac{d}{dt}|_{t=0} E(\mu + t\nu) &= \int_D \frac{d}{dt}|_{t=0}(F_1(w) - F_2(f^{\mu+t\nu}(w)))^2 dw \\
&= -\int_D 2(F_1 - F_2(f^\mu))\nabla F_2(f^\mu)\frac{d}{dt}|_{t=0} f^{\mu+t\nu} dw \\
&= -\int_D \int_D \begin{pmatrix} A \\ B \end{pmatrix} \cdot \begin{pmatrix} G_1\nu_1 + G_2\nu_2 \\ G_3\nu_1 + G_4\nu_2 \end{pmatrix} dz dw \\
&= -\int_D \left(\int_D \begin{pmatrix} AG_1 + BG_3 \\ AG_2 + BG_4 \end{pmatrix} dw \right) \cdot \begin{pmatrix} \nu_1 \\ \nu_2 \end{pmatrix} dz
\end{aligned} \tag{4.21}$$

where $\begin{pmatrix} A \\ B \end{pmatrix} = 2(F_1 - F_2(f^\mu))\nabla F_2$; $\nu = \nu_1 + i\nu_2$.

So, the descent direction for $\mu = \mu_1 + i\mu_2$ is

$$\frac{d\mu_1}{dt} = \int_D (AG_1 + BG_3)dw; \frac{d\mu_2}{dt} = \int_D (AG_2 + BG_4)dw; \tag{4.22}$$

We can iteratively optimize the energy E as follow:

$$\mu^{n+1} = \mu^n + dt \begin{pmatrix} \int_D (A^n G_1^n + B^n G_3^n)dw \\ \int_D (A^n G_2^n + B^n G_4^n)dw \end{pmatrix} \tag{4.23}$$

Figure 4.7 shows the experimental result of this example. (A) shows the standard grid on Brain 1. The standard grid is mapped by the initial map to Brain 2, which is shown as the blue grid. We optimize the map such that it minimizes the energy and the resulting map is plotted as the black grid. (C) shows the energy at each iteration. It decreases as iteration increases, which means our BHF optimization algorithm can iteratively optimize the energy functional. ∎

Therefore, with the BHF method, we can perform the optimization over the space of BCs and simplify the procedure significantly.

4.5 Applications

In this section, we outline the applications of our proposed optimization algorithm to surface registration. These applications are motivated from practical problems we encountered in medical imaging.

4.5.1 Optimized Conformal Parameterization with Landmark Matching

With the BHF method, we first develope an algorithm to effectively compute *landmark-matching optimized conformal maps* between surfaces. A landmark-matching optimized conformal map refers to a map that matches corresponding

landmarks across surfaces, while preserving the conformality as much as possible. It is important in different areas such as computer graphics and medical imaging. For example, in Human Brain Mapping, neuroscientists are often interested in finding an 1-1 correspondence between brain surfaces that matches sulcal/gyral landmark curves, which are important anatomical features. Besides matching these brain features, they also want the map to preserve the local geometry as much as possible. Conformal maps are best known as local geometry preserving and so they are commonly used. However, landmark matching cannot be guaranteed under the conformal map. Therefore, it is of interest to look for a map which is close to conformal while matching landmarks consistently.

Most existing algorithms to compute the landmark-matching optimized conformal maps cannot ensure exact landmark matching. Some existing algorithms can algin landmarks consistently, but bijectivity is usually not guaranteed especially when a large number of landmark constraints are imposed [LWC07b]. Here, we introduce a variational approach to compute the optimized conformal map iteratively by minimizing the L-2 norm of the Beltrami coefficient μ. Since μ is a measure of local conformality distortion, our proposed model are actually looking for the best map closest to conformal that matches landmarks. Also, a map is bijective as long as $|\mu| < 1$, we can easily control and guarantee the bijectivity of the maps computed in each iteration.

Given two surfaces S_1 and S_2 with the same topology. Denote the corresponding landmark curves on S_1 and S_2 by $\{\widetilde{C}_k^1\}$ and $\{\widetilde{C}_k^2\}$ respectively. We first parameterize S_1 and S_2 conformally to the common parameter domain D ($= \mathbb{D}$ or $\mathbb{S}^2 \cong \overline{\mathbb{C}}$). Let $\phi_1 : S_1 \to D$ and $\phi_2 : S_2 \to D$ be the parameterizations. We proposed to look for two maps $\varphi_1 : D \to D$ and $\varphi_2 : D \to D$ such that φ_i^{-1} ($i = 1, 2$) maps $\{\phi_i(\widetilde{C}_k)\}$ to the consistent location $\{C_k\}$ on D (See Figure 4.8),

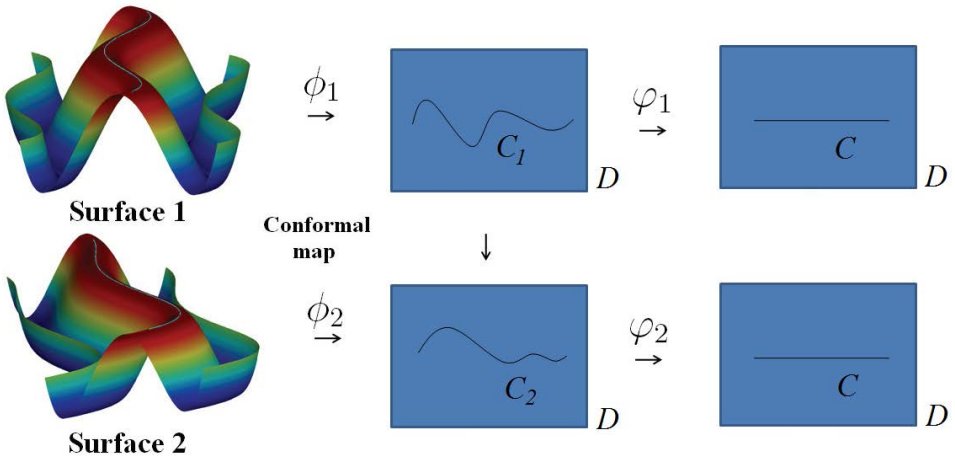

Figure 4.8: This figure shows the framework of the landmark-matching optimized conformal parameterization algorithm.

and that it minimizes the following energy functional:

$$E(\varphi_i) = \int_D |\mu_{\varphi_i}|^2 \tag{4.24}$$

Equation 4.24 ensures the landmark-matching parametrization φ_i to have the least conformality distortion. Hence, the local geometry distortion under φ_i is minimized. A landmark-matching map f between S_1 and S_2 can then be obtained by the composition map: $f := \phi_1^{-1} \circ \varphi_2^{-1} \circ \varphi_1 \circ \phi_i$. We can compute the Euler-Lagrange equation of Equation 4.24 with respect to μ_{φ_i} as follow:

$$\begin{aligned} \frac{d}{dt}|_{t=0} E(\mu_{\varphi_i} + tv) &= \int_D \frac{d}{dt}|t=0|\mu_{\varphi_i} + tv|^2 \\ &= 2\int_D [\mathbf{Re}(\mu_{\varphi_i})\mathbf{Re}(v)) + \mathbf{Im}(\mu_{\varphi_i})\mathbf{Im}(v))] \end{aligned} \tag{4.25}$$

The derivative in Equation 4.25 is negative when $v = -2\mu_{\varphi_i}$. Hence, we can iteratively minimize $E(\mu_{\varphi_i})$ by the following iterative scheme:

$$\mu_{\varphi_i}^{n+1} - \mu_{\varphi_i}^{n} = -2\mu_{\varphi_i}^{n} dt \tag{4.26}$$

. The detailed computational algorithm can be described as follow:

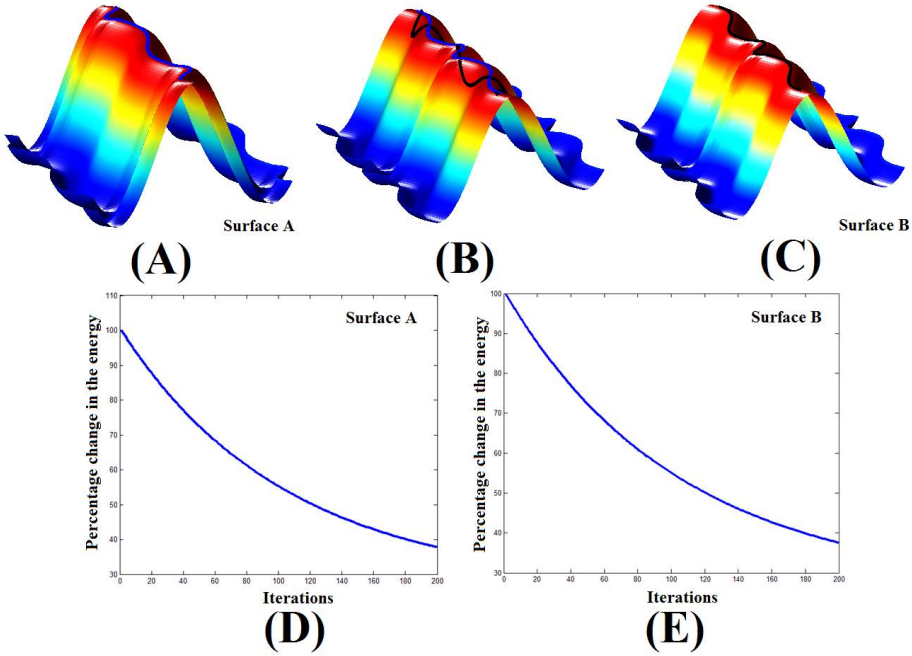

Figure 4.9: Landmark-matching optimized conformal parameterization of surfaces with 1 landmark. The blue curves on (A) and (B) represent the landmarks on the two surfaces. Under the conformal map, the landmark on Surface A cannot be mapped to the landmark on Surface B (black curve in (B)). With optimized conformal parameterization, the corresponding landmarks on each surface can be exactly matched, as shown in (C). (D) and (E) plot the percentage change in energies of the optimized conformal parameterizations for Surface A and B.

Algorithm 4.3. *Optimized conformal parameterization with landmark matching*
Input: Surfaces S_1 and S_2; Landmark curves $\widetilde{C}_k^1$ on S_1; Landmark curves $\widetilde{C}_k^2$ on S_2
Output: Optimized conformal parameterization φ_1 and φ_2 of S_1 and S_2 with landmark matching

1. *Compute the initial map φ_i^0 that align landmark curves $\{\phi_i(\widetilde{C}_k^i)\}$ to $\{C_k\}$ on D. Set $n = 0$*

2. *Compute the Beltrami coefficient $\mu_{\varphi_i}^n$ of φ_i^n. Let $\mu_{\varphi_i}^{n+1} = \mu_{\varphi_i}^n - 2\mu_{\varphi_i}^n dt$.*

3. *Compute $\vec{V}_n = V(\varphi_i^n, -2\mu_{\varphi_i}^n)F(\mu_{\varphi_i}^{n+1} - \mu_{\varphi_i}^n)$ using the BHF formula..*

4. *Let $\varphi_i^{n+1}(p) = \varphi_i^n(p) + \delta(p)\vec{V}_n(p)$, where δ is a smooth delta function on D that is equal to zero around $\{C_k^i\}$ and one elsewhere. This ensures the landmark-matching in each iteration. Set n = n+1.*

5. *Repeat Step 2 to Step 5. If $|E(\mu_{\varphi_i}^{n+1}) - E(\mu_{\varphi_i}^n)| < \epsilon$,* **Stop**.

We test our proposed method on synthetic data as well as real medical data. Figure 4.9 shows the result of matching two synthetic surfaces with one landmark on each surface. The blue curves on (A) and (B) represent the landmarks on the two surfaces. Under the conformal map, the landmark on Surface A cannot be mapped exactly to the landmark on Surface B (See black curve in (B)). Using our proposed method, the corresponding landmarks on each surface can be exactly matched, as shown in (C). (D) and (E) plot the percentage change in energies of the optimized conformal parameterizations for Surface A and B. The energies decrease as iteration increases. which indicates the decrease in the conformalilty distortion. Figure 4.10 shows the Beltrami coefficient of each optimized conformal parameterizations. The colormap shows the norm of the Beltrami coefficient.

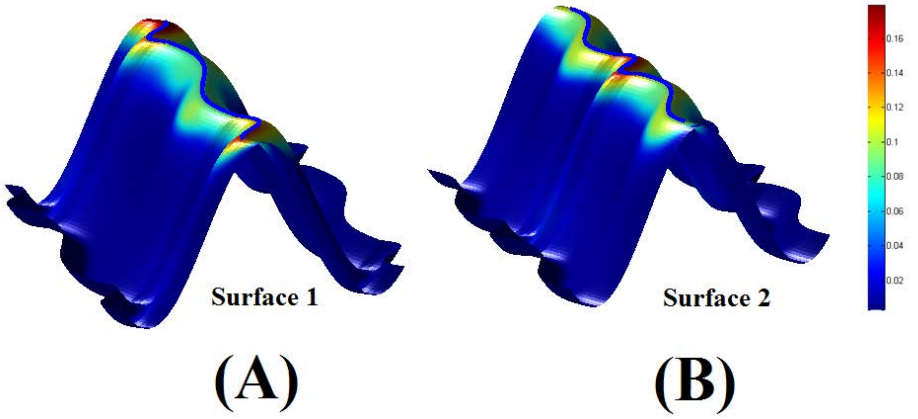

Figure 4.10: The Beltrami coefficient of each optimized conformal parameterizations of surfaces with 1 landmark. The norm of the Beltrami coefficient is very small except near the landmark curve, which means the conformality distortion is accumulated around the landmarks.

Note that the norm of the Beltrami coefficient is very small except near the landmark curve. It means the conformality distortion is accumulated around the landmarks as expected.

We also test our algorithm on synthetic surfaces with five landmarks as shown in Figure 4.11. Again, landmarks cannot be exactly matched under the conformal map (See black curves in (B)). They are exactly matched using our proposed algorithm. As shown in (D) and (E), the percentage change in energies decreases as iteration increases, meaning that conformality distortion is progressively reduced. Figure 4.12 shows the Beltrami coefficients of the optimized conformal parameterizations. Again, the norm of the Beltrami coefficient is very small except near the landmark curves.

Finally, we test our algorithm on real brain cortical hemispheric surfaces extracted from brain MRI scans, acquired from normal subjects at 1.5 T (on a GE Signa scanner). (A) and (B) shows two different brain surfaces with 3 major sulcal curves labeled on each of them (See the blue curves). Under the confor-

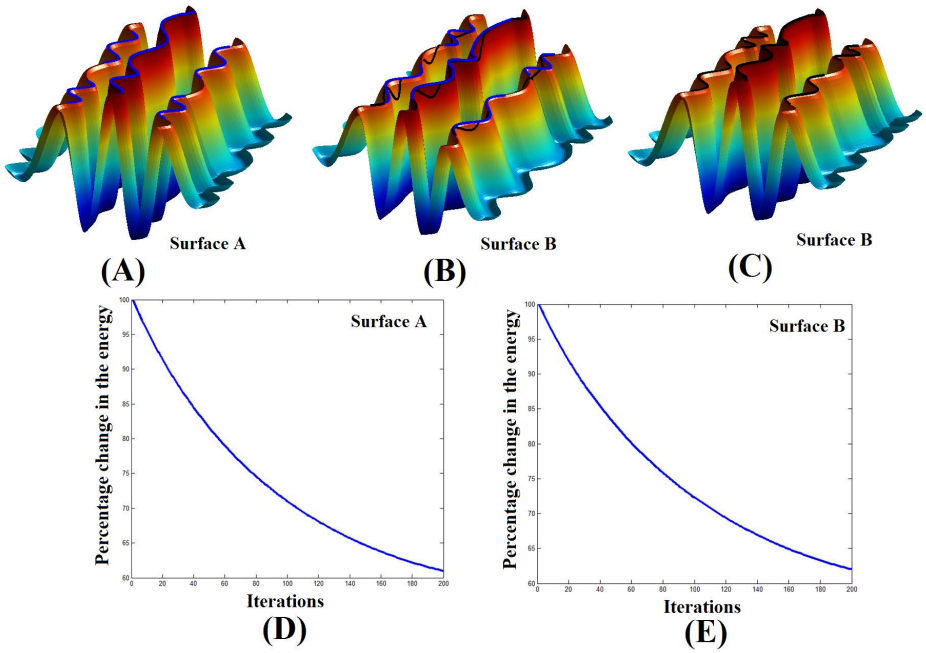

Figure 4.11: Landmark-matching optimized conformal parameterization of surfaces with 5 landmarks. The blue curves on (A) and (B) represent the landmarks on the two surfaces. Under the conformal map, the landmark on Surface A cannot be mapped to the landmark on Surface B (black curves in (B)). With optimized conformal parameterization, the corresponding landmarks on each surface can be exactly matched, as shown in (C). (D) and (E) plot the percentage change in energies of the optimized conformal parameterizations for Surface A and B.

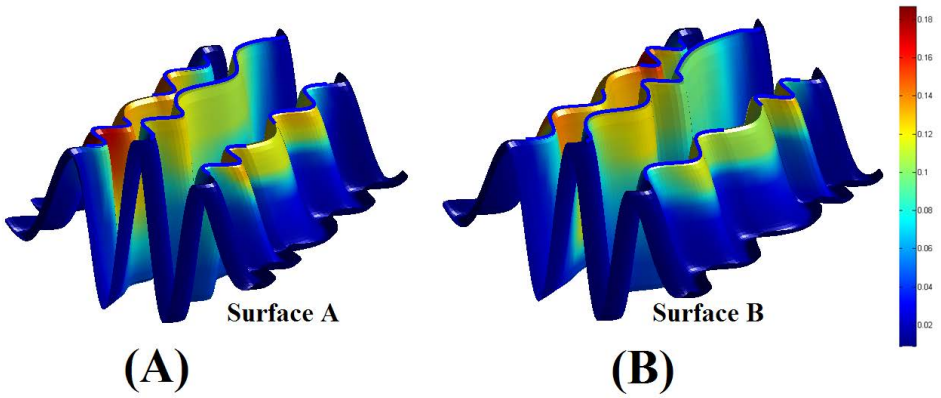

Figure 4.12: The Beltrami coefficient of each optimized conformal parameterizations of surfaces with 5 landmarks. The norm of the Beltrami coefficient is very small except near the landmark curve, which means the conformality distortion is accumulated around the landmarks.

mal map, landmarks on Brain 1 and Brain 2 are not exactly matched (See black curve in (B)). They are, however, exactly matched using our proposed algorithm as shown in (C). (D) and (E) shows the percentage change in the energies of the optimized conformal parameterizations for each surface. The energy is decreasing as iteration increases and hence the conformality distortion is gradually reduced. Figure 4.14 shows the Beltrami coefficient of the optimized conformal parameterizations for each brain surface. Again, the norm of the Beltrami coefficient is very small except near the sulci curves.

4.5.2 Hippocampal Registration with Geometric Matching

In medical imaging, there are cases when anatomical landmark features cannot be easily defined on some brain structures. In such cases, landmark-matching constraint cannot be used as a criteria to establish good correspondences between surfaces. Finding the best 1-1 correspondence between these structures becomes challenging. One typical example is the hippocampus(HP) which is a major component of the brains of humans. It belongs to the limbic system and

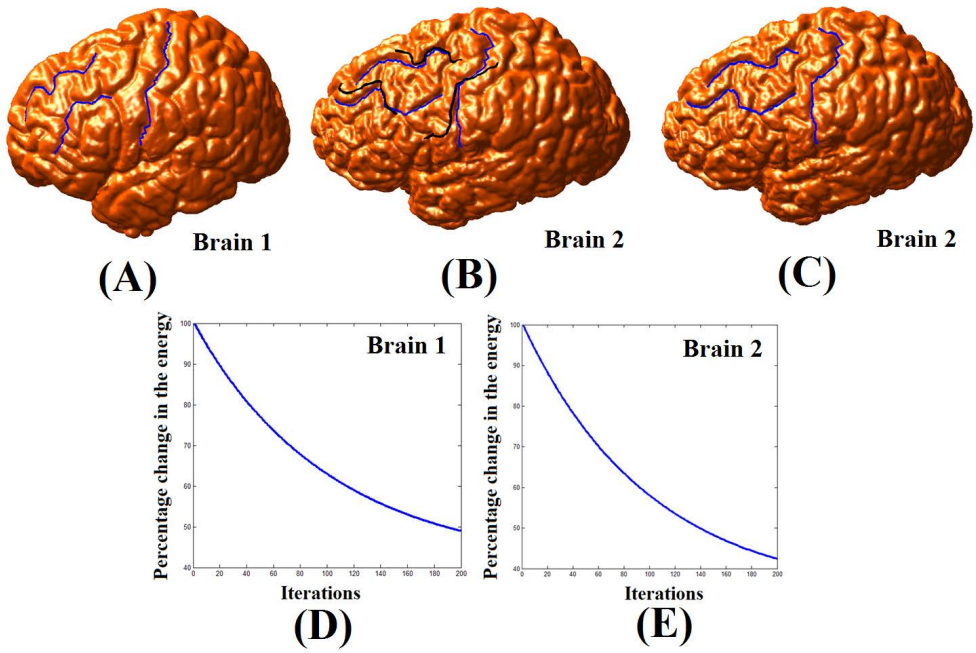

Figure 4.13: Landmark-matching optimized conformal parameterization of brain cortical hemispheric surfaces with 3 major sulcal landmarks. The blue curves on (A) and (B) represent the landmarks on the two surfaces. Under the conformal map, the landmark on Surface A cannot be mapped to the landmark on Surface B (black curves in (B)). With optimized conformal parameterization, the corresponding landmarks on each surface can be exactly matched, as shown in (C). (D) and (E) plot the percentage change in energies of the optimized conformal parameterizations for Surface A and B.

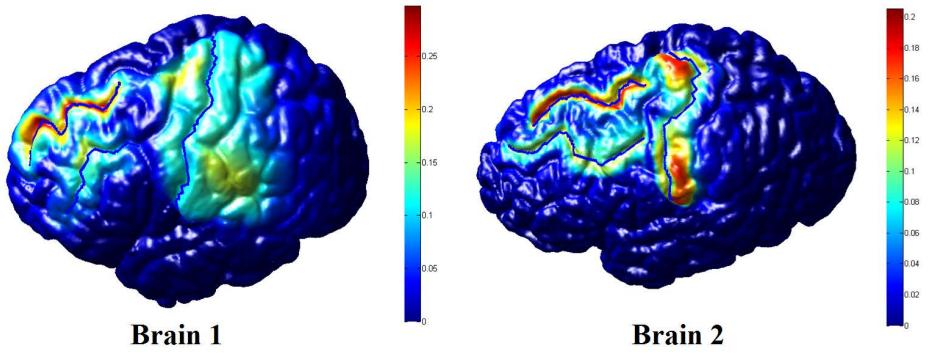

Figure 4.14: The Beltrami coefficient of each optimized conformal parameterizations of brain cortical hemispheric surfaces with 3 major sulcal landmarks. The norm of the Beltrami coefficient is very small except near the landmark curve. As expected, the conformality distortion is accumulated around the landmarks.

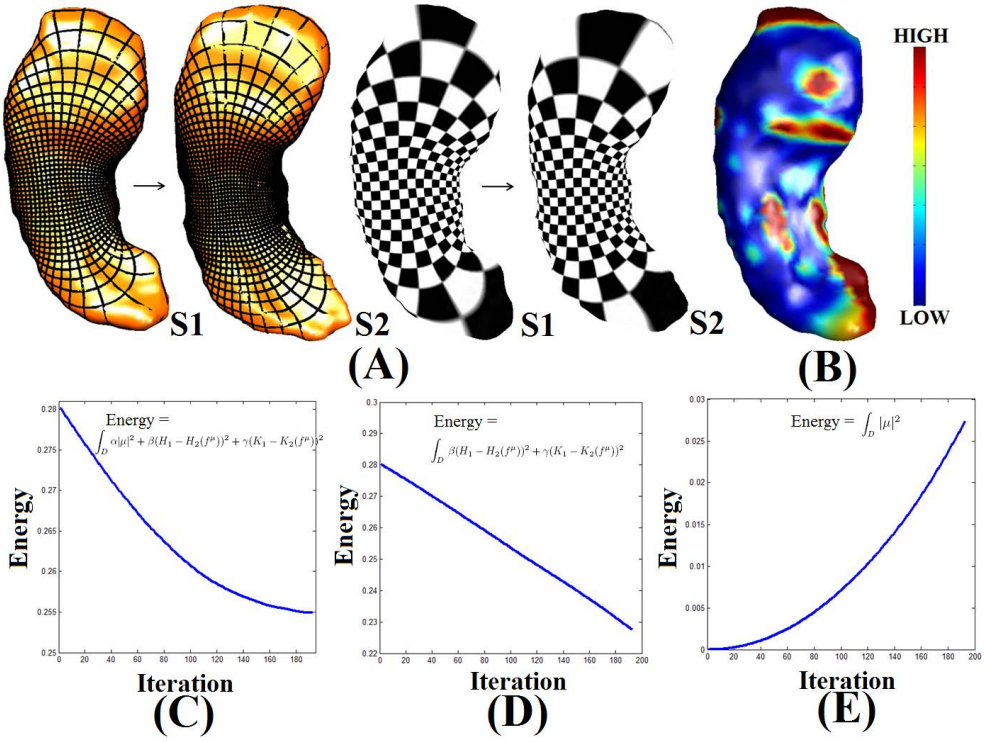

Figure 4.15: Shape registration with geometric matching using Beltrami Holomorphic flow (BHF).

plays important roles in long-term memory and spatial navigation. Surface-based shape analysis is commonly used to study local changes of HP surfaces due to pathologies such as Alzheimer disease (AD), schizophrenia and epilepsy [THZ04]. On HP surfaces, there are no well-defined anatomical landmark features. High-field structural or functional imaging, where discrete cellular fields are evident [ZET03], is still not routinely used. Finding meaningful registrations between HP surfaces becomes challenging. It is thus important to develop methods to look for good registrations between different HP surfaces without landmarks. Here we developed an algorithm to automatically register HP surfaces with complete geometric matching, avoiding the need to manually label landmark features. This is done by optimizing a compounded energy, which minimizes the L-2 norm of the Beltrami coefficient and matches curvatures defined on each surface. Given two hippocampal surfaces S_1 and S_2. The compounded energy E_{shape} is defined mathematically as:

$$E_{shape}(\mu) = \int_D |\mu|^2 + \int_D (H_1 - H_2(f^\mu))^2 + \int_D (K_1 - K_2(f^\mu))^2 \qquad (4.27)$$

where $H_1,\ H_2$ are the mean curvatures on S_1 and S_2 respectively defined on the common parameter domain D; and $K_1,\ K_2$ are the Gaussian curvatures. The first integral minimizes the conformality distortion of the surface registration. The second and the third integrals ensure the optimized registration matches the curvatures as much as possible. It turns out E_{shape} is a complete shape index which measures the dissimilarity between two surfaces. Specifically, $E_{shape} = 0$ if and only if S_1 and S_2 are geometrically equal up to a rigid motion. Therefore, surface map minimizing E_{shape} is the best registration that matches the geometric information as much as possible. We can minimize E_{shape} in Equation 4.27 iteratively, using the proposed BHF optimization algorithm. The Euler-Lagrange

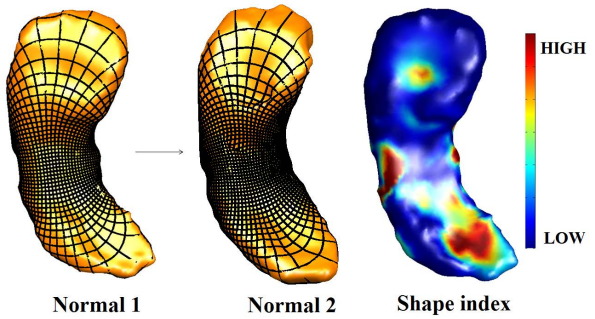

Figure 4.16: BHF registration between two normal subjects. The shape index E_{shape} is plotted on the right, which captures local shape differences.

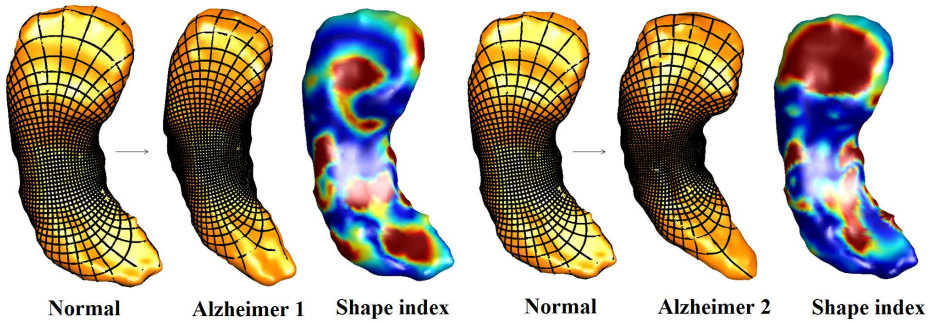

Figure 4.17: BHF registration between normal subjects and subjects with Alzheimer's disease. Their local shape differences are captured by E_{shape}.

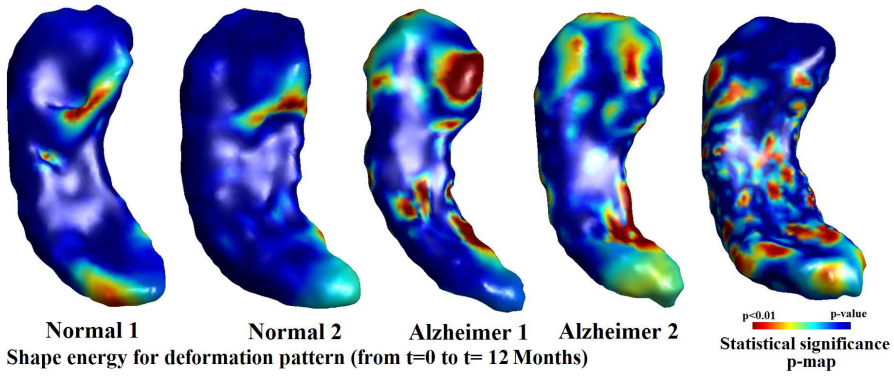

Figure 4.18: Temporal hippocampal shape changes of normal and subjects with Alzheimer's disease.

equation of Equation 4.27 can be computed as follow:

$$\begin{aligned}\frac{d}{dt}|_{t=0}E_{shape}(\mu) &= \int_D \frac{d}{dt}|_{t=0}|\mu+tv|^2 + \int_D \frac{d}{dt}|_{t=0}(H_1 - H_2(f^{\mu+tv}))^2 \\ &\quad + \int_D \frac{d}{dt}|_{t=0}(K_1 - K_2(f^{\mu+tv}))^2 \\ &= 2\int_D \mu\cdot v - 2\int_D (H_1 - H_2(f^\mu))\nabla H_2(f^\mu)\cdot \frac{df^{\mu+tv}}{dt}|_{t=0} \\ &\quad - 2\int_D (K_1 - K_2(f^\mu))\nabla K_2(f^\mu)\cdot \frac{df^{\mu+tv}}{dt}|_{t=0} \\ &= 2\int_w \{\mu(w) - \int_z [(\widetilde{H}+\widetilde{K})\cdot \begin{pmatrix} G_1 \\ G_2 \end{pmatrix}, (\widetilde{H}+\widetilde{K})\cdot \begin{pmatrix} G_3 \\ G_4 \end{pmatrix}]\}\cdot v(w)\end{aligned} \tag{4.28}$$

where $\int_w \bullet := \int_D \bullet\, dw$ and $\int_z \bullet := \int_D \bullet\, dz$ is defined as the integral over the variable w and z respectively; $\widetilde{H} := (H_1 - H_2(f^\mu))\nabla H_2(f^\mu)$; $\widetilde{K} := (K_1 - K_2(f^\mu))\nabla K_2(f^\mu)$; G_i is as defined in Equation 4.18.

The derivative in Equation 4.28 is negative when $v = -2(\mu(w) - \int_z[(\widetilde{H}+\widetilde{K})\cdot G, \mathbf{det}(\widetilde{H}+\widetilde{K}, G)]\ )$. Hence, we can iteratively minimize $E(\mu)$ by the following iterative scheme:

$$\mu^{n+1} - \mu^n = -2(\mu^n - \int_z [(\widetilde{H}^n + \widetilde{K}^n)\cdot G^n, \mathbf{det}(\widetilde{H}^n + \widetilde{K}^n, G^n)]\ )dt \tag{4.29}$$

The detailed computational algorithm can be described as follow:

Algorithm 4.4. *BHF Surface Registration*

Input: Hippocampal surfaces S_1 and S_2, step length dt, threshold ϵ

Output: Geometric matching registration f^μ and the shape index $E(f^\mu)$

1. *Compute the conformal parameterizations of S_1 and S_2. Denote them by $\phi_1 : S_1 \to D$ and $\phi_2 : S_2 \to D$*

2. *Set $\varphi^0 := \mathbf{Id} : D \to D$ and $n = 0$.*

3. *Compute the Beltrami coefficient* μ_φ^n *of* φ^n *(e.g.* $\mu_\varphi^0 = 0$*). Update* μ_φ^{n+1} *by Equation 4.29.*

4. *Compute:* $\vec{V}_n = V(\varphi^n, \mu_\varphi^{n+1} - \mu_\varphi^n)$ *using Equation 5.5. Let* $\varphi^{n+1} = \varphi^n + \vec{V}_n$*. Set n = n+1.*

5. *Repeat Step 3 to Step 5. If* $|E(\mu_\varphi^{n+1}) - E(\mu_\varphi^n)| < \epsilon$*,* **Stop**.

We tested our algorithm on 212 HP surfaces automatically extracted from 3D brain MRI scans with a validated algorithm [MTA08]. Scans were acquired from normal and diseased (AD) elderly subjects at 1.5 T (on a GE Signa scanner). Experimental results show our proposed algorithm is effective in registering HP surfaces with geometric matching. The proposed shape energy can also be used to measure local shape difference between HPs. Figure 4.15(A) shows two different HP surfaces. They are registered using our proposed BHF algorithm with geometric matching. The registration is visualized using a grid map and texture map, which shows a smooth 1-1 correspondence. The optimal shape index E_{shape} is plotted as colormap in (B). E_{shape} effectively captures the local shape difference between the surfaces. (C) shows the shape energy in each iteration. With the BHF algorithm, the shape energy decreases as the number of iterations increases. (D) shows the curvature mismatch energy ($E = \int \beta(H_1 - H_2(f))^2 + \gamma(K_1 - K_2(f))^2$). It decreases as the number of iterations increases, meaning that the geometric matching improves. (E) shows the Beltrami coefficient of the map in each iteration, which shows the conformality distortion of the map. Some conformality is intentionally lost to allow better geometric matching.

Figure 6.3 shows the BHF registration between two normal HPs. The complete shape index E_{shape} is plotted as colormap on the right. Again, E_{shape} can

accurately capture local shape differences between the normal HP surfaces.

Figure 4.17 shows the BHF hippocampal registrations between normal elderly subjects and subjects with Alzheimer's disease. The BHF registrations give smooth 1-1 correspondences between the HP surfaces. We can use the complete shape index E_{shape} to detect local shape differences between healthy and unhealthy subjects.

We also study the temporal shape changes of normal and AD HP surfaces, as shown in Figure 4.18. For each subject, we compute the deformation pattern of its HP surfaces measured at time = 0 and time = 12 Months (see [MTA09] for longitudinal scanning details). The left two panels show the temporal deformation patterns for two normal subjects. The middle two panels show the temporal deformation patterns for two AD subjects. The last column shows the statistical significance p-map measuring the difference in the deformation pattern between the normal (n=47) and AD (n=53) groups, plotted on a control HP. The deep red color highlights regions of significant statistical difference. This method can be potentially used to study factors that influence brain changes in AD.

4.6 Conclusion

In this chapter, we proposed a simple representation of bijective surface maps using Beltrami coefficients(BCs), which helps the optimization process of surface registrations. To complete the representation scheme, we develop a reconstruction algorithm of the surface diffeomorphism from a given BC, using the Beltrami holomorphic flow method. This allows us to move back and forth between BCs and surface diffeomorphisms. By formulating the variation of the associated surface map under the variation of BC, we can reformulate the variational prob-

lem over the space of surface diffeomorphisms into a variational problem over the space of BCs. It greatly simplifies the optimization procedure. More importantly, a bijective surface map is always guaranteed during the optimization process. Experimental results on synthetic examples and real medical applications show the effectiveness of our proposed algorithm for surface registration.

4.7 Appendix

I. Numerical Implementation

We will give the detailed numerical implementation about how the proposed algorithms can be computed. In practice, all surfaces are represented by meshes which consist of vertices, edges, and triangular/rectangular faces. The functions and their partial derivatives in the iterative scheme are defined on each vertex and linearly interpolated to define the value inside each triangular/rectangular face.

1. Computation of the Beltrami coefficient

Let $f = (f_1, f_2)$ be the diffeomorphism defined on the parameter domain D. The Beltrami coefficient μ_f associated uniquely to f can be computed as follow (See Equation 4.15):

$$\mu_f = [(\frac{\partial f_1}{\partial x} - \frac{\partial f_2}{\partial y}) + i(\frac{\partial f_2}{\partial x} + \frac{\partial f_1}{\partial y})]/[(\frac{\partial f_1}{\partial x} + \frac{\partial f_2}{\partial y}) + i(\frac{\partial f_2}{\partial x} - \frac{\partial f_1}{\partial y})] \tag{4.30}$$

In order to compute μ_f, we simply need to approximate the partial derivatives at each vertex: $D_x f_i(v) \approx \frac{\partial f_i}{\partial x}(v)$ and $D_y f_i(v) \approx \frac{\partial f_i}{\partial y}(v)$. We first approximate the gradient $\nabla_T f_i$ on each face T by solving:

$$\begin{pmatrix} \vec{v}_1 - \vec{v}_0 \\ \vec{v}_3 - \vec{v}_2 \end{pmatrix} \nabla_T f_i = \begin{pmatrix} \frac{f_i(\vec{v}_1) - f_i(\vec{v}_0)}{|\vec{v}_1 - \vec{v}_0|} \\ \frac{f_i(\vec{v}_3) - f_i(\vec{v}_2)}{|\vec{v}_3 - \vec{v}_2|} \end{pmatrix} \tag{4.31}$$

where $[\vec{v_0}, \vec{v_1}]$ and $[\vec{v_2}, \vec{v_3}]$ are two edges on T. After the gradient $\nabla_T f_i$ have been computed for each face T, $D_x f_i(v)$ and $D_y f_i(v)$ can be computed as follow:

$$\begin{pmatrix} D_x f_i(v) \\ D_y f_i(v) \end{pmatrix} = \sum_{T \in N_v} \nabla_T f_i / |N_v| \tag{4.32}$$

where N_v is the set of all faces around the vertex v. Hence, the Beltrami coefficient $\mu_f(v)$ can be computed by:

$$\mu_f(v) = \frac{(D_x f_1(v) - D_y f_2(v)) + i(D_x f_2(v) + D_y f_1(v))}{(D_x f_1(v) + D_y f_2(v)) + i(D_x f_2(v) - D_y f_1(v))} \tag{4.33}$$

2. Computation of the BHF reconstruction

For the BHF reconstruction algorithm, the most important step is the computation of the variation $V(f^\mu, \nu)$ of f^μ under the variation of μ. We will discuss the computation of $V(f^\mu, \nu)$ for $D = \mathbb{D}$. The computation for $D = \mathbb{S}^2 \equiv \mathbb{C}^*$ is similar. From Equation 5.5 and 4.17,

$$V(f^\mu, \nu)(w) = \int_D K(z, w) dx dy.$$

where:

$$K(z,w) = -\frac{f^\mu(w)(f^\mu(w)-1)}{\pi} \left(\frac{\nu(z)((f^\mu)_z(z))^2}{f^\mu(z)(f^\mu(z)-1)(f^\mu(z)-f^\mu(w))} + \frac{\overline{\nu(z)}(\overline{(f^\mu)_z(z)})^2}{\overline{f^\mu(z)}(1-\overline{f^\mu(z)})(1-\overline{f^\mu(z)}f^\mu(w))} \right)$$

Now, f^μ and ν are both defined on each vertex. Also, $(f^\mu)_z(v)$ can be approximated as:

$$(f^\mu)_z(v) \approx \frac{(D_x f_1(v) - D_y f_2(v)) + i(D_x f_2(v) + D_y f_1(v))}{2} \tag{4.34}$$

For each pair of vertices (v, w), $K(v, w)$ can be easily approximated. In case $K(v, w)$ is singular, we set $K(v, w) = 0$. Now, for each vertex v, we define A_v as

$$A_v = \sum_{T \in N_v} Area(T)/N_T \tag{4.35}$$

where N_T is the number of vertices on T. That is, $N_T = 3$ if T is a triangle and $N_T = 4$ if T is a rectangle. Then, $V(f^\mu, \nu)$ can be approximated by:

$$V(f^\mu, \nu)(w) = \sum_v K(v, w) A_v \tag{4.36}$$

II. Proof of Theorem 4.4.2 :

To prove the theorem, we need the following lemma.

Lemma 4.7.1. *Let $f\colon \mathbb{D} \to \mathbb{D}$ be a diffeomorphism of the unit disk fixing 0 and 1, and satisfies the Beltrami equation $f_{\overline{z}} = \mu f_z$ with μ defined on $\mathbb{D}$. Let $\tilde{f}$ be the extension of f to $\overline{\mathbb{C}}$ defined as*

$$\tilde{f}(z) = \begin{cases} f(z), & \text{if } |z| \leq 1, \\ \frac{1}{\overline{f(1/\overline{z})}}, & \text{if } |z| > 1. \end{cases} \tag{4.37}$$

Then $\tilde{f}$ satisfies the Beltrami equation

$$\tilde{f}_{\overline{z}} = \tilde{\mu} \tilde{f}_z \tag{4.38}$$

on $\overline{\mathbb{C}}$, where the Beltrami coefficient $\tilde{\mu}$ is defined as

$$\tilde{\mu}(z) = \begin{cases} \mu(z), & \text{if } |z| \leq 1, \\ \frac{z^2}{\overline{z}^2} \overline{\mu(1/\overline{z})}, & \text{if } |z| > 1. \end{cases} \tag{4.39}$$

Proof. First of all, we prove $\tilde{f}$ satisfies the Beltrami equation:

$$\tilde{f}_{\overline{z}} = \tilde{\mu} \tilde{f}_z \tag{4.40}$$

Clearly, $\tilde{f}$ satisfies equation (4.38) on $\mathbb{D}$. Outside $\mathbb{D}$, we consider f and $\tilde{f}$ as functions in z and $\overline{z}$. Note that:

$$\frac{\partial}{\partial z} \overline{f(z, \overline{z})} = \overline{\frac{\partial}{\partial z} f(z, \overline{z})} \tag{4.41}$$

We have:

$$\begin{aligned}\frac{\partial \tilde{f}(z,\overline{z})}{\partial z} &= \frac{\partial}{\partial z}\frac{1}{\overline{f(1/\overline{z},1/z)}} = -\overline{f(1/\overline{z},1/z)}^{-2}\frac{\partial}{\partial z}\overline{f(1/\overline{z},1/z)} \\ &= -\overline{f(1/\overline{z},1/z)}^{-2}\overline{\frac{\partial}{\partial \overline{z}}f(1/\overline{z},1/z)} = -\overline{f(1/\overline{z},1/z)}^{-2}\overline{(-1/\overline{z}^2)f_z(1/\overline{z},1/z)} \\ &= z^{-2}\overline{f(1/\overline{z},1/z)}^{-2}\overline{f_z(1/\overline{z},1/z)}.\end{aligned} \tag{4.42}$$

Therefore,

$$\begin{aligned}\frac{\partial \tilde{f}(z,\overline{z})}{\partial \overline{z}} &= \frac{\partial}{\partial \overline{z}}\frac{1}{\overline{f(1/\overline{z},1/z)}} = -\overline{f(1/\overline{z},1/z)}^{-2}\frac{\partial}{\partial \overline{z}}\overline{f(1/\overline{z},1/z)} \\ &= -\overline{f(1/\overline{z},1/z)}^{-2}\overline{\frac{\partial}{\partial z}f(1/\overline{z},1/z)} = -\overline{f(1/\overline{z},1/z)}^{-2}\overline{(-1/z^2)f_{\overline{z}}(1/\overline{z},1/z)} \\ &= \overline{z}^{-2}\overline{f(1/\overline{z},1/z)}^{-2}\overline{f_{\overline{z}}(1/\overline{z},1/z)} = \overline{z}^{-2}\overline{f(1/\overline{z},1/z)}^{-2}\overline{\mu(1/\overline{z})f_z(1/\overline{z},1/z)}\end{aligned} \tag{4.43}$$

Now,

$$\overline{f_z(1/\overline{z},1/z)} = z^2\overline{f(1/\overline{z},1/z)}^2\frac{\partial \tilde{f}(z,\overline{z})}{\partial z}. \tag{4.44}$$

Thus, we have,

$$\begin{aligned}\frac{\partial \tilde{f}(z,\overline{z})}{\partial \overline{z}} &= \overline{z}^{-2}\overline{f(1/\overline{z},1/z)}^{-2}\overline{\mu(1/\overline{z})f_z(1/\overline{z},1/z)} \\ &= \overline{z}^{-2}\overline{f(1/\overline{z},1/z)}^{-2}\overline{\mu(1/\overline{z})}z^2\overline{f(1/\overline{z},1/z)}^2\frac{\partial \tilde{f}(z,\overline{z})}{\partial z} \\ &= \frac{z^2}{\overline{z}^2}\overline{\mu(1/\overline{z})}\frac{\partial \tilde{f}(z,\overline{z})}{\partial z} = \tilde{\mu}(z)\frac{\partial \tilde{f}(z,\overline{z})}{\partial z}.\end{aligned} \tag{4.45}$$

□

Proof of Theorem 4.4.2 According to Quasiconformal Teichmuller Theory, there is an one-to-one correspondence between the set of quasiconformal homeomorphisms of $\overline{\mathbb{C}}$ fixing 3 points and the set of measurable complex-valued functions μ on $\overline{\mathbb{D}}$ for which $\sup|\mu| = k < 1$. If a diffeomorphism f on $\overline{\mathbb{C}}$ satisfies

equation (4.38), then $1/\overline{f(1/\overline{z})}$ also satisfies the same equation. By the uniqueness of the solution according to Theorem 4.4.1, we must have $f(z) = 1/\overline{f(1/\overline{z})}$. On $\partial\mathbb{D}$, $z = 1/\overline{z}$. This implies $f(z) = 1/\overline{f(z)}$, and hence $|f(z)| = 1$ on $\partial\mathbb{D}$. Therefore, by restricting the solution of equation (4.38) on $\overline{\mathbb{C}}$ fixing 0, 1 and ∞ to $\mathbb{D}$, we can get a diffeomorphism of $\mathbb{D}$ fixing 0 and 1. Equation (4.11) can then be applied on $\mathbb{D}$ to get diffeomorphisms of $\mathbb{D}$ fixing 0 and 1 that satisfy different Beltrami coefficients. To get the corresponding flow on $\mathbb{D}$, we evaluate the integral in equation (4.11). For simplicity, we consider $\widetilde{f} = f$, then

$$\begin{aligned} &\int_{\mathbb{C}} \frac{\nu(z)((f^\mu)_z(z))^2}{f^\mu(z)(f^\mu(z)-1)(f^\mu(z)-f^\mu(w))}\,dx\,dy \\ =&\int_{\mathbb{D}} \frac{\nu(z)((f^\mu)_z(z))^2}{f^\mu(z)(f^\mu(z)-1)(f^\mu(z)-f^\mu(w))}\,dx\,dy \\ &+\int_{\mathbb{C}\setminus\mathbb{D}} \frac{\nu(z)((f^\mu)_z(z))^2}{f^\mu(z)(f^\mu(z)-1)(f^\mu(z)-f^\mu(w))}\,dx\,dy. \end{aligned} \tag{4.46}$$

Now, outside the disk $\mathbb{D}$,

$$\nu(z) = \frac{z^2}{\overline{z}^2}\overline{\nu(1/\overline{z})} \qquad \text{and} \qquad \frac{\partial\tilde{f}(z)}{\partial z} = z^{-2}\overline{f(1/\overline{z},1/z)}^{-2}\overline{f_z(1/\overline{z},1/z)} \tag{4.47}$$

We have:

$$
\begin{aligned}
&\int_{\mathbb{C}} \frac{\nu(z)((f^\mu)_z(z))^2}{f^\mu(z)(f^\mu(z)-1)(f^\mu(z)-f^\mu(w))}\,dx\,dy \\
&= \int_{\mathbb{D}} \frac{\nu(z)((f^\mu)_z(z))^2}{f^\mu(z)(f^\mu(z)-1)(f^\mu(z)-f^\mu(w))}\,dx\,dy \\
&\quad + \int_{\mathbb{C}\setminus\mathbb{D}} \frac{\nu(z)((f^\mu)_z(z))^2}{f^\mu(z)(f^\mu(z)-1)(f^\mu(z)-f^\mu(w))}\,dx\,dy \\
&= \int_{\mathbb{D}} \frac{\nu(z)((f^\mu)_z(z))^2}{f^\mu(z)(f^\mu(z)-1)(f^\mu(z)-f^\mu(w))}\,dx\,dy \\
&\quad + \int_{\mathbb{C}\setminus\mathbb{D}} \frac{(z^2/\overline{z}^2)\overline{\nu(1/\overline{z})}((f^\mu)_z(z))^2}{f^\mu(z)(f^\mu(z)-1)(f^\mu(z)-f^\mu(w))}\,dx\,dy \qquad (4.48)\\
&= \int_{\mathbb{D}} \frac{\nu(z)((f^\mu)_z(z))^2}{f^\mu(z)(f^\mu(z)-1)(f^\mu(z)-f^\mu(w))}\,dx\,dy \\
&\quad + \int_{\mathbb{D}} \frac{(z^2/\overline{z}^2)\overline{\nu(z)}((f^\mu)_z(1/\overline{z}))^2}{\overline{f^\mu(1/\overline{z})}^{-1}(\overline{f^\mu(1/\overline{z})}^{-1}-1)(\overline{f^\mu(1/\overline{z})}^{-1}-f^\mu(w))}\frac{1}{|z|^4}\,dx\,dy \\
&= \int_{\mathbb{D}} \frac{\nu(z)((f^\mu)_z(z))^2}{f^\mu(z)(f^\mu(z)-1)(f^\mu(z)-f^\mu(w))}\,dx\,dy \\
&\quad + \int_{\mathbb{D}} \frac{\overline{\nu(z)}(\overline{(f^\mu)_z(z)})^2}{\overline{f^\mu(z)}(1-\overline{f^\mu(z)})(1-\overline{f^\mu(z)}f^\mu(w))}\,dx\,dy
\end{aligned}
$$

Substituting Equation 22 into Equation 4.11, we get an integral flow equation on $\mathbb{D}$ which is given by

$$
\begin{aligned}
\dot{f}[\nu](w) = &-\frac{f^\mu(w)(f^\mu(w)-1)}{\pi} \\
&\Bigg(\int_{\mathbb{D}} \frac{\nu(z)((f^\mu)_z(z))^2}{f^\mu(z)(f^\mu(z)-1)(f^\mu(z)-f^\mu(w))}\,dx\,dy \qquad (4.49)\\
&\quad + \int_{\mathbb{D}} \frac{\overline{\nu(z)}(\overline{(f^\mu)_z(z)})^2}{\overline{f^\mu(z)}(\overline{1-f^\mu(z)})(1-\overline{f^\mu(z)}f^\mu(w))}\,dx\,dy\Bigg).
\end{aligned}
$$

∎

CHAPTER 5

Compression of Surface Registrations using Beltrami Coefficients

5.1 Introduction

In computer vision and medical imaging, it is crucial to look for 1-1 correspondences between surfaces for further analysis. Such process is called surface registration. There are many approaches of surface registration. A widely used method is to find surfaces maps satisfying certain constraints, such as matching landmarks, and minimizing distortions, such as that given by harmonic energy [LTW10, LWC07b]. Surface maps computed from registration processes can be highly convoluted and are usually represented and stored as 3D functions in $\mathbb{R}^3$. As such, a huge storage memory is required, especially when a large set of fine surface are to be analyzed. It causes problems for data transmission and storage. This problem is particularly common in medical imaging, in which a large set of data has to be considered. Usually, a great amount of memory and bandwidth are needed to store and transmit the data of surface maps. In fact, this research was initially motivated by an actual situation in Brain Mapping research. In a project to analyze the hippocampal shape difference in patients with or without Alzheimer's disease, a thousand of hippocampal surfaces have to be registered. In order to study their time-dependent shape changes, each initial surface has to be

mapped onto several other surfaces taken at different future times. Furthermore, several maps have to be constructed between each surface pair to satisfy different matching criteria. With a typical surface mesh size of 50k vertices, the storage requirement could easily exceed 10 gigabytes, making storing and sharing surface map data a great inconvenience. Nevertheless, very little work has been done on the compression of bijective surface maps. This motivates us to look for a simple representation of surface diffeomorphisms that significantly reduces the required storage memory.

In this chapter, we propose a simple representation of surface maps using the *Beltrami coefficients*. The Beltrami coefficient is a complex-valued function defined on surfaces with supreme norm strictly less than 1. It measures the local conformality distortion of surface maps. Every surface map is associated with a Beltrami coefficient. According to the Quasi-conformal Teichmüller theory, fixing any 3 points, there is an 1-1 correspondence between the set of surface diffeomorphisms and the set of Beltrami coefficients on the source domain. In other words, every surface map can be represented by a unique Beltrami coefficient. Conversely, given a Beltrami coefficient, we can reconstruct the unique surface map associated to it. The Beltrami coefficient is a simple representation that captures many important information of the map. In this chapter, we propose the *Beltrami Holomorphic flow* (BHF) method to iteratively reconstruct the surface map associated with a given Beltrami coefficient. Using this representation, 1/3 of the required storage space is saved. Also, the Beltrami coefficient has very little constraints. The only constraint is that its supreme norm is strictly less than 1. It does not have any requirement of injectivity nor subjectivity. This allows us to further compress the Beltrami coefficient using Fourier approximations, which can further reduce the storage requirement by 90%. Fourier compression is not possible for other representations such as 3D coordinate functions, as the diffeo-

morphic property (1-1 and onto) of the resulting maps cannot be guaranteed (see Figure 5.4, 5.10).

There are three contributions in this chapter: 1. We propose the computation of Beltrami coefficients to represent bijective surface maps; 2. We propose the Beltrami Holomorphic flow (BHF) method to reconstruct surface maps from their Beltrami coefficients; 3. We propose the further compression of Beltrami coefficients by Fourier approximations, which further reduce the storage requirement by 90%.

While this chapter focuses on the compression of surface diffeomorphisms, the methodology we introduced has much broader applications than solely mapping compression. Firstly, our method allows us to have a smaller subspace for modeling and let us do statistics on the Fourier coefficients. We can also estimate new registration fields using the reduced basis, which would be more robust to noise. Thirdly, with the proposed algorithm, we can further make a statistically guided registration method, which is helpful to get a better 1-1 correspondence between surfaces. Furthermore, the Beltrami representation tells us a lot of geometric information of the surface maps, such as conformality distortion. This can be used for shape analysis between registered surfaces [LWZ10, ZLG08]. Finally, our results show that surface diffeomorphisms can be smoothly restored using only a small number of Fourier coefficients. Hence our method also has a good potential for applications in texture mapping.

This chapter is laid out as follows. In Section 2, we describe the relevant works closely related to this research. In Section 3, we describe some basic mathematical concepts related to our algorithms. In Section 4, we describe in detail the main algorithms we use to represent and compress surface diffeomorphisms with Beltrami coefficients. We also describe how surface maps can be recon-

structed from Beltrami coefficients. Experimental results are shown in Section 5. In Section 6, we draw a conclusion and describe possible future work.

5.2 Related Work

Surface registration has been studied extensively and different representations of surface maps have been proposed. Conformal parameterizations have been widely used [FST99, GWC04, GY02, HAT00, HS09, WLG07]. For example, Gu et al. [GWC04, GY02, WLG07] proposed to compute the conformal parameterizations of human brain surfaces for registration using harmonic energy minimization and holomorphic 1-forms. Hurdal et al. [HS09] proposed to compute the conformal parameterizations using circle packing and applied it to registration of human brains. To obtain landmark matching surface registrations, Wang et al. [WLC05, LWC07b] proposed to compute the optimized conformal parameterizations of brain surfaces by minimizing a compounded energy. All of the above algorithms represent surface maps with their 3D coordinate functions. Lui et al. [LTW10] proposed the use of vector fields to represent surface maps and reconstruct them through integral flow equations. They obtained shape-based landmark matching harmonic maps by looking for the best vector fields minimizing a shape energy. The use of vector fields to represent surface maps makes optimization easier, but they cannot describe all surface maps. Time dependent vector fields can be used to represent the set of all surface maps. For example, Joshi et al. [JM00] proposed the generation of large deformation diffeomorphisms for landmark point matching, where the registrations are generated as solutions to the transport equation of time dependent vector fields. The time dependent vector fields facilitate the optimization procedure, although it may not be a good representation of surface maps since it requires more memory.

Compression of mappings has also been studied. Chai et al. [CSS04] proposed the depth map compression algorithm by encoding mapppings as a simplified triangular meshes. Lewis [LE95] described a technique for compressing surface potential mapping data using transform techniques. All these methods deal with the compression of real-valued functions defined on 2D domains. For vector-valued functions, Stachera et al. [SR08] developed an algorithm to compress normal maps by decomposing them in the frequency domain. Ioup [IGL00] also proposed to compress vector map data in the frequency domain. Kolesnikov et al. [KA07] proposed an algorithm for distortion-constrained compression of vector maps, based on optimal polygonal approximations and dynamic quantizations of vector data. All these methods do not deal with preverving bijective maps between surfaces. The bijectivity (1-1, onto) of the maps can be easily lost due to lossy compression.

5.3 Theoretical Background

In this section, we describe some basic mathematical concepts related to our algorithms. For details, we refer the readers to [GL00, LV73, SY94]

A surface S with a conformal structure is called a *Riemann surface*. Given two Riemann surfaces M and N, a map $f : M \to N$ is *conformal* if it preserves the surface metric up to a multiplicative factor called the conformal factor. An immediate consequence is that every conformal map preserves angles. With the angle-preserving property, a conformal map effectively preserves the local geometry of the surface structure.

A generalization of conformal maps is the *quasi-conformal* maps, which are orientation-preserving homeomorphisms between Riemann surfaces with bounded

conformality distortion, in the sense that their first order approximations takes small circles to small ellipses of bounded eccentricity [GL00]. Thus, a conformal homeomorphism that maps a small circle to a small circle can also be regarded as quasi-conformal. Mathematically, $f\colon \mathbb{C} \to \mathbb{C}$ is quasi-conformal provided that it satisfies the Beltrami equation:

$$\frac{\partial f}{\partial \overline{z}} = \mu(z)\frac{\partial f}{\partial z}. \tag{5.1}$$

for some complex valued Lebesgue measurable μ satisfying $||\mu||_\infty < 1$. In terms of the metric tensor, consider the effect of the pullback under f of the usual Euclidean metric ds_E^2; the resulting metric is given by:

$$f^*(ds_E^2) = |\frac{\partial f}{\partial z}|^2 |dz + \mu(z)d\overline{z}|^2. \tag{5.2}$$

which, relative to the background Euclidean metric dz and $d\overline{z}$, has eigenvalues $(1 + |\mu|)^2\frac{\partial f}{\partial z}$ and $(1 - |\mu|)^2\frac{\partial f}{\partial z}$. μ is called the *Beltrami coefficient*, which is a measure of non-conformality. In particular, the map f is conformal around a small neighborhood of p when $\mu(p) = 0$. Infinitesimally, around a point p, f may be expressed with respect to its local parameter as follows:

$$\begin{aligned} f(z) &= f(p) + f_z(p)z + f_{\overline{z}}(p)\overline{z} \\ &= f(p) + f_z(p)(z + \mu(p)\overline{z}). \end{aligned} \tag{5.3}$$

Obviously, f is not conformal if and only if $\mu(p) \neq 0$. Inside the local parameter domain, f may be considered as a map composed of a translation to $f(p)$ together with a stretch map $S(z) = z + \mu(p)\overline{z}$, which is postcomposed by a multiplication of $f_z(p)$, which is conformal. All the conformal distortion of $S(z)$ is caused by $\mu(p)$. $S(z)$ is the map that causes f to map a small circle to a small ellipse. From $\mu(p)$, we can determine the angles of the directions of maximal magnification and shrinking and the amount of them as well. Specifically, the angle of maximal

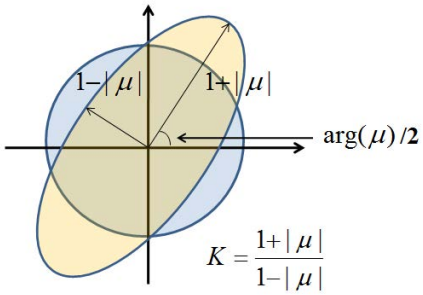

Figure 5.1: Illustration of how the Beltrami coefficient μ measures the distortion of a quasi-conformal mapping that maps a small circle to an ellipse with dilation K.

magnification is $\arg(\mu(p))/2$ with magnifying factor $1+|\mu(p)|$; The angle of maximal shrinking is the orthogonal angle $(\arg(\mu(p)) - \pi)/2$ with shrinking factor $1-|\mu(p)|$. The distortion or dilation is given by:

$$K = 1 + |\mu(p)|/1 - |\mu(p)|. \tag{5.4}$$

Thus, the Beltrami coefficient μ gives us all the information about the properties of the map (See Figure 5.1). According to Teichmüller Quasiconformal theory, there is a 1-1 correspondence between the set of Beltrami differentials and the set of diffeomorphisms $f\colon S_1 \to S_2$ fixing three points. In other word, Beltrami coefficients give us a simple way to represent surface maps.

5.4 Main Algorithms

In this section, we describe in detail the main algorithms we use to represent and compress surface diffeomorphisms with Beltrami coefficients. We also describe how a surface map can be reconstructed from its Beltrami coefficient. A flow chart representing the ideas of our algorithms is illustrated in Figure 5.2.

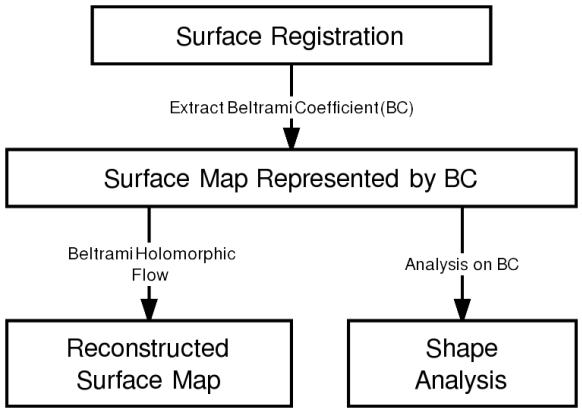

Figure 5.2: A flow chart representing the ideas of our algorithms.

5.4.1 Surface Map Representation Using Beltrami Coefficients

In computer vision and medical imaging, it is crucial to look for an 1-1 correspondence between surfaces for further analysis. Surface registration is commonly represented by 3D coordinate functions in $\mathbb{R}^3$. This representation requires lots of storage space and is difficult to manipulate. For example, the 3D coordinate functions have to a satisfy certain constraint on the Jacobian J (namely, $J > 0$) in order to preserve the 1-1 correspondence of the surface maps. Enforcing this constraint adds extra difficulty in manipulating and adjusting surface maps. It is therefore important to have a simpler representation with as few constraints as possible.

Given two surfaces S_1 and S_2 with the same topology. According to the Teichmüller Quasiconformal theory, there is a 1-1 correspondence between the set of Beltrami differentials and the set of diffeomorphisms $f\colon S_1 \to S_2$ fixing three points [GL00]. In other words, given any surface diffeomorphism $f^\mu\colon S_1 \to S_2$ and 3-point correspondence, we can represent f^μ with a uniquely determined Beltrami differential $\mu\frac{\overline{dz}}{dz}$. Beltrami differential is defined on every coordinate

patch. For genus 0 closed surfaces or simply connected open surfaces, they can be conformally parameterized with a single global patch [GWC04, GY02, WLG07]. Beltrami coefficients can then be used instead of Beltrami differentials. The Beltrami coefficient μ is a complex-valued functions defined on S_1 with $\sup|\mu| < 1$. There are no restrictions on μ that it has to be 1-1, surjective or satisfy some constraints on the Jacobian. With this representation, we can easily manipulate surface maps.

Suppose S_1 and S_2 are both either genus 0 closed surfaces or simply connected open surfaces. Let $f\colon S_1 \to S_2$, and suppose 3 points $\{p_1, p_2, p_3\}$ on S_1 correspond to 3 points on S_2 by $\{p_1, p_2, p_3\} \leftrightarrow \{q_1 = f(p_1), q_2 = f(p_2), q_3 = f(p_3)\}$ (for open surfaces with disk topology, only 2-point correspondence is needed). S_1 and S_2 can be conformally parameterized with a global patch [GWC04, JKL08]. Denote the parameterizations by $\phi_1\colon S_1 \to D$ and $\phi_2\colon S_2 \to D$, where D is either a unit sphere $\mathbb{S}^2$ or a 2D rectangle. We fix $\{p_1, p_2, p_3\}$ and $\{q_1, q_2, q_3\}$ to consistent locations on the parameter domain. For example, in the case that $D = \mathbb{S}^2$, we map $\{p_1, p_2, p_3\}$ and $\{q_1, q_2, q_3\}$ to 0 (north pole), 1 and ∞ (south pole) respectively. Here, we have identified $\mathbb{S}^2$ with the extended complex plane $\mathbb{C}^*$. Now, we can compute the Beltrami coefficient μ_f associated uniquely to f to represent f. The Beltrami coefficient μ_f can be computed by considering the composition map $\widetilde{f} = \phi_2 \circ f \circ \phi_1^{-1}\colon D \to D$. Mathematically, μ_f is given by the following formula:

$$\mu_f = \frac{\partial \widetilde{f}}{\partial \overline{z}} / \frac{\partial \widetilde{f}}{\partial z} = \frac{1}{2}\left(\frac{\partial \widetilde{f}}{\partial x} + \sqrt{-1}\frac{\partial \widetilde{f}}{\partial y}\right) / \frac{1}{2}\left(\frac{\partial \widetilde{f}}{\partial x} - \sqrt{-1}\frac{\partial \widetilde{f}}{\partial y}\right).$$

In practice, surfaces are commonly approximated by discrete meshes comprising of triangular or rectangular faces. The parameterizations map the surface meshes onto the mesh D in $\mathbb{C}$. The partial derivatives (or gradient) can be discretely approximated on each face of D. By taking average, the partial derivatives and hence the Beltrami coefficient can be computed on each vertex.

The Beltrami coefficient consists of two real functions only, namely the real and imaginary parts. Compared to the representation using 3D coordinate functions, this representation reduces 1/3 of the original storage space.

5.4.2 Reconstruction of Surface Maps

Given the Beltrami coefficient μ defined on S_1. We propose the *Beltrami Holomorphic flow* (BHF) method to reconstruct the surface diffeomorphism $f^\mu \colon S_1 \to S_2$ associated with μ. The BHF iteratively flows the identity map to f^μ. In this subsection, we describe the BHF method in detail.

The variation of f^μ under the variation of μ can be expressed explicitly. Suppose $\widetilde{\mu}(z) = \mu(z) + t\nu(z) + \mathcal{O}(t^2)$. Then, $f^{\widetilde{\mu}(z)}(w) = f^\mu(w) + tV(f^\mu, \nu)(w) + \mathcal{O}(t^2)$, where

$$V(f^\mu, \nu)(w) = -\frac{f^\mu(w)(f^\mu(w)-1)}{\pi} \times \int_D \frac{\nu(z)(f^\mu_z(z))^2 dxdy}{f^\mu(z)(f^\mu(z)-1)(f^\mu(z)-f^\mu(w))}. \tag{5.5}$$

Using this fact, we propose the BHF method to iteratively flow the identity map to f^μ. Given the parameterizations $\phi_1 \colon S_1 \to D$ and $\phi_2 \colon S_2 \to D$, we look for the map $\widetilde{f}^\mu = \phi_2 \circ f^\mu \circ \phi_1^{-1} \colon D \to D$ associated uniquely with $\widetilde{\mu} = \mu \circ \phi_1^{-1} \colon D \to \mathbb{C}$. f^μ can then be obtained by $f^\mu = \phi_2^{-1} \circ \widetilde{f}^\mu \circ \phi_1$.

We start with the identity map **Id** of which the Beltrami coefficient is equal to 0. Let N be the number of iterations. Define $\widetilde{\mu}_k = k\widetilde{\mu}/N$, $k = \{0, 1, 2, ..., N\}$. Let $\widetilde{f^{\widetilde{\mu}_k}}$ be the map associated with $\widetilde{\mu}_k$. Note that $\widetilde{f^{\widetilde{\mu}_0}} = \mathbf{Id}$ and $\widetilde{f^{\widetilde{\mu}_N}} = \widetilde{f}^\mu$. Equation 5.5 allows us to iteratively compute $\widetilde{f^{\widetilde{\mu}_k}}$ and thus obtain a sequence of maps flowing from **Id** to $\widetilde{f}^\mu$. Mathematically, the iterative scheme is given by:

$$\widetilde{f^{\widetilde{\mu}_{k+1}}} = \widetilde{f^{\widetilde{\mu}_k}} + \frac{1}{N} V(\widetilde{f^{\widetilde{\mu}_k}}, \widetilde{\mu}); \quad \widetilde{f^{\widetilde{\mu}_0}} = \mathbf{Id} \tag{5.6}$$

BHF computes a sequence of surface maps $\{\widetilde{f}^{\widetilde{\mu}_k}\}$ converging to $\widetilde{f}^{\mu}$. The approximation of $\widetilde{f}^{\widetilde{\mu}_k}$ is more accurate with a smaller time step or equivalently a larger number of iterations N. In practice, the approximations are very accurate when $N \geq 15$ (see Figure 5.9). In our experiments, we set $N = 20$.

5.4.3 Fourier Compression of Beltrami Coefficients

The Beltrami coefficient can be further compressed using Fourier approximations to reduce the storage space. An important consideration is to preserve the diffeomorphic property of the surface map after the compression. Under the representation by coordinate functions, the Jacobian has to be greater than 0 in order to ensure the diffeomorphic property. This constraint is equivalent to an inequality in the partial derivatives of the coordinate functions. Enforcing this constraint is difficult during compression and the diffeomorphic property is easily lost (see Figure 5.4, 5.10). The representation by Beltrami coefficient, however, is advantageous because it does not have any requirement for injectivity and subjectivity, making the Jacobian constraint unnecessary. The only requirement for the Beltrami coefficient μ is that it has to be a complex-valued function defined on the surface with supreme norm less than 1. We can therefore compress μ using Fourier approximations without losing the diffeomorphic property.

The Beltrami coefficient μ can be approximated as follow:

$$\mu(x, y) = \sum_{j,k=-N}^{N} c_{j,k} e^{\sqrt{-1}\pi jx/T} e^{\sqrt{-1}\pi ky/T},$$

where

$$c_{j,k} = \frac{1}{4T^2} \int_{-T}^{T} \int_{-T}^{T} \mu(x, y) e^{-\sqrt{-1}\pi jx/T} e^{-\sqrt{-1}\pi ky/T} dxdy.$$

We can use fast Fourier transform to compute the coefficients $c_{j,k}$ efficiently. In practice, we set $N = 20$ and the approximation is already very accurate (see

Figure 5.9). The Fourier compression significantly reduces the storage required to 10% of the original data size. Experimental results show that the compression of μ is stable and effective.

5.5 Experimental Results

We test our algorithm on synthetic surface data, real human brain surfaces and real hippocampal surfaces. Experimental results show that our algorithm is effective and stable.

Figure 5.3 shows the representation of a diffeomorphism from the unit square to itself using the Beltrami coefficient. (A) shows the original diffeomorphism. (B) shows the norm of the Beltrami coefficient representing the map. (C) shows the reconstructed map from the Beltrami coefficient. The dots represent the exact values of the original map. Note that the reconstructed map closely matches the original map. (D) shows the errors of the reconstructed maps versus the number of iterations under the Beltrami Holomorphic flow (BHF), which are defined as

$$Error = \sup ||f^{Re} - f||, \tag{5.7}$$

where f^{Re} is the reconstructed map. After 20 iterations, the BHF reconstructed map closely approximates the original map.

Figure 5.4(A) shows the Fourier compression result of the Beltrami coefficient μ. We take $N = 15$ in the Fourier series approximation. The reconstructed map closely matches the original map (see dots) as well. (B) shows the Fourier compression result of the coordinate functions. The Jacobian constraint is not satisfied under the compression. The diffeomorphic property is lost. Figure 5.5 shows the Fourier compression result of μ with $N = 5, 10, 15, 20$ respectively. The accuracy improves rapidly with increasingly larger N's.

We also test our algorithm on real cortical hemispheric surfaces extracted from brain MRI scans, acquired from normal and unhealthy subjects at 1.5 T (on a GE Sigma scanner). Figure 5.6(A) shows two different brain surfaces and a surface map between them. The surface map can be represented by the Beltrami coefficient. (B) shows the colormap of the norm of the Beltrami coefficient. (C) shows the reconstructed surface map from the Beltrami coefficient. The black dots represent the exact values of the original surface map. The result shows that the reconstruction of the surface map from the Beltrami coefficient is very accurate. The reconstructed map accurately approximates the original map (see black dots). Figure 5.7 shows the Fourier compression results of μ for the brain surfaces with $N = 5, 10, 15$ and 20 respectively. The error reduces rapidly as N increases.

In Figure 5.8, we test our algorithm on real hippocampal surfaces, which is an important brain structure for the study of Alzheimer's disease. (A) shows two different hippocampal surfaces and a surface diffeomorphism between them. We represent the surface map with the Beltrami coefficient and the colormap of its norm is shown in (B). (C) shows the reconstructed map from the Beltrami coefficient. Again, the black dots represent the exact location under the original map. The error as defined in Equation 5.7 versus the number of iterations during the Beltrami Holomorphic Flow (BHF) is as shown in (D). The Fourier compression results of the Beltrami coefficient for the hippocampal surfaces with $N = 5, 10, 15, 20$ are shown in Figure 5.9. The error of the reconstructed maps decreases rapidly as N increases.

However, the compression of 3D coordinate functions does not give satisfactory results. Figure 5.10(A) and 5.10(B) show the results of Fourier compression of 3D coordinate functions for the brain and hippocampal surfaces respectively.

In both cases, the diffeomorphic property is completely disrupted. In comparison, Beltrami compression gives accurate results with just a small number of coefficients.

To analyze quantitatively how well the diffeomorphic property is preserved under our algorithm, we compute a measure called the *inverse Jacobian measure*. It is defined as: $\text{Inv}(J) = \sup |1 - \frac{J}{J^{Re}}|$, where J^{Re} is the Jacobian of the reconstructed map and J is the Jacobian of the original map. J^{Re} is small when overlapping occurs. Thus, a large value of $\text{Inv}(J)$ means an occurrence of overlapping in f^{Re} and a big deviation of f^{Re} from f. Figure 5.11 shows the values of $\text{Inv}(J)$ versus the number of coefficients used under the Fourier compression of the coordinate functions and the Beltrami coefficient respectively. The red curve shows the values of $\text{Inv}(J)$ under the Fourier compression of the coordinate functions versus the number of Fourier coefficients used. Note that the values of $\text{Inv}(J)$ are quite big, meaning that overlapping occurs in f^{Re} and the diffeomorphic property is seriously distorted. The blue curve shows the values of $\text{Inv}(J)$ under the Fourier compression of the Beltrami coefficient versus the number of Fourier coefficients used. The values of $\text{Inv}(J)$ are very small, meaning that f^{Re} preserves the diffeomorphic property well and reconstructs the original map f accurately.

5.6 Conclusion

In this chapter, we address the problem of finding a simple representation of surface maps that significantly reduces the required storage memory. It is especially important in medical imaging, in which a large set of surfaces have to be registered. A great amount of storage capacity and bandwidth are needed to store and transmit the surface map data. Hence, an algorithm for compressing surface

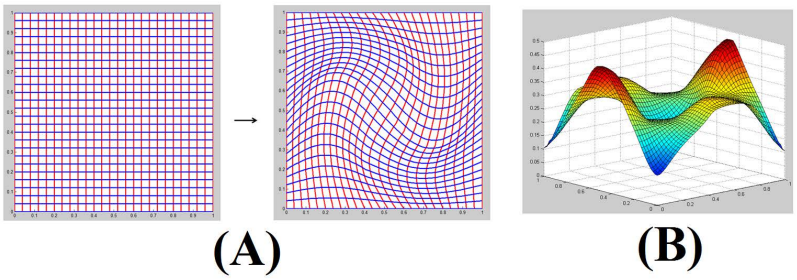

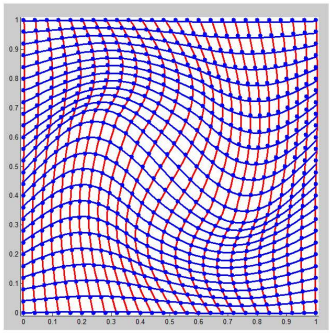

Iteration	*Error*	*Iteration*	*Error*
1	*0.2674*	*11*	*0.1395*
2	*0.2553*	*12*	*0.1256*
3	*0.2431*	*13*	*0.1114*
4	*0.2307*	*14*	*0.0970*
5	*0.2182*	*15*	*0.0823*
6	*0.2056*	*16*	*0.0673*
7	*0.1927*	*17*	*0.0520*
8	*0.1797*	*18*	*0.0366*
9	*0.1665*	*19*	*0.0210*
10	*0.1531*	*20*	*0.0166*

(C) (D)

Figure 5.3: Reconstruction of the diffeomorphism of a 2D domain from the Beltrami coefficient using Beltrami Holomorphic flow (BHF).

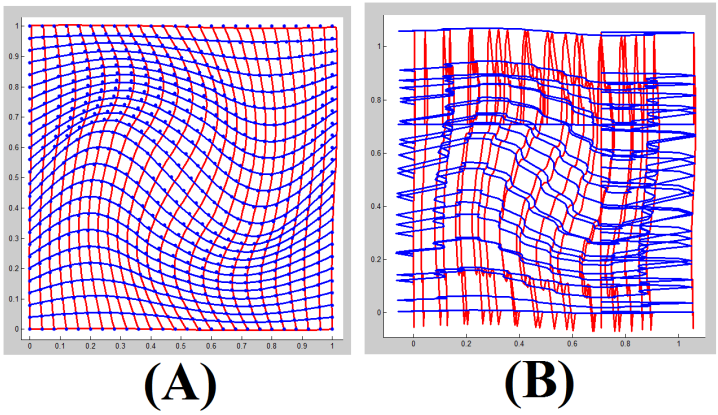

Figure 5.4: (A) shows the Fourier compression result of the Beltrami coefficient; (B) shows the Fourier compression result of the coordinate functions

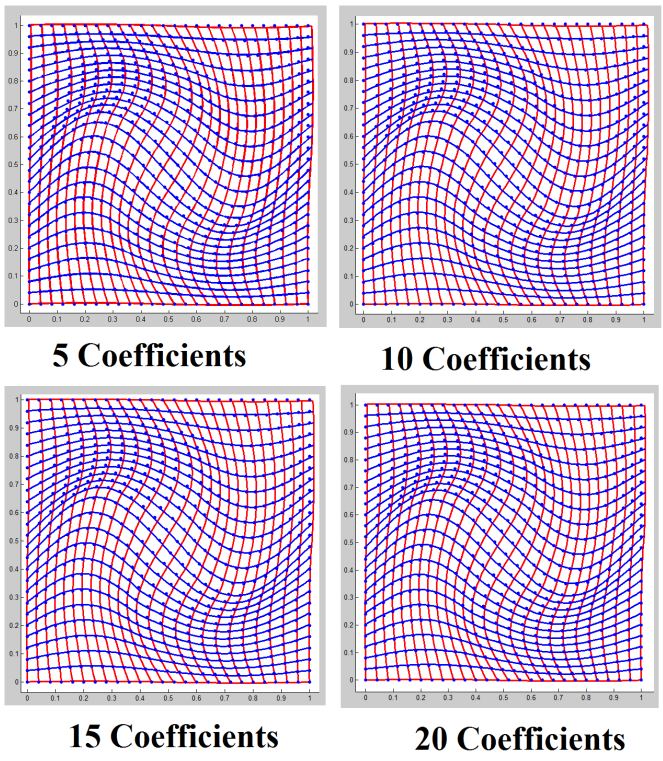

Figure 5.5: The results from Fourier compression of μ with $N = 5, 10, 15$ and 20.

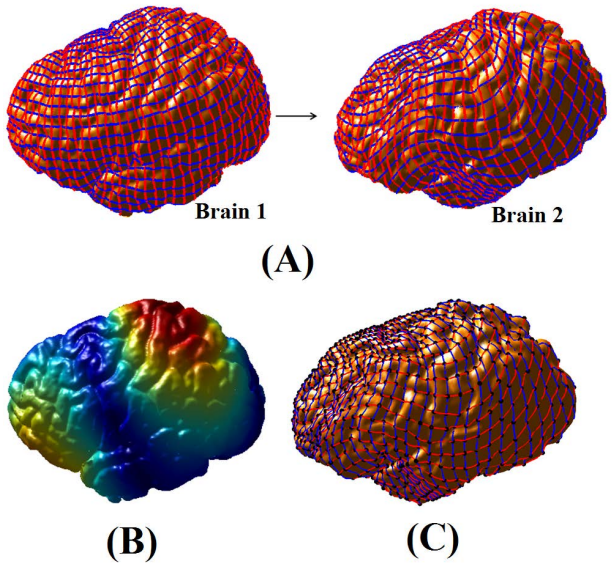

Figure 5.6: Reconstruction of a surface diffeomorphism between real human brain surfaces from its Beltrami coefficient.

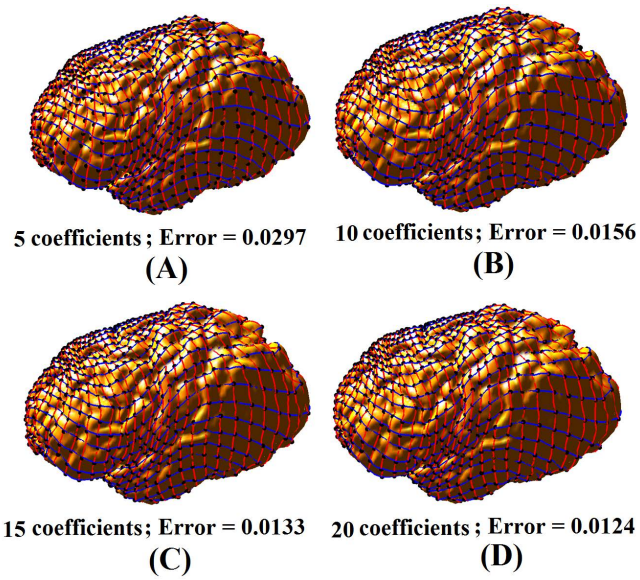

Figure 5.7: The results of Fourier compression of μ for a brain surface diffeomorphism with $N = 5, 10, 15$ and 20.

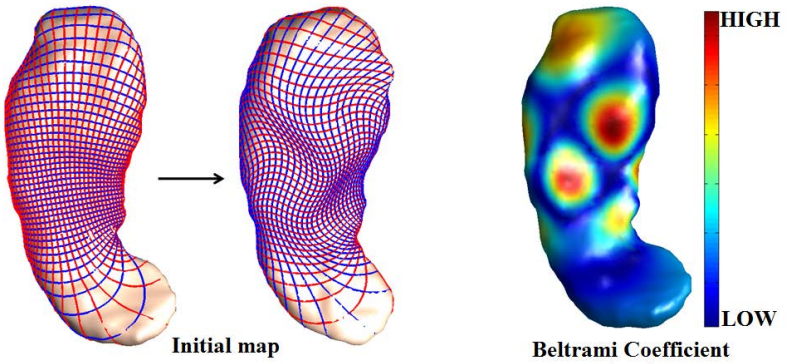

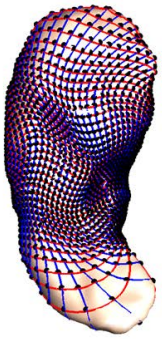

Iteration	*Error*	*Iteration*	*Error*
1	0.0958	*11*	0.0513
2	0.0915	*12*	0.0466
3	0.0872	*13*	0.0418
4	0.0829	*14*	0.0370
5	0.0785	*15*	0.0321
6	0.0741	*16*	0.0272
7	0.0696	*17*	0.0222
8	0.0651	*18*	0.0174
9	0.0606	*19*	0.0125
10	0.0560	*20*	0.0114

(C) (D)

Figure 5.8: (A) shows two different hippocampal surfaces and a surface diffeomorphism between them. We represent the surface map with its Beltrami coefficient and the colormap of its norm is shown in (B). (C) shows the reconstructed map from the Beltrami coefficient. (D) shows the errors of the intermediate maps during Beltrami Holomorphic Flow (BHF).

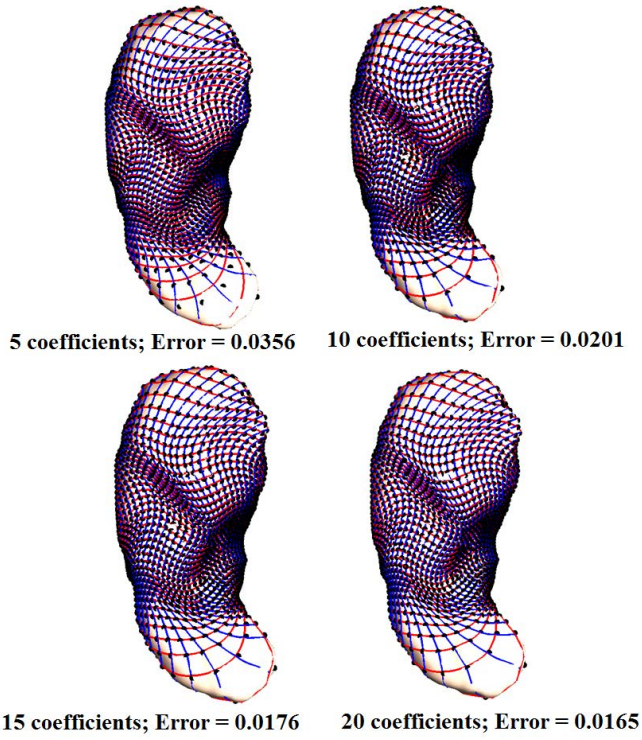

Figure 5.9: The Fourier compression results of the Beltrami coefficient for a hippocampal surface diffeomorphism with $N = 5, 10, 15$ and 20

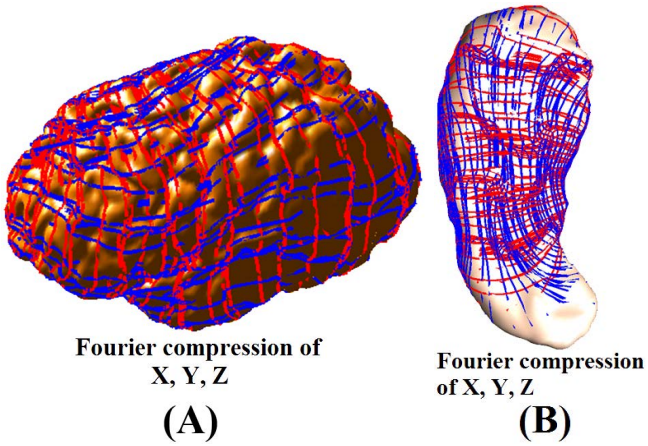

Figure 5.10: The mapped images (represented by the red and blue lines) of the reconstructed maps from the Fourier compression of 3D coordinate functions on (A) cortical surface and (B) hippocampus. Diffeomorphic properties are completely disrupted.

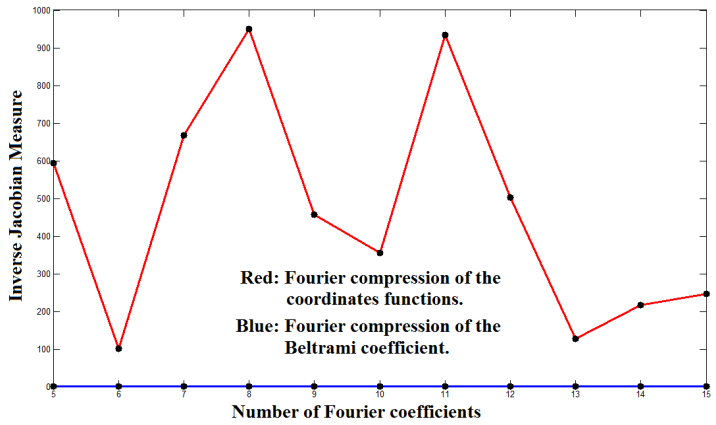

Figure 5.11: The values of Inv(J) under the Fourier compression of the coordinate functions and the Beltrami coefficient.

maps is of utmost importance. We propose a novel representation of surface maps using Beltrami coefficients. Fixing any 3 points, there is a 1-1 correspondence between the set of surface diffeomorphisms and the set of Beltrami coefficients. We propose the Beltrami Holomorphic flow (BHF) method to iteratively reconstruct the surface map with a given Beltrami coefficient. Using the Beltrami coefficient to represent the surface map reduces 1/3 of the required storage space. We can further compress the Beltrami coefficient using the Fourier approximation, which significantly reduces the storage required by 90% further. Experimental results on synthetic data, real human brain data and real hippocampus surfaces show that our method is stable and effective in accurately representing surface maps and requires less storage memory. In the future, we will further explore more potential applications of our method, such as doing statistics on the Beltrami representation for shape analysis and developing a statistically guided registration method based on the Beltrami coefficient.

CHAPTER 6

Shape-Based Diffeomorphic Registration on Hippocampal Surfaces Using Beltrami Holomorphic Flow

6.1 Introduction

The hippocampus(HP) is an important subcortical structure of the human brain that plays a key role in long-term memory and spatial navigation. Surface-based shape analysis is commonly used to study local changes of HP surfaces due to pathologies such as Alzheimer disease (AD), schizophrenia and epilepsy[THZ04]. When comparing data on two anatomical surfaces, a 1-1 correspondence must be computed to register one surface nonlinearly onto the other. On HP surfaces, there are no well-defined anatomical landmark features that can be used as a constraint to establish good correspondences. High-field structural or functional imaging, where discrete cellular fields are evident [ZET03], is still not routinely used. Finding meaningful registrations between HP surfaces becomes challenging. Inaccuracies in shape analysis are often introduced due to incorrect registrations. In fact, shape analysis and surface registration are closely related. The results of shape analysis can be highly affected by the registration, but a good registration depends largely on the appropriate choice of shape measure that captures dissimilarities between surfaces. Therefore, it is of utmost importance to combine

the two processes and define a suitable shape measure to drive the registration.

Here we developed an algorithm to automatically register HP surfaces with complete geometric matching, avoiding the need to manually label landmark features. We first propose a complete shape index using the Beltrami coefficient (BC) and curvatures, which measures subtle local differences. The shape energy is identically zero if and only if two shapes are equal up to a rigid motion. We then minimize the shape energy to obtain the best surface registration with complete geometric matching. We propose a simple representation of surface diffeomorphisms using BCs, which simplifies the optimization. We then optimize the shape energy using the Beltrami Holomorphic flow (BHF) method. The optimal shape energy obtained may also be used to measure local shape differences across subjects or time.

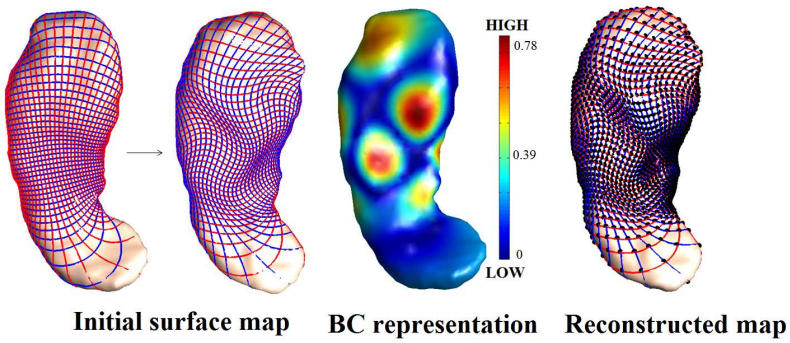

Figure 6.1: Representation of surface registration using Beltrami Coefficients

6.2 Related Work

Surface registration has been studied extensively. Conformal or quasi-conformal surface registration is commonly used [GWC04, HS09, WLG07], and gives a parameterization minimizing angular distortions. However, it cannot guarantee the matching of geometric information such as curvature across subjects. Landmark-

based diffeomorphisms are often used to compute, or adjust, cortical surface parameterizations [GVM04, LYL05, TT96]. These methods provide good registrations when corresponding landmark points on the surfaces can be labeled in advance. It is, however, difficult for HP surfaces on which there are no well-defined anatomical landmarks. Some authors have proposed driving features into correspondence based on shape information. Lyttelton et al. [LBR07] computed surface parameterizations that match surface curvature. Fischl et al. [FST99] improved the alignment of cortical folding patterns by minimizing the mean squared difference between the average convexity across a set of subjects and that of the individual. Wang et al. [WCT05] computed surface registrations that maximize the mutual information between mean curvature and conformal factor maps across subjects. Lord et al. [LHV07b] matched surfaces by minimizing the deviation from isometry. The shape indices that drive the registration process in these approaches are not complete shape measurements and do not capture shape differences completely. There are cases when two different surfaces might have the same shape value. This could lead to inaccurate registration results.

6.3 Theoretical Background

Given two Riemann surfaces M and N, a map $f : M \to N$ is *conformal* if it preserves the surface metric up to a multiplicative factor. One generalization of conformal maps is the *quasi-conformal* maps, which are orientation-preserving homeomorphisms between Riemann surfaces with bounded conformality distortion, in the sense that their first order approximations takes small circles to small ellipses of bounded eccentricity [GL00]. Thus, a conformal homeomorphism that maps a small circle to a small circle may also be regarded as quasi-conformal. Mathematically, $f : \mathbb{C} \to \mathbb{C}$ is quasi-conformal if it satisfies the Beltrami equation:

$\frac{\partial f}{\partial \bar{z}} = \mu(z)\frac{\partial f}{\partial z}$, for some complex valued function μ satisfying $||\mu||_\infty < 1$. μ is called the *Beltrami coefficient* (BC), which is a measure of non-conformality. In particular, the map f is conformal around a small neighborhood of p when $\mu(p) = 0$. From $\mu(p)$, we can determine the angles of the directions of maximal magnification and shrinking and the amount of them as well. Specifically, the angle of maximal magnification is $\arg(\mu(p))/2$ with magnifying factor $1 + |\mu(p)|$; The angle of maximal shrinking is the orthogonal angle $(\arg(\mu(p)) - \pi)/2$ with shrinking factor $1 - |\mu(p)|$. The distortion or dilation is given by: $K = (1 + |\mu(p)|)/(1 - |\mu(p)|)$.

6.4 Proposed Model

6.4.1 A Complete Shape Index

A good registration depends greatly on the appropriate choice of a shape measure to capture dissimilarities between surfaces. We propose a complete shape index E_{shape} using the Beltrami coefficient and curvatures, which measures subtle local changes completely. Given two HP surfaces S_1 and S_2. Let $f : S_1 \to S_2$ be a registration between S_1 and S_2. The complete shape index E_{shape} is defined as follow: $E_{shape}(f) = \alpha|\mu|^2 + \beta(H_1 - H_2(f))^2 + \gamma(K_1 - K_2(f))^2$ where μ is the Beltrami coefficient of f; H_1, H_2 are the mean curvatures on S_1 and S_2 respectively; and K_1, K_2 are the Gaussian curvatures. The first term measures the conformality distortion of the surface registration. The second and third terms measure the curvature mismatch. It turns out E_{shape} is a complete shape index that measures subtle shape differences between two surfaces. It can be proven that $E_{shape}(f) = 0$ if and only if S_1 and S_2 are equal up to a rigid motion. For HP shape analysis, it is good because clinically we are more interested in shape changes than their orientation. Also, by adjusting the parameters (i.e.,

α, β and γ), E_{shape} can be made equivalent to other existing shape indices. For example, when $\beta = 0$, E_{shape} is equivalent to the isometric shape index; when $\alpha = 0$, E_{shape} is equivalent to the curvature index; when $\beta = \gamma = 0$, E_{shape} measures the conformality distortion. In our work, we set $\alpha = 1$ and $\beta = \gamma = 2$ to measure complete shape changes.

We can now minimize E_{shape} to obtain the optimized surface map $\widetilde{f}$ that best matches the geometry. One advantage of using E_{shape} is that it can be defined in the space of BCs. The space of BCs is a simple functional space, which makes the optimization much easier.

6.4.2 Surface Map Representation Using Beltrami Coefficients

Surface registration is commonly parameterized using 3D coordinate functions in $\mathbb{R}^3$. This representation is difficult to manipulate. For example, the 3D coordinate functions have to satisfy certain constraints on the Jacobian J (namely, $J > 0$), to preserve the 1-1 correspondence of the surface maps. Enforcing this constraint adds extra difficulty in optimizing surface maps. The diffeomorphic property is often lost during the optimization. We propose a simple representation of surface diffeomorphisms using Beltrami coefficients (BCs). Fixing any 3 points on a pair of surfaces, there is a 1-1 correspondence between the set of surface diffeomorphisms between them and the set of BCs on the source domain.

Suppose S_1 and S_2 are both either genus 0 closed surfaces or simply connected open surfaces. S_1 and S_2 can be conformally parameterized with a global patch D[GWC04, WLG07]. Let $f\colon S_1 \to S_2$, and given 3 point correspondences. In this chapter, we chose the 3 corresponding points based on the initial conformal registration. But we can easily generalize our method by incorporating a Mobius transformation that will help us to automatically detect optimal 3-point corre-

spondences. Denote the parameterizations by $\phi_1 \colon S_1 \to D$ and $\phi_2 \colon S_2 \to D$. Now, we can compute the Beltrami coefficient μ_f associated uniquely to f to represent f (See Figure 6.1). The Beltrami coefficient μ_f can be computed by considering the composition map $\widetilde{f} = \phi_2 \circ f \circ \phi_1^{-1} \colon D \to D$. Mathematically, μ_f is given by the following formula: $\mu_f = \frac{\partial \widetilde{f}}{\partial \overline{z}} / \frac{\partial \widetilde{f}}{\partial z} = \frac{1}{2}(\frac{\partial \widetilde{f}}{\partial x} + \sqrt{-1}\frac{\partial \widetilde{f}}{\partial y}) / \frac{1}{2}(\frac{\partial \widetilde{f}}{\partial x} - \sqrt{-1}\frac{\partial \widetilde{f}}{\partial y})$.

The space of BCs is a simple functional space. There are no restrictions on μ that it has to be 1-1, surjective or satisfy some constraints on the Jacobian. Using the Beltrami representation makes the optimization process of surface maps much easier.

6.4.3 Optimized Surface Registration Matching the Geometry

E_{shape} gives us a complete shape index which measures local dissimilarities between two surfaces. Specifically, $E_{shape}(f) = 0$ if and only if S_1 and S_2 are equal up to a rigid motion. Therefore, the surface map f minimizing $E_{shape}(f)$ is the best registration that best matches the geometric information. Given two HP surfaces S_1 and S_2. We propose to find $f : S_1 \to S_2$ that minimizes $E = \int E_{Shape}(f)$. To simplify the computation, we can conformally parameterize S_1 and S_2 onto the parameter domain D. So, all computations are carried out on the simple domain D. By representing surface maps with Beltrami coefficients μ, we can define the energy on the space of BCs - a much simpler functional space for the optimization process. Mathematically, the compound energy E can be written with respect to μ as: $E(\mu) = \int_D \alpha|\mu|^2 + \beta(H_1 - H_2(f^\mu))^2 + \gamma(K_1 - K_2(f^\mu))^2$. The variation of f^μ under the variation of μ can be expressed explicitly. Suppose $\widetilde{\mu}(z) = \mu(z) + t\nu(z) + \mathcal{O}(t^2)$. Then, $f^{\widetilde{\mu}(z)}(w) = f^\mu(w) + tV(f^\mu, \nu)(w) + \mathcal{O}(t^2)$, where $V(f^\mu, \nu)(w) = -\frac{f^\mu(w)(f^\mu(w)-1)}{\pi} \int_D \frac{\nu(z)(f_z^\mu(z))^2 dxdy}{f^\mu(z)(f^\mu(z)-1)(f^\mu(z)-f^\mu(w))}$ Using the variational formula, we can derive the Euler-Lagrange equation of $E(\mu)$ easily. Specif-

ically, we can minimize $E(\mu)$ by the following iterative scheme:

$\mu^{n+1} - \mu^n = -2(\alpha\mu^n - \int_z[(\beta\widetilde{H}^n + \gamma\widetilde{K}^n) \cdot G^n, \mathbf{det}(\beta\widetilde{H}^n + \gamma\widetilde{K}^n, G^n)]\ )dt,$

where $\int_w \bullet := \int_D \bullet\ dw$ and $\int_z \bullet := \int_D \bullet\ dz$ is defined as the integral over the variable w and z respectively; $\widetilde{H} := (H_1 - H_2(f^\mu))\nabla H_2(f^\mu)$; $\widetilde{K} := (K_1 - K_2(f^\mu))\nabla K_2(f^\mu)$; $\mathbf{det}(a, b)$ is the determinant of the 2 by 2 matrix or equivalently, the norm of the cross product of a and b.

We call this iterative algorithm the *Beltrami Holomorphic flow* (BHF). Note that starting with a conformal map with $\mu = 0$, the first term of the energy ensures μ to satisfy $||\mu||_\infty < 1$. Hence, during the BHF process, the maps are guaranteed to be diffeomorphic and are holomorphic in t.

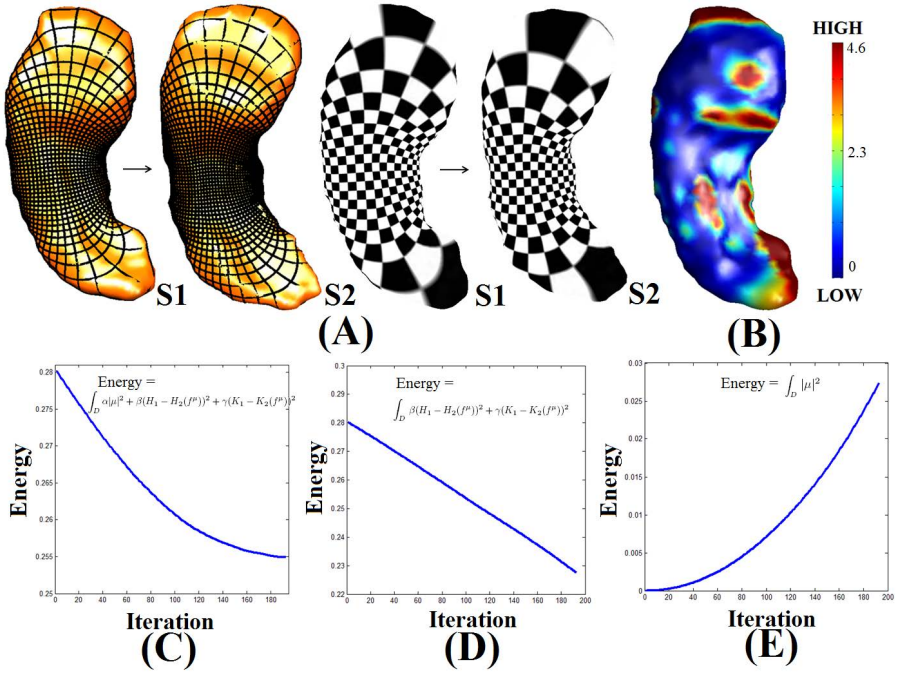

Figure 6.2: Shape registration with geometric matching using Beltrami Holomorphic flow.

6.5 Experimental Results

We tested our algorithm on 212 HP surfaces automatically extracted from 3D brain MRI scans with a validated algorithm [MTA08]. Scans were acquired from normal and diseased (AD) elderly subjects at 1.5 T (on a GE Signa scanner). Experiments have been carried out on a laptop with a 2.4 GHz DUO CPU. The algorithm takes about 4-5 minutes to compute a registration between meshes with 40K vertices.

Figure 6.1 shows the Beltrami representations of bijective surface maps. The left column shows a bijective surface map between the HP surfaces. The middle column shows the Beltrami (BC) representations of the maps. The right column shows the reconstruction of surface maps from their BCs. The reconstructed maps closely resemble the original maps, meaning that BCs can effectively represent bijective surface maps. Figure 6.2(A) shows two different HP surfaces. They are registered using our proposed BHF algorithm with geometric matching. The registration is visualized using a grid map and texture map, which shows a smooth 1-1 correspondence. The optimal shape index E_{shape} is plotted as colormap in (B). E_{shape} effectively captures the local shape difference between the surfaces. (C) shows the shape energy in each iteration. With the BHF algorithm, the shape energy decreases as the number of iterations increases. (D) shows the curvature mismatch energy ($E = \int \beta(H_1 - H_2(f))^2 + \gamma(K_1 - K_2(f))^2$). It decreases as the number of iterations increases, meaning that the geometric matching improves. (E) shows the Beltrami coefficient of the map in each iteration, which shows the conformality distortion of the map. Some conformality is intentionally lost to allow better geometric matching.

Figure 6.3 shows the BHF registration between two normal HPs. The complete shape index E_{shape} is plotted as colormap on the right. Again, E_{shape} can

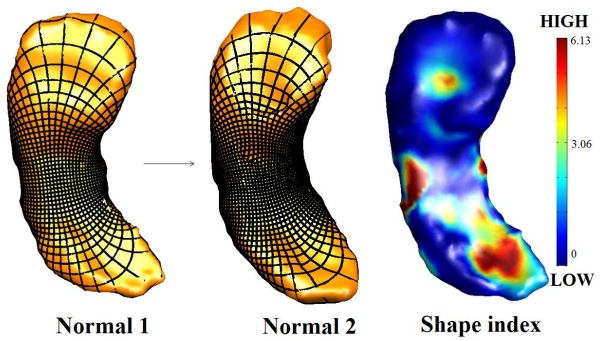

Figure 6.3: BHF registration between two normal subjects. The shape index E_{shape} is plotted on the right, which captures local shape differences.

accurately capture local shape differences between the normal HP surfaces.

Figure 6.4 shows the BHF hippocampal registrations between normal elderly subjects and subjects with Alzheimer's disease. The BHF registrations give smooth 1-1 correspondences between the HP surfaces. We can use the complete shape index E_{shape} to detect local shape differences between healthy and unhealthy subjects.

We also study the temporal shape changes of normal and AD HP surfaces, as shown in Figure 6.5. For each subject, we compute the deformation pattern of its HP surfaces measured at time = 0 and time = 12 Months (see [MTA09] for longitudinal scanning details). The left two panels show the temporal deformation patterns for two normal subjects. The middle two panels show the temporal deformation patterns for two AD subjects. The last column shows the statistical significance p-map measuring the difference in the deformation pattern between the normal (n=47) and AD (n=53) groups, plotted on a control HP. The deep red color highlights regions of significant statistical difference. This method can be potentially used to study factors that influence brain changes in AD.

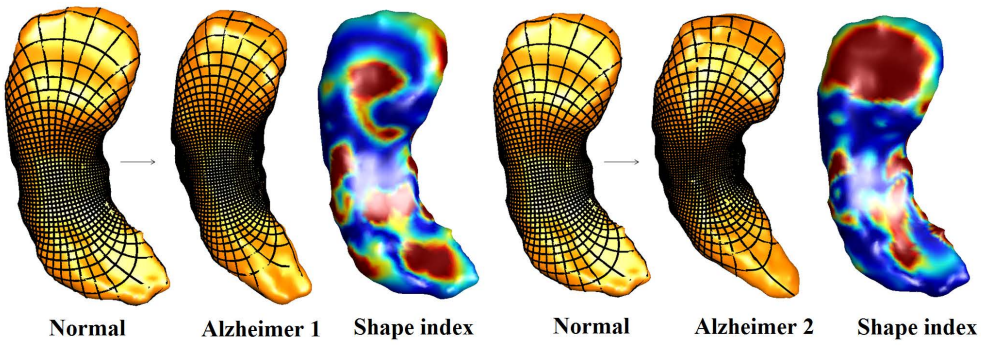

Figure 6.4: BHF registration between normal subjects and subjects with Alzheimer's disease. Their local shape differences are captured by E_{shape}.

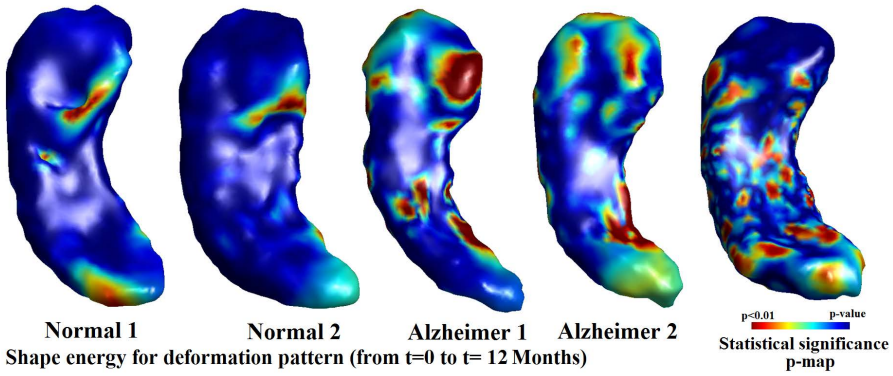

Figure 6.5: Temporal hippocampal shape changes of normal and subjects with Alzheimer's disease.

6.6 Conclusion

We developed an algorithm to automatically register HP surfaces with complete geometric matching, avoiding the need for manually-labeled landmark features. We did this by defining a complete shape index to drive the registration. Experimental results on 212 HP surfaces from normal and diseased(AD) subjects show our proposed algorithm is effective in registering HP surfaces over time and across subjects, with complete geometric matching. The proposed shape energy can also capture local shape differences between HPs for disease analysis. In future, we will use the BHF algorithm to systematically study the local shape differences and factors that affect deformation patterns between normal and AD subjects.

CHAPTER 7

Parallelizable Inpainting and Refinement of Diffeomorphisms Using Beltrami Holomorphic Flow

7.1 Introduction

In computer graphics and medical imaging, a great deal of effort is spent on processing surface diffeomorophisms. For example, in computer-aided design, fine diffeomorphisms are important for high quality texture mapping of 3D models. In brain imaging, they are crucial for the registration of cortical surfaces. However, under some situations, some parts of the surfaces may not be properly registered due to noise or highly convoluted surfaces like the cortical surface. This may make certain regions not able to register at all or result in highly distorted and/or overlapping regions. To fix this problem, we need to properly restore the missing region using existing data as much as possible.

For other situations such as video compression and computer games, the storage allowed is limited for practical reason. For example, in video compression, consecutive frames may be related by a smoothly varying diffeomorphisms, which allows further compression. In computer games, it is not practical to store the precise texture maps of thousands of in-game objects. To save storage, texture maps are often stored in a piecewise linear way with every triangle in simplified

triangular meshes. This causes unnatural distortions when objects are zoomed in too closely. To achieve the finest restoration, we need to restore the desired quality of the texture maps, like the degree of distortion and smoothness, from a compact representation as above.

Dealing with diffeomorphisms is more difficult than dealing with images, because diffeomorphisms have to be non-overlapping, which requires the Jacobian to be positive everywhere. In modifying diffeomorphisms, we must preserve these properties so that they remain smooth and bijective. This adds extra difficulty in processing them.

Motivated by the above discussion, we are interested in developing effective algorithms to either 'inpaint' the missing or distorted regions of a diffeomorphism, or refine a diffeomorphism with low resolution to higher resolution. In this chapter, we propose a novel approach to solve these two problems. The basic idea is to represent a diffeomorphism by its Beltrami coefficient. Then we may inpaint or refine it by interpolating its Beltrami coefficients instead of its coordinate functions. A new diffeomorphism can then be constructed from the inpainted/refined Beltrami coefficient, by the exact Beltrami holomorphic flow (BHF) algorithm proposed in this chapter. Compared with other methods, such as linear interpolation and adjusting its coordinate functions using existing inpainting algorithms, our method guarantees smoothness and diffeomorphic property. In the original missing region, the restored diffeomorphism follows the property of the original diffeomorphism on the non-occluded region. We apply our proposed algorithms to three practical applications, including (i) super-resolution of texture maps to sharpen and smoothen surface textures, (ii) parallelizable landmark-matching surface mapping to parameterize complicated surfaces efficiently, and (iii) inpainting of image sequences of deforming shapes. Experimental results confirm

the effectiveness and efficacy of our proposed algorithms.

7.2 Previous Work

Image inpainting and super-resolution have been extensively studied. Inpainting refers to the process of reconstructing lost or deteriorated parts of images. Image super-resolution aims to produce an aesthetically pleasing high resolution image from a low resolution image. Both image inpainting and super-resolution are related to image interpolation. Recently, different approaches for this subject have been proposed. Belahmidi [BG04] proposed a PDE-based approach to zoom images by solving anisotropic heat diffusion equations. Bertalmío et al. [BBS01] proposed to apply Navier-Stokes equations and fluid dynamics for image and video inpainting. Shen et al. [CS02] proposed mathematical models for local inpaintings of non-texture images based on the classical total variation (TV) denoising model. Later, Cha et al. [CK06] applied the PDE form of the TV energy for image zooming. Multiscale approach was also proposed. Carey et al. [KCH97] proposed an image interpolation approach based on wavelets. Although image interpolation has been well-studied, the interpolation of surface diffeomorphisms preserving bijectivity has been rarely studied. In this chapter, we focus on the interpolation of surface diffeomorphisms.

Surface registration has also been widely studied. Gu et al. [WLG07] proposed to obtain conformal surface registration by minimizing some energy functionals. Lévy et al. [LPR02] proposed a least square method to obtain conformal maps for texture mapping. To obtain a surface registration that matches important landmark features, Durrleman et al. [DPT08] developed a framework using currents, a concept from differential geometry, to match landmarks within surfaces across subjects, for the purpose of inferring the variability of brain struc-

ture in an image database. Lui et al. [LTW10] proposed to compute shape-based landmark matching registrations between brain surfaces using the integral flow method. The one-parameter subgroup within the set of all diffeomorphisms was considered and represented by smooth vector fields. Landmarks can be perfectly matched and the correspondence between landmark curves is based on shape information. Leow et al. [LYL05] proposed a level-set-based approach for matching different types of features, including points, 2D and 3D curves represented as implicit functions. Computing surface registration is generally difficult, especially on complicated surfaces. In this chapter, we propose a parallelizable method for efficient surface registration.

This chapter is mainly based on the representation of diffeomorphisms by Beltrami coefficients. Studying diffeomorphisms by Beltrami coefficient was first proposed by Lui et al. [LWZ10] for medical shape analysis. They further proposed to compute geometric matching surface registration by adjusting Beltrami coefficients [LWG10].

7.3 Theoretical Background

7.3.1 Quasiconformal Mappings and Beltrami Coefficients

A surface S with a conformal structure is called a *Riemann surface*. Given two Riemann surfaces M and N, a map $f\colon M \to N$ is *conformal* if it preserves the surface metric up to a multiplicative factor called the *conformal factor*. A generalization of conformal maps is *quasi-conformal* maps, which are orientation-preserving diffeomorphisms between Riemann surfaces with bounded conformality distortion, in the sense that their first order approximation takes small circles to small ellipses of bounded eccentricity. Thus, a conformal homeomorphism that

maps small circles to small circles is also quasiconformal.

Mathematically, $f\colon \mathbb{C} \to \mathbb{C}$ is quasiconformal if it satisfies the Beltrami equation $\frac{\partial f}{\partial \overline{z}} = \mu(z)\frac{\partial f}{\partial z}$, for some complex valued functions μ with $||\mu||_\infty < 1$. μ is called the *Beltrami coefficient*, which is a measure of non-conformality. In particular, f is conformal around a small neighborhood of p when $\mu(p) = 0$. Equivalently, f is not conformal if and only if $\mu(p) \neq 0$ at p. Inside the local parameter domain, f may be considered as a map composed of a translation to $f(p)$ together with a stretch map $S(z) = z + \mu(p)\overline{z}$, which is postcomposed by a multiplication of $f_z(p)$, which is conformal. All the conformal distortion of $S(z)$ is caused by $\mu(p)$. $S(z)$ is the map that causes f to map small circles to small ellipses. From $\mu(p)$, we can determine the angles of the directions of maximal magnification and shrinkage and the amount of them as well. Specifically, the angle of maximal magnification is $\arg(\mu(p))/2$ with magnifying factor $1 + |\mu(p)|$; the angle of maximal shrinkage is the orthogonal angle $(\arg(\mu(p)) - \pi)/2$ with shrinking factor $1 - |\mu(p)|$. The distortion or dilation is given by $K = (1 + |\mu(p)|)/(1 - |\mu(p)|)$

Thus, the Beltrami coefficient μ gives us important information about the properties of a map.

7.3.2 Adjusting Diffeomorphisms by Beltrami Holomorphic Flow

Let $f\colon \mathbb{C} \to \mathbb{C}$ be a diffeomorphism. We say that f fixes 0, 1 and ∞ if $f(0) = 0$, $f(1) = 1$ and $\lim_{z\to\infty} f(z) = \infty$. Suppose f fixes 0, 1 and ∞ and satisfies the Beltrami equation $\frac{\partial f}{\partial \overline{z}} = \mu\frac{\partial f}{\partial s}$. If we set $\mu(t) = \mu + t\nu$, then $f^{\mu(t)}(w) = f(w) + t\dot{f}(w) + o(t^2)$, where

$$\dot{f}(w) = -\frac{1}{\pi}\iint \nu(z)R(f(z), f(w))(f_z(z))^2\,dx\,dy, \tag{7.1}$$

with

$$R(z,w) := \frac{1}{z-w} - \frac{w}{z-1} + \frac{w-1}{z}. \tag{7.2}$$

This formula gives the variation of f with respect to the variation of μ. Apparantly, the integrand has singularities at $z = 0$, $z = 1$ and $z = w$. However, the integrand can be written as 3 terms, where every term has just a simple pole. Therefore, integrating them on $\mathbb{R}^2$ always give a finte answer and will not cause any singularity. We call this formula the Beltrami holomorphic flow formula.

Using this formula, we may adjust any diffeomorphism f^{μ_0} to any other diffeomorphism f^{μ}, with Beltrami coefficients μ_0 and μ respectively. When the initial $\mu = 0$, this amounts to computing f^{μ} from the identity map $f^0 = \mathrm{Id}$. Setting $\nu = \mu - \mu_0$, we compute the BHF for $f^{\mu(t)}$, where $\mu(t) = \mu_0 + t\nu$. Theoretically, the approximation of f^{μ} is given by setting $t = 1$, i.e., $f^{\mu}(w) \approx f(w) + \dot{f}(w,t)$. However, when ν is not small enough, we may face the problem of overlapping in $f^{\mu(1)}$. We will discuss how to choose an optimal t in Subsection 7.4.2.

7.3.3 TV Inpainting of 2D Image Data

Inpainting can be regarded as a process of interpolating data on the occluded region from the known data on its neighborhood. To inpaint an occluded 2D image, we can fill in the missing region by solving the Perona-Malik diffusion model:

$$\begin{cases} \frac{\partial u}{\partial t} = div(g(|\nabla u|)\nabla u) & \text{on } D; \\ u^0 = v & \text{on } D^c, \end{cases}$$

where D is the occluded region, $v\colon D^c \to R$ is the original image with occlusion, u is the approximated (inpainted) image, and $g\colon R \to R$ is an increasing function such that $g(0) = 0$ and $g(\infty) = \infty$. Note that if we replace g by $\frac{1}{\nabla u}$, we get the familiar TV smoothing model, which is well-known to preserve edges and

commonly called the TV inpainting model.

Image inpainting has been extensively studied. But very often, the inpainting of diffeomorphisms with occluded regions is also needed. For example, when surface registration cannot be done on some regions of the surface, inpainting of the registration will be necessary. However, as far as we know, no work has been done on the inpainting of 2D/3D diffeomorphisms. In this chapter, we extend the TV inpainting algorithm to inpaint diffeomorphisms with occluded regions.

7.4 Our Proposed Algorithms

In this section, we propose several algorithms to deal with the inpainting and refinement of diffeomorphisms using BHF. Although BHF deals with diffeomorphisms of 2D domains, our algorithms can be easily extended to processing surface diffeomorphisms by reparameterization onto 2D domains, such as conformal parameterizations [WLG07].

7.4.1 Exact Computation of the Beltrami Holomorphic Flow

Let $f\colon D \to D$ be a diffeomorphism on $D = [-1, 1]^2$ with $f(0) = 0$ and $f(1) = 1$. Denote the triangulation of D by $\mathrm{Tri}(D)$. For the discretized f, its value is known on every vertex of D. It is natural to assume that the actual f can be well approximated piecewise linearly on each face in $\mathrm{Tri}(D)$. On each face, the Beltrami coefficient of f is constant. We may also assume that ν, the adjustment to μ, is also piecewise constant on each face of $\mathrm{Tri}(D)$. Then $\mu(t) = \mu + t\nu$ is a piecewise constant function on D. For every $T \in \mathrm{Tri}(D)$, denote the value of ν on T as ν_T, and the value of f_z on T as $f_{z,T}$. The direction of BHF in (7.1)

becomes

$$\dot{f}(w) = \sum_{T \in \mathrm{Tri}(D)} \dot{f}(w, T), \tag{7.3}$$

where

$$\dot{f}(w, T) := -\frac{1}{\pi} \nu_T f_{z,T}^2 \iint_{z \in T} R(f(z), f(w))\, dx\, dy. \tag{7.4}$$

Note that $R(f(z), f(w))$ can be written as a sum of 3 simple fraction terms. Since $f(w)$ is constant in the integral, we may pull the factors $f(w)$ and $f(w) - 1$ in the last two terms out of the integral. Therefore to compute $\dot{f}(w, t, T)$, it suffices to compute integrals of the form $\iint_{z \in T} \frac{1}{f(z) - c}\, dx\, dy$ and sum. Note that $f(z) - c$ is a linear function in the integral. It turns out that all reciprocals of linear functions can be integrated exactly. This allows us to find the exact direction given by BHF.

With exact integration, our algorithm always give the exact derivative of f with respective to the adjustment ν in μ. The only source of error comes from the discretization of f, which is unavoidable for computations on triangular meshes. In the next subsection, we discuss the optimal step size to take after the direction given by BHF is computed.

7.4.2 Adjusting Diffeomorphisms Using BHF with Adaptive Step Size

Given a diffeomorphism $f \colon \mathbb{C} \to \mathbb{C}$ with Beltrami coefficient μ_0 fixing 0, 1 and ∞. Suppose we want to adjust its Beltrami coefficient to μ on $D = [-1, 1]^2$. After setting $\nu = \mu - \mu_0$, $\mu(t) = \mu_0 + t\nu$ and computing $\dot{f}(w)$ using the exact BHF algorithm, it may be tempting to update f by setting $t = 1$ to get the required diffeomorphism. However, although exact integration of (7.1) gives the exact flowing direction of f with respect to the change in μ, the accuracy of this first order approximation depends on $\|\nu\|_\infty$. If t is too large, overlapping may

occur and prevent the algorithm from converging. In this subsection, we propose a method which allows us to find the optimal step size t.

After computing $\dot{f}(w)$ for every vertex in $\mathrm{Tri}(D) = (\mathcal{V}, \mathcal{E}, \mathcal{F})$, the new mapping $h(w) = f(w) + t\dot{f}(w)$ satisfies the Beltrami equation with Beltrami coefficient $\sigma(t)$, which is piecewise constant on every $T \in \mathcal{F}$. When t is small, $\sigma(t)$ is approximately $\mu_0 + t\nu$. As t gets larger, the approximation gets worse. We propose to adjust f with a value of t that will not cause overlapping in h and such that $\sigma(t)$ is the best approximation to the target Beltrami coefficient μ. On every triangle $T \in \mathcal{F}$, we compute the smallest time $t_T > 0$ such that Jacobian of h on T will be zero. As $h(z_1)$, $h(z_2)$ and $h(z_3)$ move linearly as t increases, the Jacobian of h on T is quadratic in T. Therefore t_T is a root of this quadratic equation. If the Jacobian is positive for all $t > 0$, we set t_T to $+\infty$. The threashold value of t, $t_{\text{threshold}}$, is such at the Jacobian of h on at least one triangle reaches 0:

$$t_{\text{threshold}} := \min_{T \in \mathcal{F}} t_T \tag{7.5}$$

For the algorithm to work, t must be strictly less than $t_{\text{threshold}}$. We always choose t such that $t < t_{\text{threshold}}/2$ and $\sigma(t)$ best approximates μ. Using Newton's method, we find the optimal t that minimizes the L^2-norm of $\sigma(t) - \mu$:

$$t_{\text{optimal}} := \arg \min_{0 < t < t_{\text{threshold}}/2} \|\sigma(t) - \mu\|_2 \tag{7.6}$$

One may also want to use other criteria for the closeness of approximation other than the L^2-norm. In our experiments, the above choice of $t_{optimal}$ gives rapid convergence within 25 iterations most of the time, and $t_{optimal}$ could be much larger than 1 towards the end of the algorithm.

In the next 2 subsections, we make use of the exact BHF algorithm discussed thus far on the problems of inpainting and super-resizing diffeomorphisms.

7.4.3 Beltrami Inpainting of Diffeomorphisms

In this subsection, we propose an algorithm to inpaint a surface diffeomorphism on any region defined by a user. Such algorithm is extremely useful in various situations. For example, in medical imaging, part of a biological surface (e.g. cortical surface) may not be registered properly with another biological surface and shows abnormal distortions, or in video compression, where one stores the most important correspondence between 2 frames and fills in the occluded parts during playback.

To inpaint a surface diffeomorphism, we parameterize it as a diffeomorphism on $\mathbb{C}$ fixing 0, 1 and ∞, where f restricted to $D = [-1, 1]^2$ corresponds to the surface diffeomorphism. We are interested to adjust the value f takes on D. Suppose we want to inpaint a diffeomorphism $f_0 \colon \mathbb{C} \to \mathbb{C}$ on a region $\Omega \subset D$, and only the value of f_0 on $D \backslash \Omega$ is known, as if a partial registration is obtained from the non-occluded region. Our target is to smoothly reconstruct the original f_0, given that $f = f_0$ on $D \backslash \Omega$.

We propose to restore f by smoothly interpolating the Beltrami coefficient μ in the occluded region, while ensuring $f = f_0$ on $D \backslash \Omega$. Let μ_0 be the Beltrami coefficient of f_0 on $D \backslash \Omega$. Using existing algorithms on vectorial TV inpainting, we propose to define our target Beltrami coefficient μ as

$$\mu := \arg \min_{\mu = \mu_0 \text{on} D \backslash \Omega} \iint_{\Omega} \Big(|(\nabla \mathrm{Re}(\mu))(x + \sqrt{-1}y)|^2 + |(\nabla \mathrm{Im}(\mu))(x + \sqrt{-1}y)|^2 \Big)^{1/2} dx\, dy. \tag{7.7}$$

After computing the target Beltrami coefficient μ, we iteratively use the exact BHF with adaptive time step algorithm to find a diffeomorphism f minimizing

the following energy functional:

$$f = \arg \min_{f=f_0 \text{on} D\backslash\Omega} \iint_{D\backslash\Omega} |\mu(f) - \mu|^2 \, dx \, dy \tag{7.8}$$

The resulting map is the diffeomorphism that preserves the value of f_0 on $D\backslash\Omega$ and smoothly interpolates the Beltrami coefficient μ_0 of f_0 into Ω using its value on $D\backslash\Omega$. This may also be considered as the diffeomorphism which extends f_0 into Ω in the least distorted way.

In the process of iterating with BHF, it may be possible that the condition $f = f_0$ on $D\backslash\Omega$ is violated because a change in Beltrami coefficient may affect the entire map. We solve this problem by adjusting f back to f_0 on $D\backslash\Omega$ and smoothly interpolating the adjustment of f on $\partial\Omega$ into Ω. Now, we summarize the whole algorithm in Algorithm 7.1.

Algorithm 7.1 Inpaint a Diffeomorphism f_0 into Ω from its Beltrami Coefficient Using BHF

Require: A diffeomorphism $f_0 \colon D \to D \subset \mathbb{C}$ where its values on $\Omega \subset \mathbb{C}$ is unknown or need to be inpainted, represented piecewise linearly on D;

Compute the target Beltrami coefficient μ according to (7.7);

Initialize f by setting $f = f_0$ on $D\backslash\Omega$ and extending it into a piecewise linear diffeomorphism on D;

repeat

Compute the Beltrami coefficient $\mu(f)$ of f;

Update f using exact BHF with adaptive step for $\nu = \mu - \mu(f)$;

Adjust f such that $f = f_0$ on $D\backslash\Omega$;

until f converges.

In order to obtain a faster convergence, it is recommended to adjust f to satisfy $f = f_0$ on $D\backslash\Omega$ only once in a few iterations, or when $f(\partial\Omega)$ begins to

deviate mildly from $f_0(\partial\Omega)$. The results of this algorithm and its applications are shown in Section 7.5.

7.4.4 Super-Resolution of Diffeomorphisms

In this subsection, we propose a novel algorithm by modifying the inpainting algorithm in Subsection 7.4.3 to deal with the super-resolution of surface diffeomorphisms. In computer graphics, it is standard to map textures onto an object (in games or CAD programs) by specifying the position on the texture every vertex is mapped to. Then every face of the object mesh is colored by interpolating this vertex correspondence. This greatly limits the quality of texture maps by the resolution of triangular meshes. Even with bilinear or trilinear filtering, it is still unnatural if an object is zoomed in too closely. To solve this problem, our algorithm allows us to refine a diffeomorphism with high detail under the same limited vertex correspondence.

To start with, we assume that the diffeomorphism or texture mapping is reparameterized as f_0, a diffeomorphism on $\mathbb{C}$ fixing 0, 1 and ∞, where we are interested to refine the value it takes on $D = [-1, 1]^2 \subset \mathbb{C}$. Define S_L to be the grid point set $\{s_{L,ij} = -1 - \sqrt{(}-1) + ih + \sqrt{(}-1)jh | i, j = 0, 1, \ldots, L\}$, where $h_L = 2/L$. Suppose only the value of f_0 on a low resolution grid point set S_L is available. We seek to refine this diffeomorphism by reconstructing f_0 with its Beltrami coefficient interpolated to a fine point set S_H, where H is divisible by L.

First we compute the Beltrami coefficient μ_0 of f_0 on every grid element of S_L. Then we construct the target Beltrami coefficient μ by refining μ_0 using cubic interpolation. Using BHF, we construct a diffeomorphism f identical to f_0 on S_0

and minimizes the L^2-norm of $\mu(f) - \mu$:

$$f = \arg \min_{f=f_0 \text{on} S_L} \iint_{D\setminus\Omega} |\mu(f) - \mu|^2 \, dx \, dy \tag{7.9}$$

This results in a diffeomorphism with smoothly varying distortions due to the refined Beltrami coefficient μ.

In the process of iterating with BHF, it may be possible that the condition $f = f_0$ on S_L is violated. Noting that each grid element of S_L is mapped by f onto areas like quadrilaterals, we may fix this condition by mapping values of f inside each quadrilateral $\{f(s_{L,ij}, f(s_{L,(i+1)j}), f(s_{L,(i+1)(j+1)}), f(s_{L,i(j+1)})\}$ back onto the quadrilateral $\{f_0(s_{L,ij}, f_0(s_{L,(i+1)j}), f_0(s_{L,(i+1)(j+1)}), f_0(s_{L,i(j+1)})\}$ using a bilinear map preserving the diffeomorphic property of f. Now, we summarize the while algorithm in Algorithm 7.2.

Algorithm 7.2 Refine a Diffeomorphism f_0 with Known Value on a Coarse Grid from its Beltrami Coefficient Using BHF

Require: A diffeomorphism $f_0 \colon D \to D \subset \mathbb{C}$ where only its value on a coarse grid S_L is known; A finer grid S_H where its refined values are to be computed, where H is divisible by L;

Compute the Beltrami coefficient μ_0 of f_0 on S_L;

Smoothly interpolate μ_0 into μ defined on grid elements of S_H using the cubic method;

Initialize f as the identity function;

repeat

Compute the Beltrami coefficient $\mu(f)$ of f;

Update f using exact BHF with adaptive step for $\nu = \mu - \mu(f)$;

Adjust f such that $f = f_0$ on S_L;

until f converges.

To obtain a faster convergence, we may also adjust f to satisfy $f = f_0$ on S_L

only once in a few iterations, or when $f(S_L)$ begins to deviate mildly from $f_0(S_L)$. In the next section, we show our results by applying algorithms in this section on the inpainting and super-resolution of texture mappings and diffeomorphisms, on both 2D and 3D examples and applications in brain imaging.

7.5 Results and Discussion

In this section, we present the results of our BHF inpainting and refinement algorithms on 2D and 3D examples and demonstrate their effectiveness of our proposed algorithms.

7.5.1 BHF Inpainting of a Highly Distorted Diffeomorphism

In this subsection, we apply the BHF inpainting algorithm on a diffeomorphism $f\colon [-1,1]^2 \to [-1,1]^2$, shown in Figure 7.1, with the inpainting region $\Omega \subset [-1,1]^2$ highlighted. From the plot of its Beltrami coefficient, f is highly distorted. The inpainting region lies on its most distorted area, making the inpainting problem challenging.

Applying the BHF inpainting algorithm on Ω, we restore the lost region of f by constructing a diffeomorphism with a smoothly inpainted Beltrami coefficient. As shown in Figure 7.2(a), the texture in the inpainting region smoothly blends into the surrounding texture, giving a natural diffeomorphism with continuous varying distortion. On the other hand, the result of inpainting using linear interpolation of coordinate functions of f shows only continuation on 3 sides of Ω due to the non-convexity of $f^{-1}(\Omega)$. The texture also shows a sudden jump near the boundary of Ω, giving a very unnatural mapping. The result shows that to reconstruct a diffeomorphism correctly, a careful consideration has to be given to the higher

(a) (b)

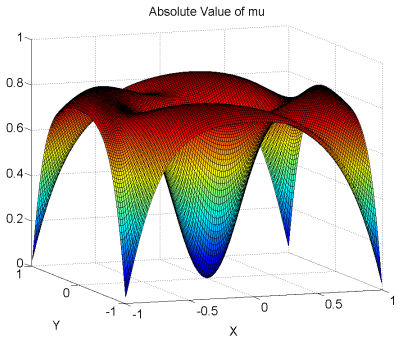

(c)

Figure 7.1: A highly distorted diffeomorphism f of $[-1,1]^2$. (a) shows the domain of f textured with a regular grid pattern. (b) shows how the texture is mapped under f onto $[-1,1]^2$, with the inpainting region highlighted. (c) shows a plot of the modulus of its Beltrami coefficient μ, indicating the high distortion of f.

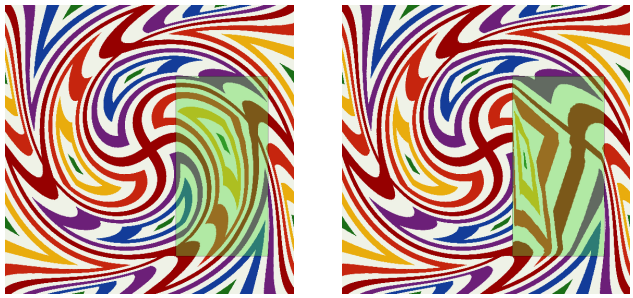

(a) (b)

Figure 7.2: A comparison of the result of the BHF inpainting algorithm (a) and the failed result using linear interpolation (b), with the inpainting region highlighted.

order changes of the diffeomorphism, which is achieved by smoothly inpainting the Beltrami coefficient using our algorithm.

7.5.2 BHF Inpainting of Image Sequences of Deforming Shapes

In this subsection, we demonstrate how the BHF inpainting algorithm can be applied to process image sequences of deforming shapes, which has many applications in areas such as video processing and shape analysis of medical images over time. In this example, we aim at restoring the correspondence of 2 frames in an image sequence of a gingerbread man figure, where the second frame is distorted and occluded by unknown foreground object represented by a black region (see Figure 7.3). This is challenging for conventional image inpainting algorithms due to the size of the occluded region and the additional distortions.

First of all, we independently register the top and bottom non-occluded regions between the first and second frames. As illustrated in Figure 7.4, this can be done by marking a number of correspondences between 2 frames in each region, and registering each region separately using existing algorithms [LTW10]. After this, the Beltrami coefficient of the registration in the non-occluded regions

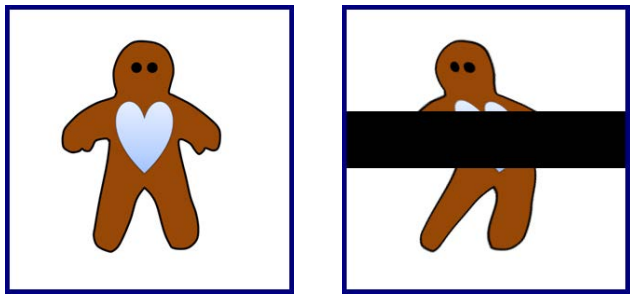

(a) (b)

Figure 7.3: An image sequence of a gingerbread man showing the initial frame (a) and the second frame with distortion and occlusion (b).

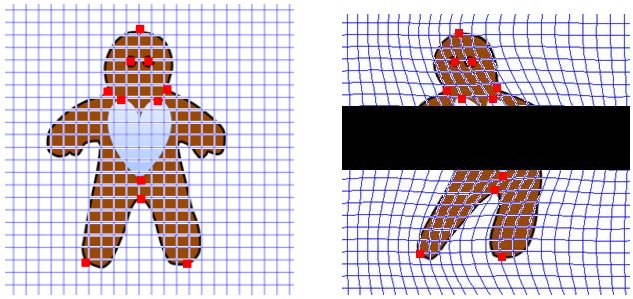

(a) (b)

Figure 7.4: The highlighting of feature points and the registration between the top and bottom parts of frame 1 and 2.

can be computed. Using the BHF inpainting algorithm, we inpaint the Beltrami coefficient in the occluded region and construct the whole registration between the first and second frames, preserving the already registered top and bottom parts. The final diffeomorphism is shown in Figure 7.5(a). As can be seen, the complete diffeomorpism follows the pattern and geometry of the local registrations, and continues smoothly into the middle occluded region. Figure 7.5(b) shows the complete gingerbread man with the occluded region filled from the first frame using the complete diffeomorphism.

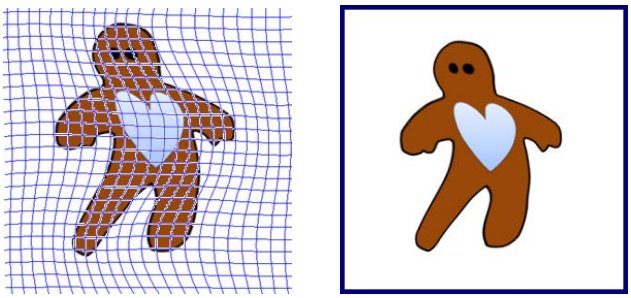

(a) (b)

Figure 7.5: The result of registering frames 1 and 2 using the BHF inpainting algorithm. (a) shows the final registration. (b) shows the complete gingerbread man with the occluded region filled.

(a) (b)

Figure 7.6: Application of the BHF refinement algorithm on a 2D diffeomorphism. (a) shows a coarse diffeomorphism represented with 17 by 17 points. (a) shows the refinement result to 129 by 129 points using the BHF refinement algorithm.

7.5.3 Super-Resolution of Diffeomorphisms Using the BHF Refinement Algorithm

In this subsection, we apply the BHF refinement algorithm on the super-resolution of diffeomorphisms. In our first test, a coarse version of the highly distorted diffeomorphism in Subsection 7.5.1 is used, which is represented with 17 by 17 points. As shown in Figure 7.6(a), the use of such sparse data causes unnatural jaggy visualization, which is similar to a texture mapping onto a coarse triangular mesh.

Using the BHF refinement algorithm, we refine the coarse mapping into a fine diffeomorphism of 129 by 129 points by interpolating the original 16 by 16 Beltrami coefficient on each face to a 128 by 128 version, and reconstructing a 129 by 129 diffeomorphism, fixing its values on the coarse 17 by 17 grid. The result of the refinement is shown in Figure 7.6(b), which is very smooth and almost looks identical to the original high resolution diffeomorphism. This shows that our algorithm can smoothly refine a diffeomorphism even only a tiny fraction of data is available.

Next we demonstrate the effectiveness of the algorithm in a real 3D texture mapping example. In this test, initially we have a face model represented by a 33 by 33 regular triangular mesh and textured with a highly convoluted texture mapping. As we can see in Figure 7.7(a) and 7.7(b), the coarse triangulation resulted in a poor visualization of the texture. Using the BHF refinement algorithm for surfaces, we refine this coarse texture map into a fine 129 by 129 texture map using only the initial coarse data. The result shown in Figure 7.7(c) and 7.7(d) is very smooth, as if textured using a much higher resolution mapping. This illustrates the effectiveness of our algorithm to represent texture maps in much higher details than the triangular mesh used.

7.5.4 Application in Cortical Surface Parameterization

Finally, we apply the BHF inpainting algorithm to efficiently compute a landmark-matching surface parameterization of the cortical surface. In brain imaging, it is often necessary to map feature landmark lines, such as the sulcal and gyral lines highlighted by doctors, onto consistent locations of a parameter domain, where further analysis takes place. On convoluted surfaces such as the cortical surface, this involves mapping a large number of landmark curves onto consistent

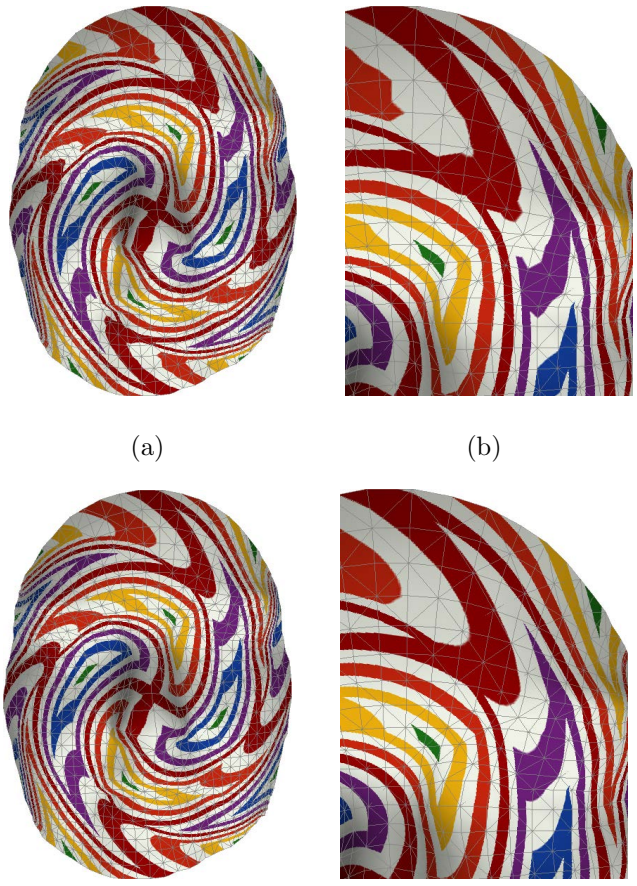

(a) (b)

(c) (d)

Figure 7.7: Application of the BHF refinement algorithm on 3D texture mapping. (a) shows a normally visualized texture mapping on a coarse 33 by 33 mesh. (b) shows a zoom-in version to illustrate its low quality. (c) shows the refined texture mapping on the same mesh after BHF refinement. (d) shows a zoom-in version to illustrate its fine details.

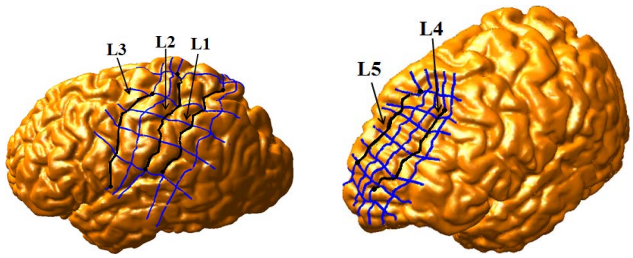

(a) (b)

Figure 7.8: Breaking down a parameterization problem of the cortical surface into 2 subproblems and solve all problems simultaneously. (a) shows the first subproblem involving 3 feature curves. (b) shows the second subproblem involving 2 feature curves.

locations, making the solution infeasible.

We demonstrate the use of the BHF inpainting algorithm to solve this problem efficiently. Instead of solving the problem with all feature curves at once, we first compute consistent parameterizations of a few landmarks lines at a time. As shown in Figure 7.8, we divide a problem involving 5 feature curves on a cortical surface into 2 subproblems involving 2 and 3 feature curves respectively, and solve each subproblem with existing registration algorithms [LTW10]. This breaks down the large problem into easier subproblems which can be solved simultaneously.

After each subproblem is solved, we place the local parameterizations into a larger parameter domain. Then a global parameterization that extends the two local parameterizations is computed using the BHF inpainting algorithm, as shown in Figure 7.9. The resulting global parameterization is a landmark-matching parameterization that smoothly extends the existing local parameterizations.

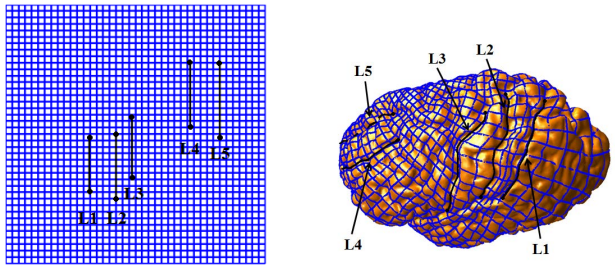

(a) (b)

Figure 7.9: The final result for the large parameterization problem. (a) shows a global parameter domain containing 2 local parameter domains. (b) shows the global parameterization computed using the BHF inpainting algorithm.

7.6 Conclusion

In this chapter, we derived an exact formula for the adjustment of diffeomorphisms using BHF, under the practical assumption that the diffeomorphism is piecewise linear on a triangular mesh. Using this exact algorithm, we further proposed 2 algorithms for the inpainting and refinement of diffeomorphisms. We applied these algorithms on the inpainting of a highly distorted diffeomorphism, the inpainting of image sequences of deforming shapes, the super-resolution of diffeomorphisms and the global parameterization of cortical surfaces by combining local parameterizations. The results show that our algorithms could always reproduce fine details from diffeomorphisms with missing parts or with very low resolution, where other methods produced unnatural or overlapping results. This demonstrates the great versatility of our proposed algorithms on areas from texture mapping to video processing, and from computer graphics to medical imaging. In the future, we plan to improve the efficiency of algorithms by implementing them on GPUs and propose more areas in which they could be used.

References

[AHT99] S. Angenent, S. Haker, A. Tannenbaum, and R. Kikinis. "On the Laplace-Beltrami operator and brain surface flattening." *Medical Imaging, IEEE Transactions on*, **18**(8):700–711, Aug. 1999.

[BBS01] M. Bertalmio, A.L. Bertozzi, and G. Sapiro. "Navier-stokes, fluid dynamics, and image and video inpainting." In *Computer Vision and Pattern Recognition, 2001. CVPR 2001. Proceedings of the 2001 IEEE Computer Society Conference on*, volume 1, pp. I–355–I–362, 2001.

[BG04] A. Belahmidi and F. Guichard. "A partial differential equation approach to image zoom." In *Image Processing, 2004. ICIP '04. 2004 International Conference on*, volume 1, pp. 649–652, Oct. 2004.

[CK06] Y. Cha and S. Kim. "Edge-forming methods for image zooming." *Journal of Mathematical Imaging and Vision*, **25**:353–364, 2006.

[CL03] Bennett Chow and Feng Luo. "Combinatorial Ricci flows on surfaces." *Journal Differential Geometry*, **63**(1):97–129, 2003.

[CS02] T.F. Chan and J. Shen. "Mathematical models for local nontexture inpaintings." *SIAM J. Appl. Math*, **62**:1019–1043, 2002.

[CSS04] Bing-Bing Chai, Sriram Sethuraman, Harpreet S. Sawhney, and Paul Hatrack. "Depth map compression for real-time view-based rendering." *Pattern Recognition Letters*, **25**:755–766, 2004.

[CWR03] Moo K. Chung, Keith J. Worsley, Steve Robbins, Tomáš Paus, Jonathan Taylor, Jay N. Giedd, Judith L. Rapoport, and Alan C. Evans. "Deformation-based surface morphometry applied to gray matter deformation." *NeuroImage*, **18**:198–213, 2003.

[DPT08] S. Durrleman, X. Pennec, A. Trouve, P. Thompson, and N. Ayache. "Inferring brain variability from diffeomorphic deformations of currents: an integrative approach." *Medical Image Analysis*, **12**(5):626–637, 2008.

[FST99] Bruce Fischl, Martin I. Sereno, Roger B.H. Tootell, and Anders M. Dale. "High-resolution intersubject averaging and a coordinate system for the cortical surface." *Human Brain Mapping*, **8**:272–284, 1999.

[GL00] F. P. Gardiner and N. Lakic. *Quasiconformal Teichmüller theory*. American Mathematics Society, 2000.

[GM98] Ulf Grenander and Michael I. Miller. "Computational anatomy: an emerging discipline." *Quarterly of Applied Mathematics*, **56**(4), 1998.

[GVK99] Christian Gaser, Hans peter Volz, Stefan Kiebel, Stefan Riehemann, and Heinrich Sauer. "Detecting structural changes in whole brain based on nonlinear deformations - application to schizophrenia research." *Neuroimage*, **10**:107–113, 1999.

[GVM04] J. Glaunès, Marc Vaillant, and Michael I. Miller. "Landmark matching via large deformation diffeomorphisms on the sphere." *J. Maths. Imaging and Vision*, **20**:179–200, 2004.

[GWC04] Xianfeng Gu, Yalin Wang, Tony F. Chan, Paul M. Thompson, and Shing-Tung Yau. "Genus zero surface conformal mapping and its application to brain surface mapping." *IEEE Transactions on Medical Imaging*, **23**(8):949–958, August 2004.

[GY02] Xianfeng Gu and Shing-Tung Yau. "Computing conformal structures of surfaces." *Communications in Information and Systems*, **2**(2):121–146, 2002.

[Ham88] Richard S. Hamilton. "The Ricci flow on surfaces." *Mathematics and General Relativity (Santa Cruz, CA, 1986), Contemp. Math. Amer.Math.Soc. Providence, RI*, **71**, 1988.

[HAT00] S. Haker, S. Angenent, A. Tannenbaum, R. Kikinis, G. Sapiro, and M. Halle. "Conformal surface parameterization for texture mapping." *Visualization and Computer Graphics, IEEE Transactions on*, **6**(2):181–189, Apr.–Jun. 2000.

[HS09] M. K. Hurdal and K. Stephenson. "Discrete conformal methods for cortical brain flattening." *Neuroimage*, **45**:86–98, 2009.

[IGL00] Juliette W. Ioup, Marlin L. Gendron, and Maura C. Lohrenz. "Vector map data compression with wavelets." *Journal of Navigation*, **53**:437–449, 2000.

[JKL08] M. Jin, J. Kim, F. Luo, and X. Gu. "Discrete surface Ricci flow." *IEEE Transactions on Visualization and Computer Graphics*, **14**(5):1030–1043, 2008.

[JM00] S.C. Joshi and M.I. Miller. "Landmark matching via large deformation diffeomorphisms." *IEEE Transactions on Image Processing*, **9**(8):1357–1370, 2000.

[JSR04] L. Ju, J. Stern, K. Rehm, K. Schaper, M. Hurdal, and D. Rottenberg. "Cortical surface flattening using least square conformal mapping with minimal metric distortion." *IEEE International Symposium on Biomedical Imaging*, pp. 77–80, 2004.

[KA07] Alexander Kolesnikov and Alexander Akimov. "Distortion-constrained compression of vector maps." *Proceedings of the 2007 ACM Symposium on Applied Computing*, pp. 8–12, 2007.

[KCH97] W. Knox Carey, D.B. Chuang, and S.S. Hemami. "Regularity-preserving image interpolation." In *Image Processing, 1997. Proceedings., International Conference on*, volume 1, pp. 901–904, oct 1997.

[LBR07] Oliver Lyttelton, Maxime Bouchera, Steven Robbinsa, and Alan Evans. "An unbiased iterative group registration template for cortical surface analysis." *NeuroImage*, **34**:1535–1544, 2007.

[LE95] J.D. Lewis and M.J. English. "Compression of body surface potential maps using image compression techniques." *Proceeding of Computers in Cardiology*, pp. 401–404, 1995.

[LHV07a] N.A. Lord, J. Ho, and B.C. Vemuri. "USSR: a unified framework for simultaneous smoothing, segmentation, and registration of multiple images." In *Computer Vision, 2007. ICCV 2007. IEEE 11th International Conference on*, pp. 1–6, Oct. 2007.

[LHV07b] N.A. Lord, J. Ho, B.C. Vemuri, and S. Eisenschenk. "Simultaneous registration and parcellation of bilateral hippocampal surface pairs for local asymmetry quantification." *Medical Imaging, IEEE Transactions on*, **26**(4):471–478, April 2007.

[LPR02] Bruno Lévy, Sylvain Petitjean, Nicolas Ray, and Jérôme Maillot. "Least squares conformal maps for automatic texture atlas generation." In *SIGGRAPH 02 Conference Proceedings*, pp. 362–371, 2002.

[LTW08] Lok Ming Lui, Sheshadri Thiruvenkadam, Yalin Wang, Tony Chan, and Paul Thompson. "Optimized conformal parameterization of cortical surfaces using shape based matching of landmark curves." *11th MICCAI*, 2008.

[LTW10] Lok Ming Lui, Sheshadri Thiruvenkadam, Yalin Wang, Paul M. Thompson, and Tony F. Chan. "Optimized conformal surface registration with shape-based landmark matching." *SIAM J. Img. Sci.*, **3**:52–78, February 2010.

[Luo04] Feng Luo. "Combinatorial Yamabe flow on surfaces." *Commun. Contemp. Math.*, **6**(5):765–780, 2004.

[LV73] O. Lehto and K.I. Virtanen. *Quasiconformal mappings in the plane*. Springer-Verlag, New York, 1973.

[LWC07a] L. M. Lui, Y. Wang, T. F. Chan, and P. M. Thompson. "Brain anatomical feature detection by solving partial differential equations on general manifolds." *Discrete and Continuous Dynamical Systems B*, **7**(3):605–618, May 2007.

[LWC07b] Lok Ming Lui, Yalin Wang, Tony F. Chana, and Paul Thompson. "Landmark constrained genus zero surface conformal mapping and its application to brain mapping research." *Applied Numerical Mathematics*, **57**:847–858, 2007.

[LWG10] L.M. Lui, T.W. Wong, X.F. Gu, P.M. Thompson, T.F. Chan, and S.T. Yau. "Shape-based diffeomorphic registration on hippocampal surfaces using beltrami holomorphic flow." In *Proceedings of the 13th MICCAI'10: Part II*, pp. 323–330, 2010.

[LWZ10] Lok Ming Lui, Tsz Wai Wong, Wei Zeng, Xianfeng Gu, Paul Thompson, Tony Chan, and Shing-Tung Yau. "Detecting shape deformations using Yamabe flow and Beltrami coefficents." *Journal of Inverse Problem and Imaging (IPI): Special Issue in Medical Imaging*, **4**(2):311–333, 2010.

[LYL05] A. Leow, C.L. Yu, S.J. Lee, S.C. Huang, H. Protas, R. Nicolson, K.M. Hayashi, A.W. Toga, and P.M. Thompson. "Brain structural mapping using a novel hybrid implicit/explicit framework based on the level-set method." *NeuroImage*, **24**(3):910–927, 2005.

[MTA08] Jonathan H. Morra, Zhuowen Tu, Liana G. Apostolova, Amity E. Green, Christina Avedissian, Sarah K. Madsen, Neelroop Parikshak, Xue Hua, Arthur W. Toga, Clifford R. Jack, Michael W. Weiner, Paul M. Thompson, and Alzheimer's Disease Neuroimaging Initiative. "Validation of a fully automated 3D hippocampal segmentation method using subjects with Alzheimer's disease mild cognitive impairment, and elderly controls." *NeuroImage*, **43**(1):59–68, 2008.

[MTA09] Jonathan H. Morra, Zhuowen Tu, Liana G. Apostolova, Amity E. Green, Christina Avedissian, Sarah K. Madsen, Neelroop Parikshak, Arthur W. Toga, Clifford R. Jack, Norbert Schuff, Michael W. Weiner,

and Paul M. Thompson. "Automated mapping of hippocampal atrophy in 1-year repeat MRI data in 490 subjects with Alzheimer's disease, mild cognitive impairment, and elderly controls." *NeuroImage*, **45**(1):S3–15, 2009.

[PFG06] Kilian M. Pohl, John Fisher, A W. Eric L. Grimson, A Ron Kikinis, and William M. Wells B. "A Bayesian model for joint segmentation and registration." *NeuroImage*, **31**:228–239, 2006.

[PP93] Ulrich Pinkall and Konrad Polthier. "Computing discrete minimal surfaces and their conjugates." *Experimental Mathematics*, **2**:15–36, 1993.

[SR08] J. Stachera and P. Rokita. "Normal map compression based on BTC and wavelet coding." *Proceeding of Real-Time Image Processing*, **6811**:68110S.1–68110S.8, January 2008.

[SRL07] Yonggang Shi, Allan L. Reiss, Agatha D. Lee, Rebecca A. Dutton, Ursula Bellugi, Albert M. Galaburda, Julie R. Korenberg, Debra L. Mills, Ivo Dinov, Paul M. Thompson, and Arthur W. Toga. "Hamilton-Jacobi skeletons on cortical surfaces with applications in characterizing the gyrification pattern in Williams syndrome." *IEEE ISBI*, 2007.

[STD07] Yonggang Shi, Paul M. Thompson, Ivo Dinov, Stanley Osher, and Arthur W. Toga. "Direct cortical mapping via solving partial differential equations on implicit surfaces." *Medical Image Analysis*, **11**(3):207–223, 2007.

[SY94] Richard Schoen and Shing-Tung Yau. *Lectures on differential geometry*. International Press of Boston, 1994.

[TGW00] Paul Thompson, Jay N. Giedd, Roger P. Woods, David MacDonald, Alan C. Evans, and Arthur W. Toga. "Growth patterns in the developing brain detected by using continuum-mechanical tensor maps." *Nature*, **404**(6774), March 2000.

[THZ04] Paul M. Thompson, Kiralee M. Hayashi, A Greig I. De Zubicaray, B Andrew L. Janke, David M. Doddrell, and Arthur W. Toga A. "Mapping hippocampal and ventricular change in Alzheimer disease." *NeuroImage*, **22**(4):1754–66, 2004.

[TRL06] D. Tosun, A. L. Reiss, A. D. Lee, R. A. Dutton, K. M. Hayashi, U. Bellugi, A. M. Galaburda, J. R. Korenberg, D. L. Mills, A W. Toga, and P. M. Thompson. "Use of 3-D cortical morphometry for

mapping increased cortical gyrification and complexity in Williams syndrome." *IEEE ISBI*, 2006.

[TT96] P. Thompson and A.W. Toga. "A surface-based technique for warping three-dimensional images of the brain." *Medical Imaging, IEEE Transactions on*, **15**(4):402–417, Aug. 1996.

[US05] G. Unal and G. Slabaugh. "Coupled PDEs for non-rigid registration and segmentation." In *Computer Vision and Pattern Recognition, 2005. CVPR 2005. IEEE Computer Society Conference on*, volume 1, pp. 168–175, June 2005.

[VMY04] M. Vaillant, M. I. Miller, L. Younes, and A. Trouvé. "Statistics on diffeomorphisms via tangent space representations." *NeuroImage*, **23**:S161–S169, 2004.

[WCT05] Y. Wang, Ming-Chang Chiang, and Paul M. Thompson. "Automated surface matching using mutual information applied to Riemann surface structures." *Proceeding in Medical Image Computing and Computer-Assisted Intervention MICCAI 2005*, **2**:666–674, 2005.

[WLC05] Yalin Wang, Lok Ming Lui, Tony F. Chan, and Paul M. Thompson. "Optimization of brain conformal mapping with landmarks." *Proceeding in Medical Image Computing and Computer-Assisted Internvention - MICCAI 2005*, pp. 675–683, 2005.

[WLG07] Yalin Wang, Lok Ming Lui, Xianfeng Gu, K.M. Hayashi, T.F. Chan, A.W. Toga, P.M. Thompson, and Shing-Tung Yau. "Brain surface conformal parameterization using Riemann surface structure." *Medical Imaging, IEEE Transactions on*, **26**(6):853–865, June 2007.

[ZET03] Michael M. Zeineh, Stephen A. Engel, Paul M. Thompson, and Susan Y. Bookheimer. "Dynamics of the hippocampus during encoding and retrieval of face-name pairs." *NeuroImage*, **299**(5606):577–580, 2003.

[ZLG08] W. Zeng, L.M. Lui, X. Gu, and S.-T. Yau. "Shape analysis by conformal modules." *Journal of Methods and Applications of Analysis*, **15**(4):539–556, 2008.

[ZSG10] Wei Zeng, D. Samaras, and D. Gu. "Ricci flow for 3D shape analysis." *Pattern Analysis and Machine Intelligence, IEEE Transactions on*, **32**(4):662–677, April 2010.

[ZYZ08] Wei Zeng, Xiaotian Yin, Yun Zeng, Yukun Lai, Xianfeng Gu, and Dimitris Samaras. "3D face matching and registration based on hyperbolic Ricci flow." *Computer Vision and Pattern Recognition Workshop*, **0**:1–8, 2008.

[ZZW08] Wei Zeng, Yun Zeng, Yang Wang, Xiaotian Yin, Xianfeng Gu, and Dimitris Samaras. "3D non-rigid surface matching and registration based on holomorphic differentials." In *ECCV08*, pp. 1–14, 2008.